Wearable Technologies for Embodied Human-Robot Interaction

Thèse Nº 7266

Carine ROGNON

2019

EPFL
ÉCOLE POLYTECHNIQUE
FÉDÉRALE DE LAUSANNE

If you were born without wings
do nothing to prevent them from growing.
— Coco Chanel

How one sees the world depends on
how one is acting on it.
—

Pour William,
mon rayon de soleil…

Acknowledgements

I would like to express my deepest gratitude to all the people who made this journey possible.

I would like to thank **Prof. Dario Floreano** for giving me the opportunity to carry out my PhD in his laboratory and for advertising my project, which gave me multiple great opportunities to meet people from the community and beyond. I would like to thank our administrative assistant **Michelle** for simplifying my life and always finding solutions to my administrative issues. Your importance is too often overlooked. I am also thankful to **Corinne**, our doctoral school secretary, for always being there to listen and help me.

I would like to say a very special thanks to my amazing mentor **Stefano** for having me persevere in this thesis. Since the first day, when I was away, and even after leaving the lab, you were there for me no matter the situation. Without you, I would never have finished this thesis. Your support and advice allowed me to reach the achievements of this work. I am infinitely grateful to you. I would never say it enough: "You are my academic hero!"

A big thanks to all the past and present **LIS members** for the awesome moments we spend together! All the fun, cooking battles, barbecues, ski trip, beers at Sat and of course the science, will be memories that I will cherish for life. In particular, thank you to **Vivek** who has been very thoughtful with me. You always took the time for me, to help me or to calm me down. Another huge thank you to **Matt E.** for being "ride or die" with me in stormy moments of my life. You never judged me and your honesty helped me to get through these periods. I would also like to thank **Davide** for being so optimistic with my project and always being willing to test new devices. Thank you to **Enrica** for being so kind and helpful both on the academic side and as a friend.

I would like to express my deepest gratitude to **Prof. Allison Okamura** for giving me the opportunity to gain experience in her lab at Stanford. In addition to be a great advisor, you changed my vision of science and taught me precious knowledge that made me grow as a scientist and as a person. You set a great example for me. I would also like to thank all **Charm Lab members** for adopting me in your lab and for being so kind. In particular, **Margaret K.** for your endless patience, your aptitude to always see the positive side of any situations and for the great conversations we have on so many topics. Thanks to **Julie** for including me at so many occasions and for being there went I needed it. Thanks to **Sophia, Margaret C.** and **Laura** for your help and enthusiasm. My adventure at Stanford would not have been the same without **Vincent** whose positivism even helped me to finish a marathon! Thanks also to **Sam** for sharing numerous adventures and controversial discussions.

Acknowledgements

I would like to thank my demo-buddy **Jenifer** for the great moments we shared during the multiples events we have done together, and also for handling the stress due to the flight simulator. Also, together we learned the hard way that you should not trust Google Map in New York City :).

I would like to thanks the lab members from **BioRob** and **RRL** for sharing parts of my journey. In particular **Amy** for your valuable help, and **Matt R., Salman** and **Robin** for motivating me through running sessions among other things. A special thank you to **Ale** for "saving" me so many times with all kind of IT issues.

I would also like to thank the members of my jury, **Prof. Heike Vallery**, **Prof. Mark Cutkosky**, **Prof. Roger Gassert** and **Prof. Auke Ijspeert** who honored me by agreeing to review this work, and provided highly valuable comments.

Besides all the work related aspects, I would also thank my dear friends who supported me during all the time at EPFL. In particular my dream team – **Flavien** (special thanks for being, with so much optimism, my cavia so many times!), **Ludo, Daniel, Nico, Gaetan, Daphné, David M.** – who helped me to put the size of my problems in perspectives. I would like to thanks my friend since forever, **Sarah**, for being there during all the challenges of my life and for giving me a reason – William – to do well. Thanks to **Louise** for listening to me endlessly and bringing other points of view on my issues. I would like to thanks all the member of the **Rushteam**, my triathlon team, in particular **Cendrine** and **Estelle** for motivating me to get out of the lab every once in a while and for their positivism.

I am endlessly thankful to my parents **Monique** and **Philippe** for always encouraging me, being optimistic about my life choices and for supporting me even in the darkest moments of this thesis. You allow me to dream big as I know that you will be there to catch me if I fall. Thanks to my sister **Emilie** for making me laugh (and I learned since the youngest age to not drink Coke at the same time) and for sharing the "Rainforest" and "petit paquet" at Yoga.

At last but not least, my biggest thought goes to my beloved **Matthieu**. You have been caring for me in every situations and it is thanks to you if I am here today. You have been my rock, allowing me to succeed in this PhD. Thanks also to your family who been supportive among all the years.

Lausanne, 28 Mai 2019   Carine Rognon

Abstract

Robotic teleoperation is fundamental to augment the resilience, precision, and force of robots with the cognition of the operator. However, current interfaces, such as joysticks and remote controllers, are often complicated to handle since they require cognitive effort and learned skills. Wearable interfaces can enable more natural and intuitive interactions with robots, which would make robotic teleoperation accessible to a larger population of users for demanding tasks, such as manipulation or search-and-rescue.

The aim of this thesis is to explore solutions to simplify our interactions with robots promoting their access to a broader range of the population. To achieve this, we are presenting a soft upper body exoskeleton, called the FlyJacket, for the bidirectional control of fixed-wing drones. Drones can greatly benefit us as they extend our perception and range of action. The exoskeleton controls a drone by recording torso movement and, through embedded haptic feedback devices, renders either kinesthetic guidance to improve the flight performance or tactile feedback to render the sensation of flying.

We developed and tested an interface to control both a simulated and a real drone. The FlyJacket is a soft exoskeleton with arm support conceived to address the challenges of adapting to different morphologies and supporting the user during flight to prevent fatigue. We demonstrated that this novel interface allowed more consistent performance than when performing the same task with a remote controller and users felt more immersed into the flight.

Interacting with a robot can be greatly enhanced by having multiple channels of sensorial feedback to increase the awareness of the operator. Information on the state of the drone can be intuitively rendered with haptic feedback. To create this bidirectional interaction with the drone, the two types of haptic feedback – kinesthetic and tactile – have been explored.

Kinesthetic feedback was implemented with a cable-driven system to give haptic guidance to the user's torso position. Performing user studies, we could determine that the embedded kinesthetic guidance improved the flight performance and that a quadratically shaped force feedback curve was the most adequate profile to guide the user. We also established the minimal force difference, defined the perceived magnitude of this system and studied the learning process of users.

Tactile feedback was investigated to render the sensation of flying by enhancing flight awareness, realism and immersion. To this end, we developed and embedded a new type of soft actuator that was compliant and lightweight such that it remained wearable and portable. Four tactile devices, placed on the torso, provided feedback by compressing closed air pouches against the skin rendering the sensation of air pressure. A mechanical model and simulation

of the pouch device were developed to determine appropriate parameters. We evaluated whether it conveyed useful information to the user and whether it enhanced the experience of flying. We demonstrated that users were able to understand the direction of the cues without prompting, could distinguish the cues quickly, and do so with high accuracy. The device was also used in a simulated flight task and users indicated that it increased the flight realism. We believe that the contributions of this thesis provide insights to the design of intuitive interfaces for human-robot interaction and increases their accessibility to a wider range of the population.

Keywords

Résumé

La téléopération robotique est fondamentale pour augmenter la résilience, la précision et la force des robots grâce aux capacités cognitives de l'opérateur. Cependant, les interfaces actuelles, telles que les joysticks et les télécommandes, sont souvent compliquées à manipuler car elles nécessitent un effort cognitif et des compétences pointues qui requièrent un apprentissage. Les interfaces sous forme de technologie vestimentaire peuvent permettre des interactions plus naturelles et intuitives avec les robots, ce qui rendrait la téléopération robotique accessible à un plus grand nombre d'utilisateurs pour des tâches exigeantes, telles que les manipulations délicates ou les missions de recherche et de sauvetage.

Le but de cette thèse est d'explorer des solutions pour simplifier nos interactions avec les robots, facilitant ainsi leur accès à une population plus large. Pour ce faire, nous présentons un exosquelette flexible pour le haut du corps, appelé FlyJacket, destiné au contrôle bidirectionnel des drones à voilure fixes. Les drones peuvent nous être grandement utiles car ils élargissent notre perception et notre rayon d'action. L'exosquelette contrôle un drone en enregistrant les mouvements du torse et, au moyen de dispositifs de retour haptiques intégrés, fournit un guidage kinesthésique pour améliorer les performances de vol ou un retour tactile pour donner la sensation de voler.

Nous avons développé et testé une interface permettant de contrôler à la fois un drone en simulation et un drone réel. La FlyJacket est un exosquelette flexible incluant un support de bras. Elle a été conçue pour relever les défis d'adaptation de l'exosquelette à différentes morphologies et pour soutenir les bras de l'utilisateur pendant le vol afin de prévenir leur fatigue. Nous avons démontré que cette nouvelle interface permet des performances plus homogènes que lors de l'exécution de la même tâche avec une télécommande et que les utilisateurs se sentent davantage immergés dans le vol.

L'interaction avec un robot peut être grandement améliorée en incluant plusieurs canaux de retour sensoriel afin d'augmenter la prise de conscience de l'opérateur. Les informations sur le status du drone peuvent être rendues intuitivement à l'aide d'un retour haptique. Pour créer cette interaction bidirectionnelle avec le drone, les deux types de retour haptique - kinesthésique et tactile - ont été explorés.

Le retour kinesthésique a été mis en œuvre avec un système de câbles pour donner des informations relatives à la position du torse de l'utilisateur. En effectuant des études auprès des utilisateurs, nous avons pu déterminer que ce guidage kinesthésique améliorait les performances de vol et qu'une courbe de retour de force de forme quadratique était le profil le plus approprié pour guider l'utilisateur. Nous avons également établi la différence de force

Abstract

minimale requise pour être perçue par l'utilisateur, déterminé la perception de l'amplitude d'une force donnée par ce système et étudié le processus d'apprentissage des utilisateurs.

Le retour tactile a été étudié pour donner la sensation de voler en améliorant le ressenti du vol, le réalisme et l'immersion. À cette fin, nous avons développé et intégré un nouveau type d'actionneur flexible, qui est souple et léger, que l'on peut porter à la manière d'un vêtement et qui reste transportable. Quatre actionneurs tactiles, placés sur le torse, fournissent un retour de force en comprimant des poches d'air fermées contre la peau, ce qui permet de recréer une sensation semblable à la pression de l'air. Un modèle mécanique et une simulation de l'actionneur ont été développés pour déterminer les paramètres appropriés. Nous avons évalué si cela transmettait des informations utiles à l'utilisateur et si cela améliorait l'expérience de vol. Nous avons démontré que les utilisateurs sont en mesure de comprendre la direction indiquée par le retour de force sans aide extérieure, peuvent distinguer rapidement ces directions, et le faire avec une grande précision. Le dispositif a été également testé avec un vol simulé et les utilisateurs ont indiqué qu'il augmente son réalisme.

Nous pensons que les contributions de cette thèse permettent de mieux comprendre la conception d'interfaces pour des interactions plus intuitives entre l'humain et les robots, accroissant ainsi leur accessibilité à une plus grande partie de la population.

Mots-clés

Interaction Humain-Robot, Télérobotique et Téléopération, Réalité Virtuelle et Interfaces, Robotique Endossable, Haptique Endossable, Assistance Kinesthésique, Retour Tactile, Applications de la Robotiques Flexible, Drones

Contents

Contents

List of Figures

List of Tables

List of Acronyms

- HRI: Human-Robot Interface

- ROM: Range Of Motion

- VR: Virtual Reality

- MCU: Microcontroller Unit

- IMU: Inertial Measurement Unit

- SPI: Serial Peripheral Interface

- AS: condition "Arms \ Support"

- ANS: condition "Arms \ No Support"

- NA: condition "No Arms"

- RC: Remote Controller

- RMS: Root Mean Square

- GSS: Gas Spring Support

- SBS: Static Balancing Support

- NS: No Support

- 1PF: 1st Percentile Female

- 99PM: 99th Percentile Male

- DOF: Degree Of Freedom

- EMG: Electromyogram

- MVC: Maximal Voluntary Contraction

- JND: Just Noticeable Difference

- wp: waypoint

Introduction

Robots are becoming pervasive in both domestic and professional environments. They can bring benefit to an individual in many situations, extending our range of action and increasing our safety. Indeed, nowadays robots are widely used in dangerous situations such as in nuclear plants and chemical industries, scenes of natural hazards, and more generally in search-and-rescue missions [1, 2]. We also take advantage of robots for physically demanding tasks such as construction and car assembly lines [3]. Furthermore, robots have proven to be useful for performing tasks where humans are not able to physically reach either due to environmental risk or size constraints [4] such as space [5], undersea [6], micro- and nanoscale exploration [7] or performing sophisticated surgeries [8].

Telerobotics involves the remote control of a robot by a human as operator [9]. In this system, cognitive decisions are made by the human while the robot is responsible for their direct action within the environment. The use of telerobotics can augment robot awareness. Having the human cognition skills (i.e. decision making, creativity and problem solving) for high-level tasks completed by the augmented physical skills of the robot (force, dexterity, or another type of locomotion) can achieve complex tasks and enhance mission performance. More specifically, the term "teleoperation" stresses the task-level operations of telerobotics.

Teleoperation experiences a long history with its first documented use back in the 1940's in nuclear research by Raymond C. Goertz who used a teleoperated system to handle radioactive material [9]. Applications in nuclear power activities began to decline in the 1980's but telerobotics had already become well established in many other fields such as medicine, undersea and space missions [9]. Ever since, the teleoperation of robots has continued to extend to various fields including industries and leisure.

However, current human-robot interfaces (HRIs), such as joysticks, keyboards, and touch screens, are neither natural [10] nor intuitive for the user as they require training and concentration during operation [2, 11]. In many cases, this limits the use of robots to highly trained professionals [4, 12]. Indeed, telerobotics is often restricted to expert users that undergo significant training to master the control of robots. The most limiting issues are the complexity of the control interface, which requires high attention and induces cognitive fatigue for the user during long term operation, and the restricted feedback on the robot's state, which creates uncertainty regarding its trajectory or position [2, 11]. Consequently, there is a growing de-
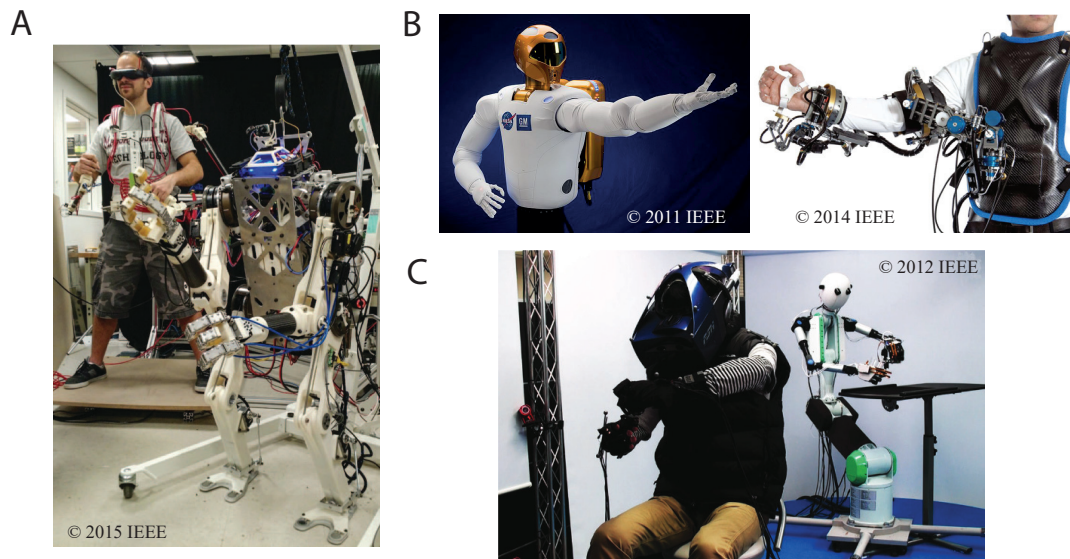
Figure 1 – Examples of telerobotics systems. A) HERMES humanoid system showing the operator and humanoid robot [13]. B) Robonaut (left) [5] and the X-ARM 2 exoskeleton (right) [16]. C) TELESAR V system showing the master (left) and the slave (right) [15].

mand for new types of intuitive HRIs to grant naive users access to this technology, broadening its use to a wider population and applications.

Recent investigations have focused on finding easier approaches to teleoperate robots by having more natural and intuitive control, and more extended sensorial feedback. In order to enhance the ease of use of telerobotic systems, focus has been placed on wearable devices. With such devices, the human can control a robot using intuitive body movements instead of handling a remote controller. Using a wearable device also allows rendering sensations felt by the robot directly on the body of the human – using haptic feedback – which can enhance task immersion and trigger sensory channels other than vision and audition [13]. For example, during robot manipulation tasks, the operator needs to perceive the force that the robot applies on the object to ensure stable grasping [14, 15]. In the case of a drone, teleoperators could potentially react quicker to perturbations such as wind gusts or turbulence when provided with both haptic and visual feedback, rather than relying on visual feedback alone. By exploiting the presence of spinal reflexes, the reaction time can be shorted three-fold [13]. Furthermore, using only one sensory channel, for example vision, to process the information from the robot, can be very tiring and can cause the operator to make mistakes leading to the task failure [2].

The main focus of this thesis is to study and develop new wearable technologies for embodied human-robot interaction by designing wearable and portable interfaces with embedded, haptic feedback devices. The interface presented in this thesis can control and receive feedback from a fixed-wing drone. Drones can bring a lot of benefits to the human as they can extend our perception and range of action. In addition, we wanted to demonstrate that it was possible

to intuitively interact with non-homologous robots, when the humans' command possibilities differ from the robot's desired behavior. Our aim is to simplify these interactions to facilitate a drone's use to a larger range of the population.

Figure 2 – Examples of wearable devices. A) Cable-driven lower limb exoskeleton [17]. B) Cable-driven hand exoskeleton [18]. C) Cable-driven upper body exoskeleton [19]. D) Pneumatic upper body exoskeleton [20]. E) Pneumatic hand exoskeleton [21]. F) Slide spring mechanism for hand exoskeleton [22].

Wearable Interfaces

Wearable interfaces are created by taking human-centred criteria into consideration. At first, the customization and ergonomics of the wearable device have to be studied. Humans vary considerably in shape, size, and dimension. To engage users, the look and feel of the wearable devices should enable customization considering the mass and proportions of physical anatomy. This also affects the physical shape of the wearable devices and how users perceive them. For instance, ergonomic design is important in haptic devices that require significant load transmission to the operator's body in a manner that minimizes bulkiness and prioritizes comfort. One important step towards functional ergonomics is applying our existing understanding of human physiology. This includes the knowledge of human anatomical pressure sensitivity [23] to locate proper anchoring points and skin strain field mapping [24] to prevent slippage between the device and the skin.

Secondly, the comfort of the wearable device plays an essential role in the design. The users should not experience any discomfort and pain, which is a consideration that guides texture, shape, and weight of the device. The form factor of objects that interface with the body should be determined by their interaction with the human form, factoring in the dynamics of movements, and ensuring that these movements are not unintentionally obstructed.

Third, the intuitiveness and cognitive load of the interaction of the user with the wearable interface, i.e. correctly interpreting the feedback provided by the wearable devices, has to be taken into consideration. A straightforward interface enhances the usability of the device, and increases the user's engagement. The wearable device should resort to a minimalistic design that includes only the necessary interaction channels required to accomplish the robotic task.

Typically, wearable interfaces to control robots are made of rigid materials, which enable efficient support of the human motion, postures, and force transmission [13, 16, 25]. However, most of these interfaces are heavy, cumbersome and do not have good user acceptance. Therefore, they do not satisfy the first two aforementioned criteria. Recently, investigations have focused on developing soft exoskeletons to reduce the weight and enhance user acceptance. These devices can be cable-driven [17, 18, 19], pneumatically actuated [20, 21], or use sliding spring mechanisms [22] (see Fig. 2). Their intrinsic compliance grants users freedom to move and adapts to different body types. These characteristics can also compensate for misalignments between centers of rotation of the human body and the joints of the exoskeleton. Such misalignments are a well-known problem for rigid exoskeletons as even a small mismatch in kinematics can induce a moment on the human body, leading to injuries [26]. However, the achievable support and force transmission of a soft exoskeleton is substantially lower than for rigid devices.

Haptic Feedback

Using wearable devices to interact with robots has shown to simplify the interaction [27, 28]. However, the user frequently lacks information about the state of the robot and the environment because they must rely only on visual feedback [13, 29].

The provision of sensory feedback serves to inform the teleoperator about the state of the robot and its environment. The human body is equipped with various sensory systems that gather feedback. This includes sensory information arising from vision (eyes), audition (ears), tactile sensation (skin), kinesthetic awareness (joints, muscles, and connective tissues), and balance (vestibular organs). When interacting with the environment, through the teleoperation of a robot or not, it is essential to feel the forces produced by our surrounding. Haptics - which is the sense of touch - enable humans to perform a wide variety of inspection and manipulation. Without this sensory channel, we would have great difficulty to interact with our environment as we would be unaware of contact with objects, the amount of force transmitted, or surface properties, which can be crucial in interaction tasks such as handling a tool. Furthermore, haptic feedback acts as a protective mechanism; we can feel when the forces are becoming dangerously high, and intuitively remove our limbs before getting hurt. This kind of information cannot be transmitted by vision or audition without a learning process. Having haptic feedback embedded in the wearable device is therefore a very important feature for situational awareness and immersion [30]. Controlling a robot without having haptic feedback results in being deprived of an important sensing modality, which considerably complicates interaction with the environment. In addition, the types of tasks that human teleoperators need to perform often require a considerable amount of effort and it is very tiring to treat all information within only one sensory channel (e.g. vision) which can cause the operator to fatigue and induce them to make mistakes.

The benefits of haptic feedback for improving telerobotic performance have been demonstrated in several applications spanning different fields of human-robot teleoperation. Examples include space telerobotic applications [16, 31], medical applications [32, 33, 34], search-and-rescue operations [13], underwater applications [6], or navigation [35, 36, 37].

Haptic feedback is typically described in two modalities: kinesthetic and tactile feedback [38]. Kinesthetic feedback, which depends on the proprioception of body parts, is sensed by muscles, tendons and joints through muscle spindles and Golgi tendon organs. Kinesthetic awareness senses movement and force, typically associated with force-displacement relationships. It helps inform us about the torque applied on our joints and the position (and derivatives thereof) of our body parts. The most popular kinesthetic device is probably the Phantom Omni. It is a grounded device that can provide a broad range of force feedback in three dimensions to the fingertips. Wearable technologies use an exoskeleton to give kinesthetic feedback by moving one body part relative to another [16, 25]. Some devices do not actively move body parts but on the contrary prevent motion using clutches [39, 40]. When kinesthetic feedback must be given without fixation points to the ground or links between two

body parts, one solution is to use the flywheel principle [41, 42, 43].

Tactile sensations, which refer to sensations at skin level such as pressure, vibrations or shear, are sensed by the mechanoreceptors embedded in the skin. Each mechanoreceptor perceives a specific type of haptic stimulus and their density differs regarding to body parts [44]. When designing a haptic device, the density and specialization of the mechanoreceptors present on the body part where the device will be applied should be taken into account. The design of the tactile device should also consider the type of sensation that should be recreated, which can be very complex due to the large amount of sensations that the skin can sense. The most widely used actuators to give tactile feedback are vibrotactors. These actuators have the advantage of being lightweight and, thanks to the possibility of varying the frequency and amplitude of the vibration, can give a large range of sensations such as tapping on a surface, textures or puncturing membranes [45]. However, they can not render some types of sensation such as large normal pressure on the skin. Recent investigations have focused on pneumatic actuators due to their intrinsic compliance, which enables a safe interaction with the body [46], [47]. Multiple sensations can also be recreated with pneumatic actuators. However, they require a system of valves and a compressor which are noisy and prevent the portability of the system. Another kind of tactile feedback is electro-stimulation. Like the vibrotactors, this technique allows to give many different kinds of sensation by changing the amplitude and frequency of the stimulation [48, 49]. However, electrical stimulation is sometimes found to be unpleasant and is tiring for muscles when used for several minutes. A normal force can be rendered using pins [50] but they are usually bulky and not compliant. Liquid coupled dielectric elastomers have the advantage of being small, silent and cost effective [51] but also have several drawbacks for wearable use; the required high voltage is usually negatively perceived by users, and the given forces are relatively small. Skin stretch devices are also used to transmit information such as movements and directions [52, 53]. These mechanical devices are usually electrically-driven, which enhances the portability. Tactile feedback is also always present in kinesthetic feedback devices as they are in contact with the body, stimulating the skin. Therefore, the interaction of the kinesthetic device with the body has to be considered to give the right tactile sensations.

Haptic feedback is mostly used to give two types of information; (1) task guidance to improve the performance or (2) to recreate sensations that are not available. Both kinesthetic and tactile feedback can be used to deliver either of these two types of information. Haptic guidance requires knowledge about the environment where the robot operates. For example, within navigation either a predetermined path can be followed or obstacles can be sensed during motion for collision avoidance [35]. Haptic guidance can also be used for task training in many fields such as rehabilitation [54, 55], sports [56, 57] or medicine [32]. Guidance can be provided to the user to move either away from the cue (repulsive feedback) or toward the cue (attractive feedback). Both repulsive and attractive feedback showed similar improvement in task performance but investigations suggest different learning mechanisms [32, 58, 59]. The amount of guiding force influences substantially the performance [60]. Providing too much guidance leads to passiveness of the user while not enough guidance will not improve the task

performance [61]. The task should be challenging enough to induce active participation from the user. This "sweet spot" is individual and task dependant, and may also vary regarding to the daily motivation of the user.

Haptic feedback can be used to recreate sensations that are not available at the operator location such as during teleoperation, in virtual reality (VR) or when having an amputated limb. In the case of teleoperation, sensors are required on the robots to feel the environment and an effective communication channel between the robot and the human is required to insure imperceptible time-delay. Recreating sensations felt by the robot in its environment will deepen the operator's immersion in the task, prompting more natural behavior. Having a more intuitive interaction reduces the operator workload and therefore reduces possible mistakes. When the aim of the haptic feedback is to deepen embodiment, sensation realism is critical. However, more realistic haptics are not necessarily better. Indeed, if the fidelity of the haptic sensation increases but is not matching with other sensory feedback (such as visual and auditory cues), or if the sensations do not correspond to the user's expectation, the subjective impression of realism actually worsens and an embodiment can not be reached. We refer this degradation as the uncanny valley of haptics [62]. Additionally, more sensation is not necessarily better because too much information can confuse the user and also degrade the interaction.

Drone Teleoperation

Among the various types of robots, drones are among the fastest growing in personal and professional environments because of their capability to extend human perception and range of action in unprecedented ways [1]. Fields of application include aerial mapping, agriculture, military applications, search-and-rescue, transportation and delivery [11]. In most of these fields, drones work cooperatively with users as they increase the perception of human spaces and provide information that would not be available from a ground perspective [63, 64]. However, the use of joysticks or remote controllers for drone teleoperation is a non-intuitive and challenging task, which becomes cognitively demanding during long-term operations [65]. The development of more intuitive control interfaces could improve flight efficiency, reduce errors, and allow users to shift their attention from the task of control to the evaluation of the information provided by the drone.

Human-drone interfaces could be improved by focusing on natural human gestures captured by wearable sensors. Indeed, the use of wearable devices, such as exoskeletons, has been shown to enhance control intuitiveness and immersion [54, 66]. Over the last decade, the development of gesture-based interfaces for flight control have focused on the use of upper body movements to control the flight with two different approaches. The first approach relies on moving platforms that can support the entire weight of the person. For example, using the Birdly (Somniacs SA, Zurich, Switzerland) or the Hypersuit (Theory, Paris, France), the person lies horizontally on the platform with the arms spread out on wing-like structures to control a

simulated bird or wing-suit (see Fig. 3). These platforms make use of a VR headset to provide a first-person view from the flying agent's perspective. Flight control is achieved by moving the hands or the arms. The wing-like structure supports the arms weight, preventing physical fatigue during long flight sessions. Although these platforms were designed as VR devices for instilling the impression of flying, we have shown that they can also be used for immersive control of a real drone [67]. Despite the impressive rendering of flight experiences, these platforms suffer from two drawbacks when it comes to drone control: the support structures tend to constrain the range of human gestures to very few degrees of freedom (e.g. wrist rotation) and they are bulky and heavy, which prevents their usability in deployable drone operation.
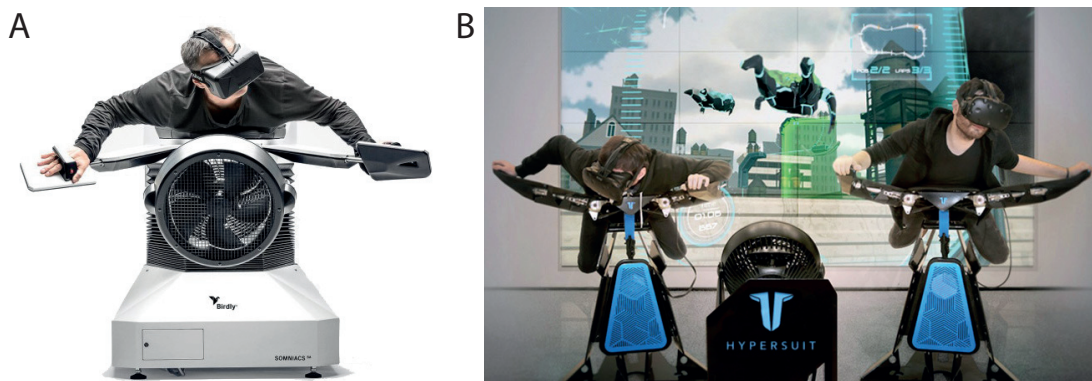
Figure 3 – Examples of flight simulator platforms. A) Birdly (Somniacs SA, Zurich, Switzerland). B) Hypersuit (Theory, Paris, France).

The second approach lets users command the drone with upper body movements recorded by external tracking systems [68, 69, 70]. Here the person is free to use a larger variety of gestures to control the drone, but the lack of body support can cause fatigue. Furthermore, the necessity of external devices for tracking body motion limits the method to indoor use. Yet, one study used EMG sensors on the forearm to control a drone [71]. For most of the cited studies, the control is carried out from a third-person view or through a monitor, which limits the immersion.

In a previous study [72], the authors identified an intuitive upper body movement pattern that naive users exploited to fly a fixed-wing drone. This embodied flight style, which allows the user to directly control the pitch and roll of a drone using torso movements, reduces learning time and increases performance when compared to the use of traditional remote controllers. The established movements to control the drone are the following: the user is seated and bends his torso forward and backward in the sagittal plane to control the pitch up and down maneuvers respectively, and a combination of bending on the sides in the frontal plane and twisting in the transverse plane, is used to control the roll angle of the drone. The mapping between torso movements and drone commands is linear. An illustration of these movements

can be found in Fig. 1.4 in Chapter 1.

As discussed earlier, providing haptic feedback during teleoperation increases the performance. For complex tasks such as flying, adding haptic feedback led to a faster reaction time than solely relying on visual and auditory feedback [73, 74]. Previous work provided haptic feedback from the drone through a hand-held remote controller to give additional information to the operator about the state of system, such as the distance to obstacles [36, 73], the drone position (Motion Pilot, Ecublens, Switzerland), or drone velocity [74, 75]. In the case of flying a drone using intuitive body gesture, additional information about the body position in space or the attitude of the drone could be given to the user in order to further improve the flight precision. Rendering flight information using haptic feedback on the user's torso could provide a collocated feedback that is more natural and easier to process [76].

Thesis Outline

In this thesis, we developed an upper body soft exoskeleton - called the FlyJacket - for a bidirectional interaction with drones. The FlyJacket is conceived for teleoperation during search-and-rescue missions. Indeed, during these missions, drones are used to gather information from the environment to help the rescuers to plan the mission and distribute efficiently their resources. However, with current interfaces, they need to have an operator that undergoes a long training to master the control of the drone, hence the necessity of having more intuitive interactions to reduce this training. To be deployable, the design of the exoskeleton has to be carefully studied to remain lightweight and portable, and to support body parts during long operation. Therefore, the design challenges of the interface are discussed in Chapters 1 and 2 by studying and testing a wearable textile-based exoskeleton and an advanced arm support. To improve the awareness of the operator, information on the state of the drone can be intuitively rendered with haptic feedback. Two types of haptic feedback were implemented in this exoskeleton and analyzed: a cable-driven kinesthetic feedback device for guidance, described in Chapters 3 and 4, and a tactile feedback device made of closed air pouches to render the sensations of flying, described in Chapters 5 and 6.

Publication Note: The material presented in the summary list is adapted from abstracts of the publications mentioned in each section.

Chapter 1, **Wearable: An Upper Body Soft Exoskeleton for Immersive Drone Control**

This chapter presents strategies to address the challenges of a wearable and portable interface. It describes a soft exoskeleton, called FlyJacket, which includes a motion-tracking device to monitor body movements and an arm support system to prevent fatigue. The design considers the efficiency of the force transmission, the comfort of the interface and the freedom of motion, and a steady connection for motion-tracking devices, while remaining portable. A

user study was performed with participants flying a simulated fixed-wing drone to validate the performance of the interface and the teleoperation of a real drone was demonstrated.

The main contributions of Chapter 1 are:

- The development of an upper body soft exoskeleton to control a drone with intuitive body movements.

- The lower performance variance between participants when using the developed exoskeleton regarding to the traditional remote controller.

- The significant reduction in fatigue perception when using the arm support.

- The demonstration of the feasibility of a flight with a real drone.

Chapter 2, **Wearable: A Portable Arm Support to Reduce Muscle Activity During Flight**

The arm support presented in Chapter 1 supports the user's arm but does not fully compensate the shoulder torque at all arm positions. In this chapter, we present an advanced passive arm support that can cover more than 97% of the ROM required to fly with the FlyJacket while being adaptable to 98% of the population and remaining portable. The performance analysis of the arm support is described with a mechanical model and its implementation is validated with both a mechanical characterization and a user study, which measured the flight performance, the shoulder muscle activity and the user acceptance.

The main contributions of Chapter 2 are:

- The development of a passive arm support with better users' morphologies adaptation and gravity compensation along the flight ROM than the arm support presented in Chapter 1.

- The reduction of the muscular activity which induces a better support in shoulder rotation.

Chapter 3, **Kinesthetic Feedback: Guidance with a Soft Exoskeleton to Reduce Error in Drone Teleoperation**

Kinesthetic feedback acts on the position of a body part and can therefore be used to correct gestures. In this chapter, we present the integration of a cable-driven kinesthetic guidance in the FlyJacket. The aim of the device is to apply a force relative to the distance between the drone and a pre-determined trajectory to correct user torso orientation and improve the flight precision. Four different guidance profiles (three linear profiles with different stiffness and one quadratic) were tested.

The main contributions of Chapter 3 are:

10

- The development of a kinesthetic feedback and its integration in the soft exoskeleton.

- The improvement in flight performance induced by the quadratically shaped feedback.

Chapter 4, **Kinesthetic Feedback: Perception and Learning with Cable-Driven Guidance in Exosuit Teleoperation**

This chapter introduces the results of psychophysical and motor learning user studies to assess the effect of cable-driven kinesthetic guidance described in the previous chapter. Experiences to determine the Just Noticeable Difference, the coefficient of the Stevens' Power Law, and the effect of the kinesthetic feedback on motor learning were conducted.

The main contributions of Chapter 4 are:

- The results of the Just Noticeable Difference experience which showed that the perception of force difference on the users' torso scales linearly with the amplitude of the force exerted through the cables.

- The determination of the coefficient of the Stevens' Power Law being close to one which indicated that the perceived force was similar to the magnitude of the stimulus.

- The motor learning study which revealed that the guidance improved user performance in training, but that this improvement was not retained when subjects were evaluated without guidance.

Chapter 5, **Tactile Feedback: Soft Haptic Device to Render the Sensation of Flying like a Drone**

Flight sensation can be recreated through tactile feedback to enhance the flight awareness, realism and immersion. In this chapter, we describe a soft tactile device placed on the torso which provides feedback by compressing a set of closed air pouches against the skin to recreate the sensation of air pressure. A mechanical model and simulation of a pouch device were developed to determine appropriate parameters. A set of pouch devices were constructed and integrated into the soft exoskeleton and their mechanical performance evaluated. The tactile device was also tested in a flight stabilization task.

The main contributions of Chapter 5 are:

- The development of a soft tactile device and its incorporation to the soft exoskeleton.

- The development of a simulated model to test the characteristics of the tactile device.

- The highly similar results between the simulation and the data recorded on the built hardware.

- The results of the flight stabilization task which showed that adding haptic feedback reduced the user's workload and improved their state awareness.

Chapter 6, **Tactile Feedback: Perception of a Wearable Haptic Feedback Device to Render the Sensation of Flight**

In this last chapter, we evaluate the tactile feedback described in the previous chapter with a user study to test whether it can convey useful haptic information to the user and whether the feedback enhances the user experience of flying.

The main contributions of Chapter 6 are:

- The ability of the participants to understand the directional cues without prompting.

- The high accuracy and short time to distinguish directional cues from the tactile device by the participants.

- The improvement in flight realism induced by the tactile device.

1 Wearable: An Upper Body Soft Exoskeleton for Immersive Drone Control

1.1 Introduction

In this first chapter, we introduce a different approach to wearable drone control that attempts to capture the best features of what have been discussed in the introduction of this thesis. In order to have more embodied interaction with drone, an upper body wearable interface to record gestures and send commands to the drone has been designed. Using wearable technology can promote the naturalness and intuitiveness of the control as users directly move their body to map the desired movement of the drone and do not have to learn to handle an external object such as a remote controller. The use a soft, wearable interface enhances user acceptance and portability of the device. Together with a design comprising multiple adjustments to adapt to body morphology variation, these criteria allow a large range of the population to fit in the jacket and promote interaction with drone. The interface consists of a sensorised upper-body soft exoskeleton, coupled with virtual reality (VR) or first-person view goggles that maps torso movements into control instructions for a fixed-wing drone flying at a constant speed and equipped with a frontal camera. The exosuit, which we call FlyJacket, is equipped with unobtrusive and removable arm supports, which allow users to fly with their arms spread out without experiencing fatigue. This jacket integrates sensors for body motion
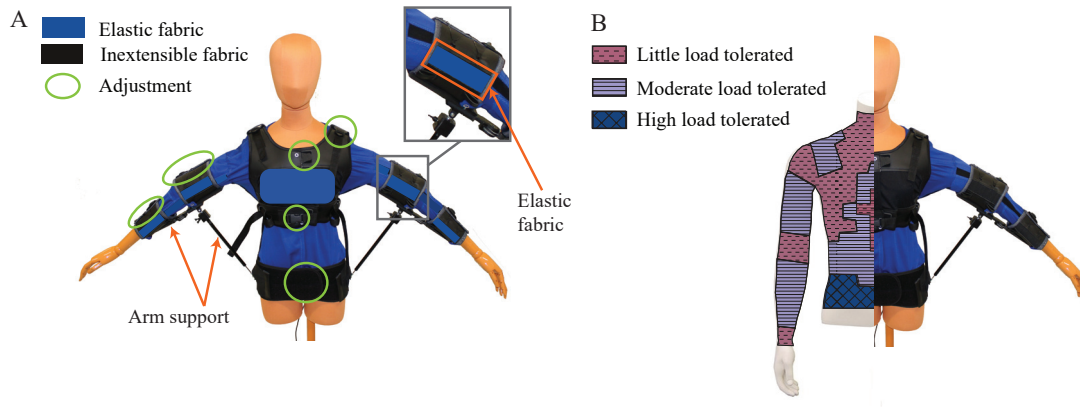
Figure 1.1 – The FlyJacket. A) Front view of the jacket, this view includes a magnification of the upper arm section that contains an elastic segment. For sake of clarity, blue areas indicate elastic fabric in this picture and black areas indicate inextensible fabric. The middle of the chest part and the elastic bands of the upper arm and forearm parts are left in the original black color in the following pictures. B) Comparison of the jacket design with the map of tolerated loads on the upper body (adapted from [23] and [26]).

detection and can easily fit into a backpack for rapid deployment in diverse situations, such as rescue missions, inspection, or personal leisure. For instance, Section 1.4 describes an application for search-and-rescue. The user flies a drone with the jacket and exploits the video feedback to identify points of interest, such as injured persons or hazards, and can tag them to create a georeferenced map for future interventions.

1.2 Exosuit Design

The design of an upper body exosuit for gesture control requires three main challenges to be addressed. The first challenge is to ensure freedom of motion and adaptation to different morphologies and both genders. A second challenge is to efficiently exchange forces between the user and the exosuit which requires a tight interaction to prevent parasitic motions that may deteriorate body motion detection. Also, a tight interaction between the body and the wearable is required to avoid slippage between the skin and the device that may lead to discomfort or injuries. The exchange of forces from the exosuit to the human must be localized in areas of the body that can withstand high pressure. For example, body joints and the chest are very sensitive to pressure, while the arm and the pelvis can be heavily loaded without pain [23, 26]. The third and final challenge is to prevent users' fatigue caused by remaining in unusual or tiring postures for extended periods of time. Other desirable features include a small size and weight of the exosuit, the use of breathable materials to prevent sweating, and a design that allows users to easily put on and remove the exosuit without external aid.

1.2.1 Fabric Design

The first two challenges are addressed by combining a layer made of elastic fabric, shown in blue, with elements of inextensible fabric shown in black in Fig. 1.1 A. The softness and extensibility of the elastic layer, made of sport fabric (100% polyester mesh knit), allow the user's motion freedom and adaptation to different morphologies and genders. In addition, the intrinsic compliance of the soft material can compensate for misalignments between center of rotation of the human and the exoskeleton's joint. Such misalignments are a well-known problem for rigid exoskeletons [77, 78] as even a small mismatch in kinematics can induce a moment on the human body, leading to injuries. As shown in Fig. 1.1, the shoulder joints, elbow joints, a space for breast and the lower part of the torso of the exosuit are made of elastic fabric. This elastic fabric is also breathable and can evacuate sweat during intense flight sessions. The inextensible elements made of leather are connected to the elastic layer with snap buttons. These inextensible elements provide strong anchoring areas to the body as they can be strongly tightened to these regions with adjustments in order to transmit forces without slippage between the body and the exosuit. The inextensible elements are located on the upper torso, the pelvis, the arms and forearms, which are regions that can tolerate moderate to heavy loads (see Fig. 1.1 B) [23, 26]. The inextensible elements are equipped with adjustments, shown by green circles in Fig. 1.1 A and magnified in Fig. 1.2 (A to D), that allow preserving motion freedom and adaptability of the jacket to different morphologies and body dimensions (minimal and maximal dimensions are given in Fig. 1.2). To adjust the tightening at the arm and forearm, cable lacing with a Boa closure system (Boa Technology Inc. Denver, USA) allows adapting their diameter with only one hand (see Fig. 1.2 C and D). The leather parts of the arms possess an elastic segment to allow changes in arm volume due to muscular contraction during motion (see magnification of Fig. 1.1 A). At the upper shoulder and at the middle of the torso tightening can be adapted with an inextensible fabric band and ladder-lock buckles (see Fig. 1.2 A and B). The inextensible chest band is in series with an elastic segment that provides some compliance during change in the torso circumference due to breathing. The middle of the chest is made of elastic fabric to allow extra room for the breast (see Fig. 1.2 B). On the back of the belt there is an elastic pocket to store electronics (see Fig. 1.3 A). Thanks to these adjustments and combination of textile stiffness, the FlyJacket can fit 95 % of the population [79] .

1.2.2 Arm Support

A previous study on naïve individuals showed that torso movements are a natural and immersive way of flying a fixed-wing drone [72]. This study found that drone pitch can be intuitively controlled by bending the torso forward and backward in the sagittal plane and drone roll can be controlled by a combination of bending in the frontal plane and rotation along the longitudinal axis of the torso (see Fig. 1.4 E and F). Even if with this flight style the arms were not used to directly control the drone attitude, during trials we observed that participants instinctively spread out their arms when flying with either the elbows straight (see Fig. 1.3 A)

Body region	Minimum diameter (mm)	Maximum diameter (mm)
Forearm	180	300
Arm	220	360
Torso	680	1100
Hips	730	940*

* additionnal fabric with velcro can increase the maximum diameter
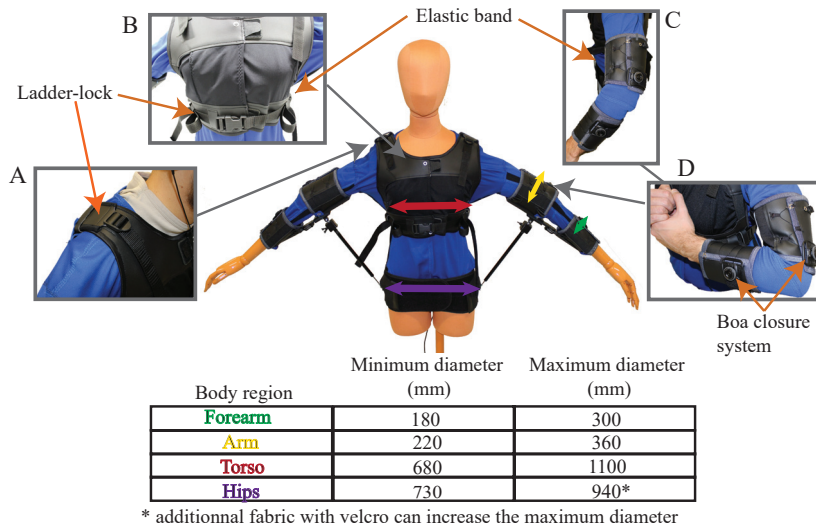
Figure 1.2 – FlyJacket adjustment possibilities and size range at different locations. A) Magnification of the ladder-lock adjustment at the shoulder. B) Magnification of the middle region of the torso part. C) Magnification of the arm extended. D) Magnification of the behavior of the FlyJacket when the arm is bent.

or bent (Fig. 1.3 B). In this position, two forces are acting on the arms: the arm's weight (W_a) which induces adduction, and the forearm's weight (W_f) which also induces adduction and, if the elbow is bent, an internal rotation of the shoulder (Fig. 1.3 B). Keeping this position for extended periods of time is tiring as shoulder muscles must counteract the moments induced by these forces. Therefore, the challenge of keeping the arms in this tiring posture is tackled in the FlyJacket by adding two arm supports that prevent fatigue (see Fig. 1.3). Research on body support has gradually shifted from bulky and heavy multi-joint systems [78, 80] to lightweight and wearable soft devices. Some soft body supports use actuated cables anchored to body segments [19, 81, 82]. However, drawbacks of this approach are the large standoff needed to create sufficient torque and the compressive loads applied to the joints during actuation. Another approach is to use pneumatic pouches [20, 83, 84]. The main disadvantage of pneumatic devices is the need for a compressor for the actuation, which prevents portability. Additionally, support of multiple joints would require a complex design of pouches and valves, which is not practical.

Thus, in the FlyJacket, we chose to use a linear passive gas spring (Eckold AG, Switzerland) between the upper arm and hips (see Fig. 1.3) because this region of the body is the best suited to bear the high forces generated by the arm support [23] (Fig. 1.1 B). The main advantage of the proposed design is that it does not attempt to mimic the shoulder joint anatomy, such as exoskeletons in [66, 54, 80]; resulting in a simpler design without major reductions in the range of motion (ROM). The arm and forearm are supported by two plates made of 3D printed Acrytonitrite Butadiene Styrene (ABS) (see Fig. 1.3 D) with small cushions inside for comfort. These plates are interconnected by two passive joints: a rotating joint made of ball bearings to
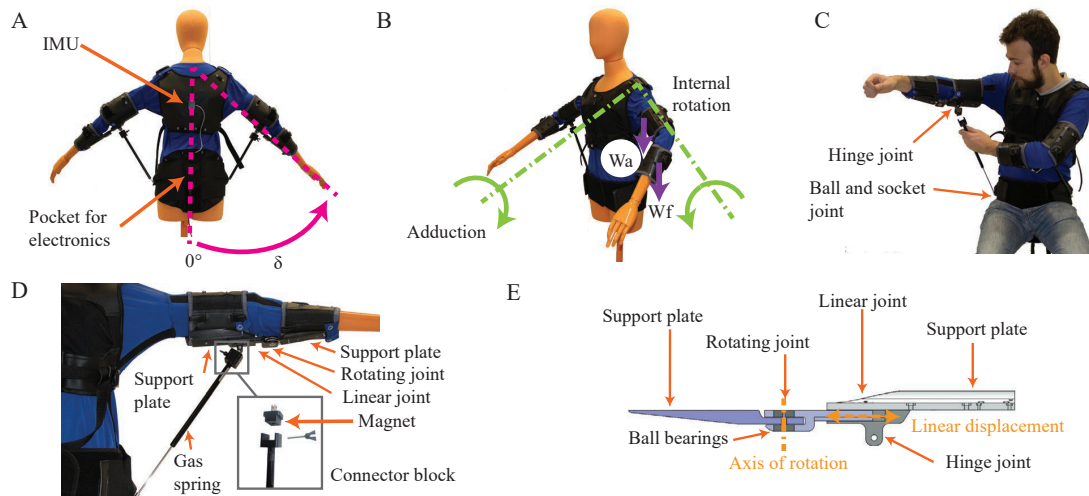
Figure 1.3 – FlyJacket arm support. A) Back view of the jacket. B) Perspective view of the jacket describing the forces and momentum acting on the arm. C) Participant disconnecting the arm support while wearing the FlyJacket. D) Description of the main components that constitute the arm support; this view includes a magnification of the arm support connector block. E) Longitudinal section view of the arm support highlighting the axis of rotation and the linear displacement of the elbow joint.

bend the elbow and a linear joint to absorb misalignments between the center of rotation of the elbow and the rotating joint of the support (see Fig. 1.3 E). The connection between the gas spring and the waist belt is made of a ball and socket joint (Fig. 1.3 C). The connection to the arm plates consists of a hinge joint. This solution allows resisting to the internal shoulder rotation induced by the forearm's weight therefore preventing fatigue (see Fig. 1.3 B). The ROM in shoulder internal rotation is almost fully constrained in order to provide shoulder support, but still giving the possibility to the user to put and remove the VR goggles by themselves. ROM in adduction/abduction movement is limited in order to support the arm's weight in resting position (δ = 40°, Fig. 1.3 A) and because of the limited length of the gas spring (δ = 120°). The arm support plates can be easily disconnected from the gas springs, thanks to a connector made of magnets that facilitate the placement of the gas spring. This support is secured by a screw to resist strong acceleration (see magnification in Fig. 1.3 D). Gas spring supports can be entirely removed from the jacket if the user prefers to use another flight style, for example with the arms along the body. Although the gas spring used in the experiments described here is passive and calibrated to provide arm buoyancy, the same design could be actuated by a linear motor to provide haptic feedback from the drone wings to the arm level.

1.2.3 Movement Tracking System

The full movement recording system is composed of a Transmission Unit to send commands to the drone, a Microcontroller Unit (MCU, STM32F100, STMicroelectronics, Geneva, Switzer-
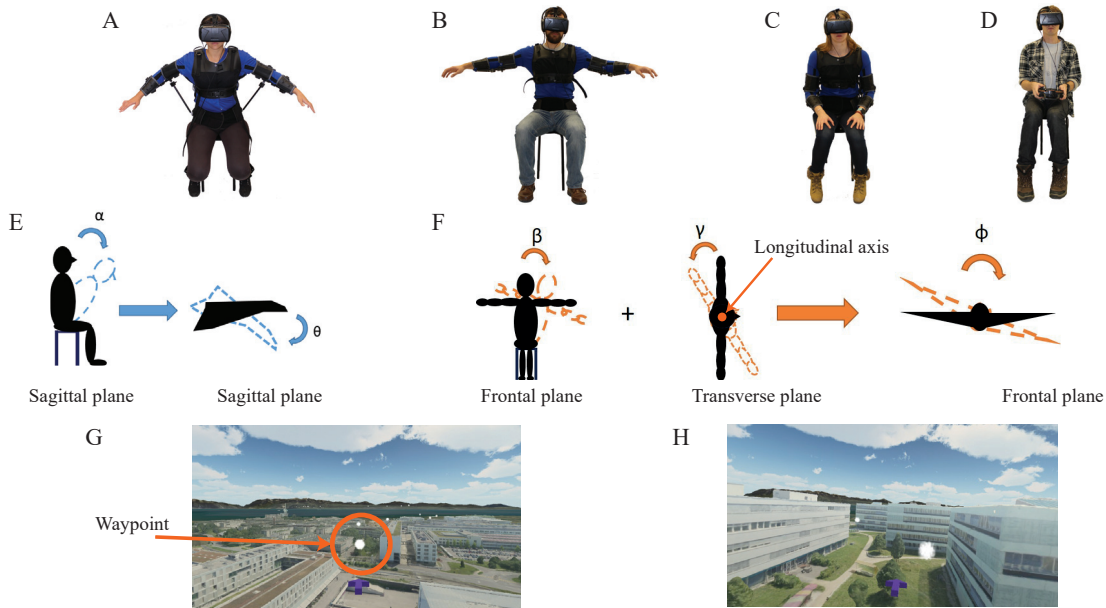
Figure 1.4 – Experimental setup. A) Body position and setup for the condition "Arms / Support" (AS). B) Body position and setup for the condition "Arms / No support" (ANS). C) Body position and setup for the condition "No arms" (NA). D) Body position and setup for the condition "Remote controller" (RC). E) Movement mapping between the torso bending angle (α) in the sagittal plane and the drone to control the drone's pitch (θ). F) Movement mapping between the combination of the torso bending angle (β) in the frontal plane and the rotation (γ) along the body longitudinal axis and the drone to control the drone's roll (ϕ). G) Flight environment for the task in open environment displaying waypoints. H) Flight environment for the task in cluttered environment.

land) for real-time processing located in the electronics pocket, and an Inertial Measurement Unit (IMU) (LSM9DS1, STMicroelectronics) located on the back of the leather element on the upper torso (Fig. 1.3 A). The IMU is connected to the MCU via a Serial Peripheral Interface (SPI). The IMU records the motion and the MCU processes in real-time this information to send posture commands to the simulated drone on the PC or to a real drone. Then, the steady connection offered by the leather element that supports the IMU enables precise tracking of torso motion without interference from motion of other body parts, such as the arms. For this first study on the FlyJacket, a simple flight style using only the torso to control a drone was used. However, other flight styles can be implemented and additional IMUs can be inserted on the inextensible element on the upper arms, forearms or pelvis to record the motion of these body parts.

1.3 Experimental Validation

In order to assess the exosuit for drone control and the effectiveness of the arm support system, 32 participants (25 men and 7 women, age 27.3 ± 5.9 years; mean ± SD) controlled

a simulated fixed-wing drone either with torso movements wearing the FlyJacket, or with a remote controller (Hobbyking 6CH RC Flight Simulator System, Hobbyking, Kwun-Tong, Hong Kong). In both cases, they used VR googles (Oculus Rift Development Kit 2, Oculus VR, Menlo Park, USA).

Each participant performed the experiment under only one flying condition. 24 participants used the FlyJacket in one of the three following conditions (8 participants per condition): arms spread out with arm support (condition "Arms \ Support" (AS), Fig. 1.4 A), arms spread out without arm support (condition "Arms \ No Support" (ANS), Fig. 1.4 B), arms along the body (condition "No arms" (NA), Fig. 1.4 C). In the condition of NA, the participants were asked to place the palm of their hands on their thighs in whichever position they found most comfortable. For these three conditions, participants were using the flight style reported in [25], where torso movements are mapped into pitch and roll input for the drone as illustrated in Fig. 1.4 E and F. To prevent any Euler angles singularities and also dangerous movements for the user, the maximum angles of the drone in the simulator have been bound to $\pm 85°$ for both the pitch and the roll maneuvers. The orientation of the pilot's trunk is computed with a gradient descent algorithm implemented in the MCU based on the measurements of the IMU located in the middle of the upper back (see Fig. 1.3 A). Such an estimation method was selected for its performance and ability to operate at low sampling rates, which significantly reduces the power consumption [85]. Since the body movement dynamic is low, the gradient descent algorithm was run at a frequency of 20 Hz, which in pilot experiments proved to be a reasonable compromise between tracking accuracy and power consumption. Within these conditions, the static RMS error of the IMU was less than 2° and the dynamic RMS error less than 7°. Moreover, we performed tests at various sampling rates and no differences were identified between them.

For a control experiment, 8 participants controlled the simulated drone with a conventional remote controller (condition "Remote Controller" (RC), Fig. 1.4 D). Pitch and roll were controlled by moving the joystick up and down, and left and right, respectively.

All participants flew a drone in a simulator developed in Unity3D (Unity Technologies, San Francisco, CA, USA). The simulator physics is based on the eBee, a fixed-wing drone developed by SenseFly (Parrot Group, Paris, France), flying at a constant cruise speed of $12 \frac{m}{s}$. This is the nominal speed of drones during imaging and mapping tasks.

Half of the participants had no prior experience with simulated or real aircraft flying operations. After statistical analysis, no correlations were found between the prior experience on flying a simulated or real aircraft and the performance of the participants in any conditions. Also, participant level of expertise in between conditions was statistically the same. The same analysis was done with the number of hours of computer gaming and the same results were found. During the tasks, participant's performance was evaluated when flying through waypoints represented by small clouds (see Fig. 1.4 G and H). These waypoints were forming a trajectory in the sky and disappeared when they were reached. The waypoints sequence

was randomized, but the number of maneuvers (up/down/right/left) was the same for every task. This evaluation was preceded by a training period composed of two tasks. At first, they had to follow the direction of an arrow positioned in front of them. The arrow was pointing consecutively "right", "left", "up", and "down" twice. The goal of this task, which lasted one minute, was to make the participants perform every flight control movement at least once. The second task was one and a half minutes of free flight in a 3D reconstruction of our campus. The goal of the training was to enable the participant to feel comfortable with the control of the flight. After the short training period, participants performed two evaluation tasks where they had to reach 34 waypoints positioned at high altitude ("open environment", Fig. 1.4 G) and then 34 waypoints positioned between buildings ("cluttered environment", Fig. 1.4 H). The second task aimed to be more stressful and required sharper changes of direction as participants had to avoid buildings. An arrow pointing toward the next waypoint to reach is used to help the participant.

To compute the performance, the distance between the center of the waypoint and the point where the trajectory of the drone crosses a plane drawn perpendicular to the line connecting the previous and next waypoint is recorded for the 34 waypoints [67]. Performance per participant is computed as the Root Mean Square (RMS) of this distance over the 34 waypoints of a task.

At the end of the experiment, participants filled out a questionnaire about comfort and immersiveness. Questions were asked in the form of a Likert scale (an example is given in Fig. 1.6 A). To compare performance and questionnaire answers between conditions, a Wilcoxon Rank Sum test was performed and, in order to analyze the variance difference between conditions, an F-test for equal variances was performed. All calculations done in this study, including statistical analysis and correlation, were computed in MATLAB (MathWorks, Massachusetts, USA). The EPFL Institutional Review Board procedures approved the study and the participants provided written informed consent.

1.3.1 Flight Control Performance

No significant difference in flight performance was found between the conditions with the exosuit and the condition with the remote controller, for tasks in both the open environment (see Fig. 1.5 A) and the cluttered environment (see Fig. 1.5 C). These results suggest that the exosuit design and control strategy were comparable to a conventional remote controller. The higher overall RMS error for all conditions in the cluttered environment task with respect to the open environment is suggestive that it is a more difficult task.

However, significant differences were found in both tasks for the three exosuit conditions: in the open environment task, NA condition was significantly worse than the AS condition ($p = 0.021$), and in the cluttered environment, the NA condition was significantly worse than both AS ($p = 0.021$) and ANS ($p = 0.049$) conditions. These results suggest that subjects were more accurate in controlling the drone with the torso motion when the arms were spread out.
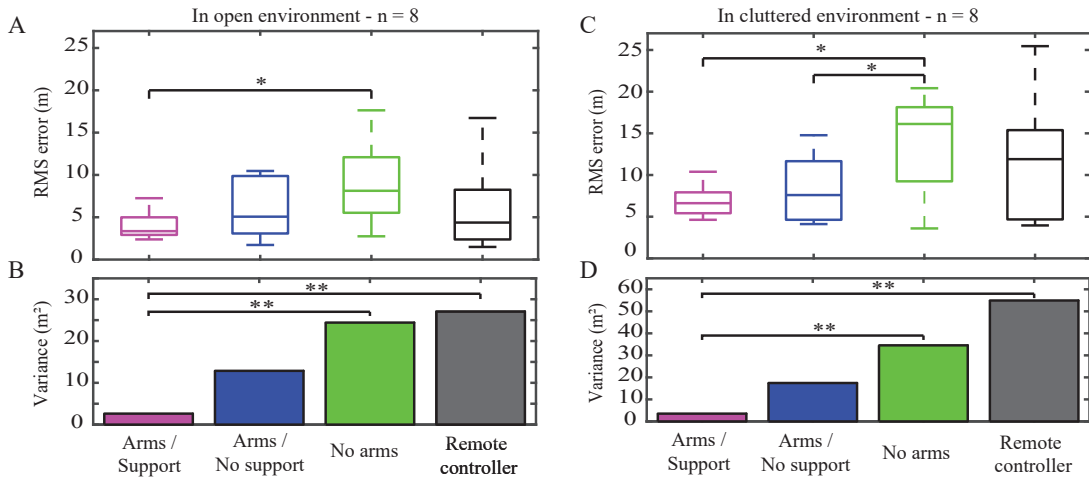
Figure 1.5 – Performance results. A) RMS error for the task in open environment. B) Variance of the RMS error for the task in open environment. C) RMS error for the task in cluttered environment. D) Variance of the RMS error for the task in cluttered environment. (*) denotes $p < 0.05$ and a double asterisk (**) denotes $p < 0.01$.

Furthermore, the performance variance was significantly larger in the RC condition than in the AS condition in both the open environment task ($p = 0.006$, Fig. 1.5 B) and in the cluttered environment task ($p = 0.002$, Fig. 1.5 D). This suggests that some subjects had more difficulty in piloting the drone with the remote controller than with the exosuit with the arm support. The same observation can be made when comparing the performance variance of the NA condition that is significantly larger than AS condition both in open environment ($p = 0.009$, Fig. 1.5 B) and cluttered environment ($p = 0.008$, Fig. 1.5 D).

1.3.2 Questionnaire Results

At the end of the flight sessions, participants had to fill a questionnaire where they rated on a Likert scale (from 1 to 7) how strongly they agreed with a set of statements (an example is shown in Fig. 1.6 A). These are displayed on top of each sub figure B to F of Fig. 1.6. The statements were measuring the subjective feeling of the participant regarding the proposed gesture controls (Fig. 1.6 B, C and D) and their physical comfort (Fig. 1.6 E and F).

Significant differences for the gesture control were found between the condition using the exosuit with the arms spread out (conditions AS and ANS) and the RC. Participants felt better control over the flight trajectory in the condition AS than with the RC ($p = 0.009$, Fig. 1.6 B). Significant differences were also found in the kind of gesture proposed; both AS and ANS conditions have significantly better rating than the RC condition, as shown in Fig. 1.6 C ($p = 0.002$ between AS and RC, and $p = 0.001$ between ANS and RC) and Fig. 1.6 D ($p = 0.015$ between AS and RC, and $p = 0.012$ between ANS and RC). In addition, participants would use the flight gestures with the arm spread out more than with the arms along the body (Fig. 1.6 C,

21
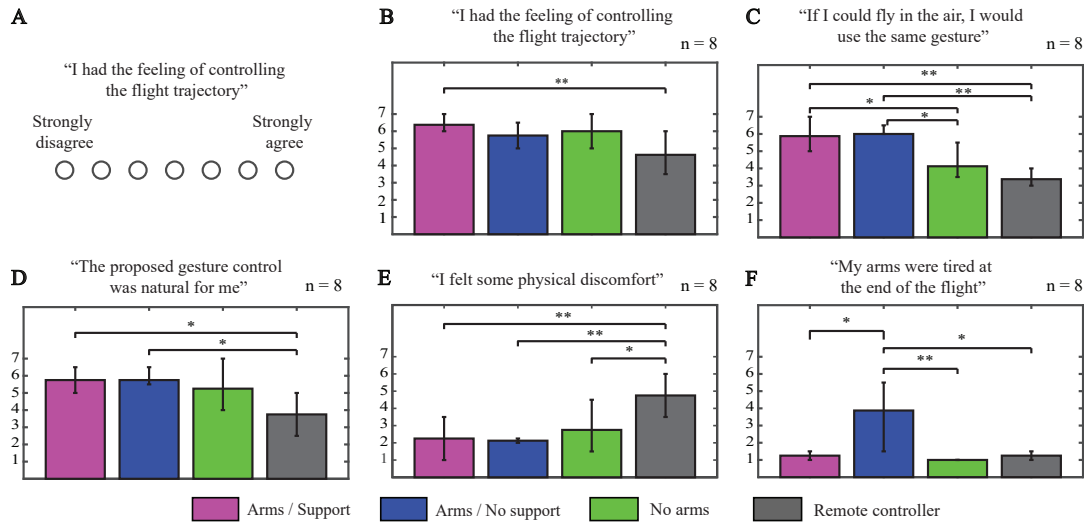
Figure 1.6 – Questionnaire results. A) Example of the Likert scale questionnaire. B-F) Questionnaire results, statements are shown on top of each graphs. (*) denotes $p < 0.05$ and a double asterisk (**) denotes $p < 0.01$.

$p = 0.034$ between AS and NA, and $p = 0.018$ between ANS and NA).

Regarding the physical comfort, participants rated a significantly higher discomfort with the remote controller than with all the flight conditions using the exosuit (Fig. 1.6 E, $p = 0.009$ between AS and RC, $p = 0.001$ between ANS and RC and $p = 0.021$ between NA and RC). Participants felt more arm fatigue when flying in the condition ANS than all three other conditions (Fig. 1.6 F, $p = 0.023$ between ANS and AS, $p = 0.007$ between ANS and NA and $p = 0.023$ between ANS and RC). However, they felt the same level of arm fatigue between conditions AS than NA and RC.

1.4 Flying with Real Drones

The FlyJacket was also tested for the teleoperation of a real drone. The flight was performed with a quadcopter (Bebop 2, Parrot Drones, Paris, France) mimicking the flight dynamic of a fixed-wing drone (see details of the control in [34]). The drone can stream real-time video feedback to the goggles of the user. The test simulates a search-and-rescue mission where the user operates a drone to geotag points of interest, for example injured people or dangerous areas. These points of interest will subsequently populate a map that can facilitate the planning of the intervention. In the test, the user was wearing the FlyJacket with the arm support and a smart glove capable to detect predefined finger gestures through capacitive sensors placed on each finger and on the palm (see Fig. 1.7 A and B. For example, setting a point of interest is triggered by pressing the middle or the ring finger against the thumb depending on the point category. The glove can be also used to send high level commands to the drone, for example automatic take-off, landing and return home. The trajectory of the
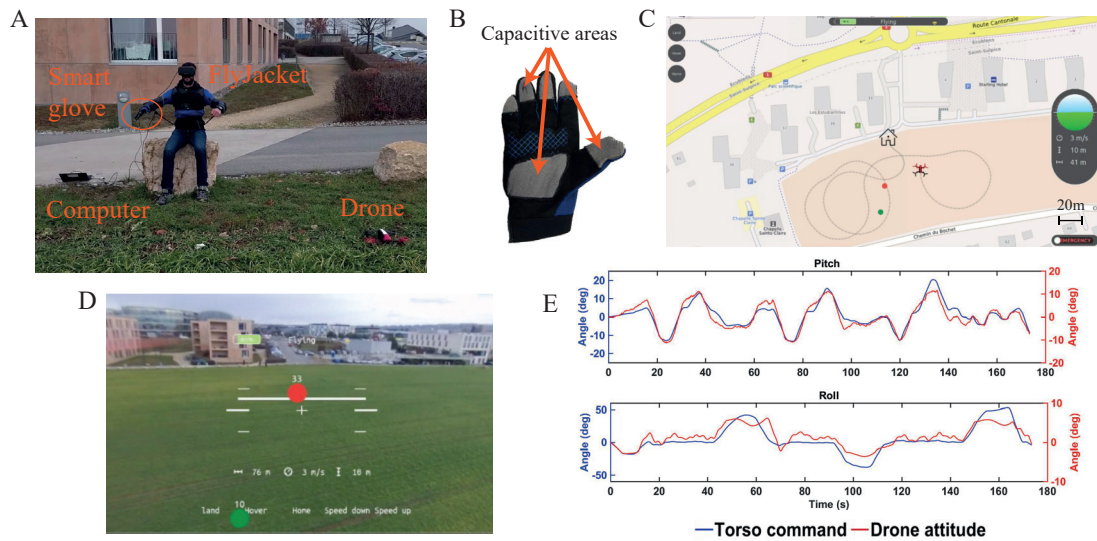
Figure 1.7 – Real teleoperation of a drone. A) User and setup. B) Smart glove with capacitive sensors. C) Map and drone route. D) View from the head mounted display. E) Logs of the flight.

drone can be followed on a computer (see Fig. 1.7 C). Red and green dots are points of interest set by the user during the flight. Different colors can be used to describe the nature of the recorded point, for example, in the simulated rescue mission, green for injured people to be rescued and red for dangerous areas. The point of interest appears in the center of the field of view of the drone (white cross in Fig. 1.7 D). The numbers above the recorded points indicate the estimated distance between the point and the drone in meters. Points of interests can be added and removed from the flight directly during the flight. Fig. 1.7 E shows the log of the torso body movements and the corresponding response of the drone orientation for both pitch and roll.

1.5 Conclusion

The presented exosuit, the FlyJacket, addresses the challenges of controlling a fixed-wing drone in a natural and immersive way while being portable and fitting various morphologies. The whole system can easily fit in a backpack and be transported in the field. A simple but efficient arm support prevents arm fatigue without reducing user's performance. Indeed, experimental results demonstrate that participants found the jacket comfortable, natural and intuitive, and were able to easily control a simulated drone with it. The level of discomfort was very low and participants used the free comments section of the questionnaire to report that they only felt dizziness due to the VR goggles, a well-known problem [35], which is not caused by the exosuit.

The flight performance of the exosuit is comparable to a remote controller. However, the

performance variation across the participants is significantly smaller when using the exosuit with the arm support in both open and cluttered environments. These results show that all participants could reach a low RMS error using the exosuit with the arm support unlike participants using the remote controller. A possible explanation for the significantly lower performance variance when users pilot with the torso, is that the visual feedback, that is present also while flying with the remote controller, is complemented by the vestibular and somatosensory feedbacks that have a direct correlation with the attitude of the drone [86].

In addition, the use of the exosuit with the arms spread out is preferred by the participants, and in general they find this control more natural than flying with the remote controller. They also have greater feeling of controlling the trajectory. Moreover, participants reported in the questionnaire significantly less physical discomfort using the FlyJacket than the remote controller. This difference is caused by a higher level of dizziness felt when flying using the remote controller. We hypothesize that, as the participant's body stays static when using the remote controller, the sensation of motion sickness due to the VR goggles is intensified (as suggested also in [87]).

When comparing the different flight styles of the exosuit, the RMS error is significantly higher when flying with the arms along the body than when flying with the arm spread out with the arms support. The median of the RMS error is also higher than for all other flight conditions. The error difference is even greater when participants fly in a cluttered, and therefore more stressful, environment in which more precise manoeuvers are required. One possible explanation is that participants had difficulties performing precise maneuvers with their arms along their body, while having their arms spread out would allow them finer control of the rotation of their torso. This could be explained by the fact that small torso rotations correspond to large displacements of the arm extremities, which could improve proprioception [88]. Also, one can use the arms for reactive inertial torque. In addition, regarding the questionnaire results, both flight styles with the arms spread out are preferred by participants.

There were no significant differences in participants' performance and feeling when having the arm support or not. Moreover, performance is not prevented by the support and it does not induce any discomfort. The only difference is that the feeling of arm fatigue is significantly higher when flying with the arms spread out and no support than for all other flight conditions. The same low level of fatigue was perceived by the participants flying with the arm support as the one flying with the arms along the body.

Finally, the FlyJacket has been demonstrated for the teleoperation of a real drone. The user performed a survey flight to locate points of interest on the ground. As the exosuit leaves the hands free, the user can easily grasp objects such as the head mounted display when setting up the device. Finally, the free hands allow to exploit hand-held devices in order to perform complementary tasks such as geotagging points of interests or sending high level commands to the drone.

2 Wearable: A Portable Arm Support to Reduce Muscle Activity During Flight

---

Publication Note: The material presented in this chapter is adapted from:

- C. Rognon, L. Grossen, S. Mintchev, J. Miehlbradt, S. Micera and D. Floreano. *"A Portable and Passive Gravity Compensation Arm Support for Drone Teleoperation"*, in preparation.

The two first authors contributed equally to this work. C. Rognon supervised the design and development of the arm support, performed the user study together with J. Miehlbradt, analyzed the results and wrote the manuscript. L. Grossen designed and developed the arm support, performed the mechanical characterization, and contributed to write the manuscript.

2.1 Introduction

In the previous chapter, a simple passive arm support composed of a gas spring placed between the waist and the upper arm was integrated in the FlyJacket to prevent arm fatigue. Results showed that the sensation of fatigue felt by the user was significantly reduced. However, the gravity compensation was poor, the arm range of motion (ROM) was limited and no tunings were available to adapt to different users' morphologies.

As one of the envisaged applications of the FlyJacket is search-and-rescue, the arm support is required to allow the ROM necessary to perform the task while remaining portable to enable deployability in the field. Portable arm supports in the form of exoskeletons have been developed for human power enhancement [89] or to help workers in their tasks [90, 91, 92]. Ekso Bionics (Richmond, CA, USA) even commercialized an upper body exoskeleton for fatigue reduction during overhead manufacturing, assembly, and construction. Research has also focused on exoskeletons for shoulder support in the frame of rehabilitation [93, 80]. These devices have the advantage to be portable, enabling the patient to perform daily life activity

at home. To enhance user acceptance, compliance to the body, and safety, soft exoskeletons have been in the focus of recent work [82, 84, 20, 94, 95]. Pneumatically actuated arm supports allow a safe interaction with the human body due to their intrinsic compliance. Yet, to be actuated they require a compressor which limits the portability. Soft supports (i.e. pneumatic or cable-driven exoskeleton) are compliant and usually more lightweight than rigid structures but their efficiency and force transmission are significantly lower.

In this chapter, we present an advanced arm support – called Static Balancing Support (SBS) – that can cover more than 97% of the ROM required to fly with the FlyJacket while being adaptable to 98% of the population and remaining portable. First, the device's design was studied. Its effectiveness was simulated along the flight ROM and compared with the arm support described in Chapter 1, called Gas Spring Support (GSS). Then, the built SBS device performances were characterized mechanically and with a user study. For the mechanical characterization, the output torque of the SBS was measured and compared with the torque induced by the arm weight. For the user study, twelve participants performed a flight task with three different arm support conditions – SBS, GSS, and No Support (NS) – and their performance and shoulder muscle activity were compared.

2.2 Analysis of the Requirements

The arm support is conceived as a separate module that can be added to the existing FlyJacket. The function of the device is to compensate the arm weight while remaining transparent to the user. For this purpose, the arm support should fulfill three main requirements: (i) it should balance the weight for every pose assumed by the arm during operation, (ii) its workspace should be compatible with the user ROM during operation, and (ii) its structure and balancing strength should adapt to different users' morphologies, in particular different upper body lengths and arms weights.

The ROM of the user during the flight is produced by two joint angles; the waist joint and the shoulder joint (see Fig. 2.1). Although sagittal bending of the torso uses the hip joint while the lateral bending uses the lumbosacral joints, we approximated for simplification that both joints are collocated. The required ROM of these two joints are based on the data collected directly during the user studies of Chapter 1 and of [72], and are summarized in Table 2.1. They include all angles recorded during these two user studies. However, not all angle combinations have been observed and participants most of the time used smaller joint angles. The zero position ($\alpha = 0°$) for the shoulder corresponds to the arm position at 90° regarding to the torso. The ROM relative to each body dimension can be calculated with Eq. A.5 and A.6 (see Appendix A). An example of arm ROM is illustrated by the purple region in Fig. 2.1.

In order to allow access to this technology for a wide range of people, the arm support should be adaptable to different body morphologies. As a requirement, the device is modelled based on body dimensions from the 1st percentile female, hereafter denoted as "1PF", until the 99th percentile male, denoted "99PM", size and body mass of the US population [96] and [97].

Table 2.1 – Range of Motion Used During Flight

Body Movement	Angle (°)	
	Min	Max
Torso flexion / extension	-30	40
Torso lateral	-20	20
Torso twist	-60	60
Shoulder abduction	-60	5
Shoulder flexion	-40	0
Shoulder rotation	-5	5

Table 2.2 – Body Dimensions for the 1st Percentile Female and the 99th Percentile Male

Body Parts	1st Percentile Female	99th Percentile Male
Total arm mass A_m (kg)	1.86	6.56
Upper arm length L_a (m)	0.234	0.312
Upper trunk height U_{th} (m)	0.269	0.353
Lower trunk height L_{th} (m)	0.213	0.265
Half chest width C_w (m)	0.138	0.203
Half hip width H_w (m)	0.142	0.214

See Fig. A.1 in the Appendix A for the location of the dimensions

Using these data, the device would fit 98% of the population. The dimensions for the upper body are summarized in Table 2.2.

2.3 Design and Working Principle

The arm support presented in this chapter is composed of an articulated mechanism that can follow the upper body gestures of the user, and an elastic element to passively balance the arm weight. The mechanism consists of an arm and a torso segment connected with a revolute joint (see Fig. 2.1). The arm segment is fixed on the upper arm just before the elbow joint, and the torso segment is connected on the hip where the arm weight is redirected. The hip has a higher load tolerance comparing to other parts of the upper body, which makes it a good fixation point to redirect the load [23].

To fulfill the first requirement, the arm support exploits a gravity compensation strategy known as static balancing [98]. A spring integrated in the torso segment generates a force to balance the arm weight (W). The spring force is transmitted to the arm segment by a cable with a lever arm Δs. The result is a torque (Γ) that rotates the arm segment upward balancing the arm weight at any position within the workspace of the mechanism (Requirement i). Differently to active balancing exoskeletons with electric or pneumatic motors, static balancing is implemented with passive mechanisms that do not require any source of energy. This solution minimizes the bulkiness of the device and foster portability by decreasing dependency from power sources.
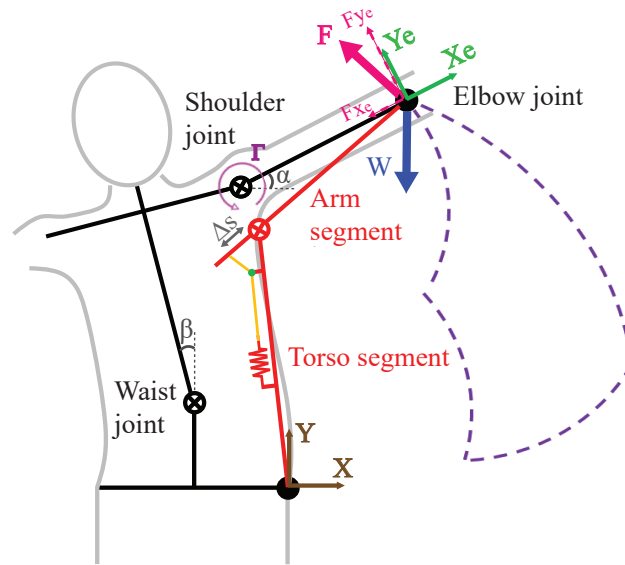
Figure 2.1 – Schema of the Static Balancing Support (SBS) and the induced forces and torque. Two different coordinate systems are used: The XY coordinate system for the positions and the $X_e Y_e$ coordinate system for the force projections. The force generated by the mechanism can be decomposed in two components in the $X_e Y_e$ coordinate system: the gravity compensation contribution on Y_e and the parasitic forces in the arm on X_e. Example of ROM domain is shown in purple dashed line.

The kinematics of the arm support are designed to minimize the mismatches between the mechanism workspace and the user ROM (Requirement ii). This result is achieved by integrating a revolute joint between the arm segment and the upper arm, and a spherical joint to connect the torso segment to the hip. The combination of these joints allows to accommodate the majority of the body movements described in Table 2.1.

Requirement iii is fulfilled by the possibility to adjust the length of the arm and hip segments, and the lever arm Δs of the spring to match different user morphologies and arm weights respectively.

2.3.1 Performance Analysis

The performance of the arm support, in particular its balancing efficacy, undesired parasitic effects, and workspace, have been simulated using MATLAB according to the analytical model presented in the Appendix A. To evaluate the balancing efficacy and the undesired parasitic effects it is convenient to consider the balancing force F generated by the arm support at its attachment point near the elbow (see Fig. 2.1). This force can be projected in the local refence frame $XeYe$ and decomposed in two components: the gravity compensation contribution (F_{ye}) that is responsible for the balancing torque Γ that limits user fatigue, and a parasitic force (F_{xe}) directed along the arm, which produces an undesired sliding motion of the fixation of

Figure 2.2 – Normalized torque error ($T_{errV.norm}$) over the reachable ROM. A) For the SBS for the 1PF. B) For the SBS for the 99PM. C) For the GSS for the 1PF. D) For the GSS for the 99PM.

the arm support along the arm of the user. The balancing efficacy can be quantified with the torque error normalized by the arm weight:

$$T_{errV.norm} = \frac{F_{errY_e} \cdot L_a}{A_m} \tag{2.1}$$

while a measure of the undesired parasitic effect is the force along X_e normalized by the arm weight:

$$F_{X_e,norm} = \frac{F_{X_e}}{A_m} \tag{2.2}$$

with the variables described in Table 2.2 and in the Appendix A.

Fig. 2.2 shows the results for the normalized torque error ($T_{errV.norm}$) for both the Static Balancing Support (SBS) (Fig. 2.2 A for the 1PF and B for the 99PM) and the Gas Spring Support (GSS) (Fig. 2.2 C for the 1PF and D for the 99PM) within the flight ROM. We can observe that with the SBS, almost the entire ROM can be reached (98.2% for the 1PF and 97.8% for the 99PM) with the exception of the very bottom region. Indeed, the user cannot abduct their arm at -65° if they are bending their torso at 20° on the same side. However, this ROM is rarely performed by the participant during the flight. On the other hand, when using the GSS, the user can reach only a sub-portion of the ROM required for the flight (58.4% for the 1PF and 24.4% for the 99PM).

For the SBS, the normalized torque error ($T_{errV.norm}$) is relatively uniform and small along the ROM with a mean value of -0.005 $\frac{Nm}{kg}$ for the 1PF and -0.002 $\frac{Nm}{kg}$ for the 99PM over the ROM and a maximum of -0.024 $\frac{Nm}{kg}$ and -0.101 $\frac{Nm}{kg}$ respectively, at the lower part of the ROM. For
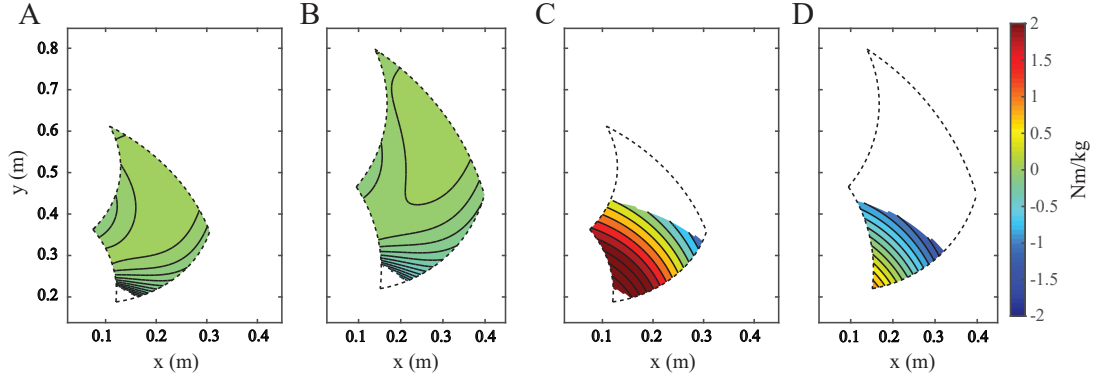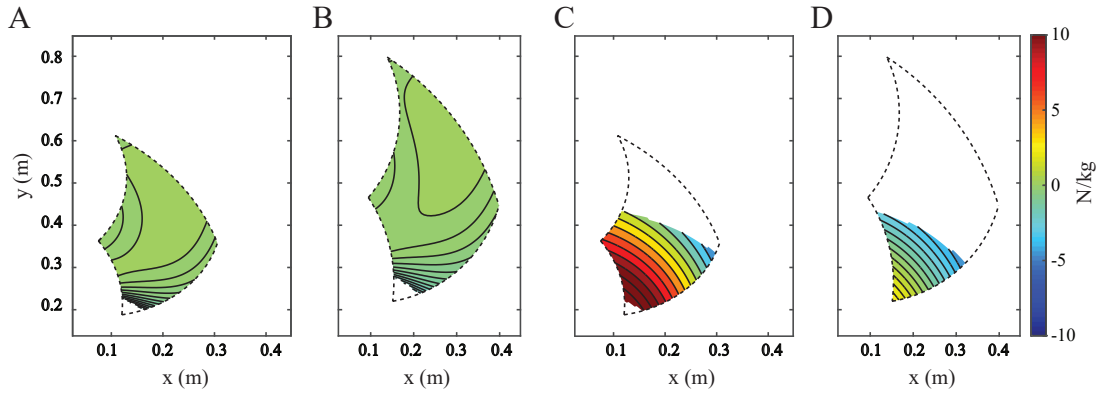
Figure 2.3 – Normalized parasitic force ($F_{X_e,norm}$) over the reachable ROM. A) For the SBS for the 1PF. B) For the SBS for the 99PM. C) For the GSS for the 1PF. D) For the GSS for the 99PM.

the GSS, the normalized torque error is more important with a mean value more than 130 times higher for the 1PF (0.684 $\frac{Nm}{kg}$) and 30 times for the 99PM (-0.058 $\frac{Nm}{kg}$) and a maximum of 1.915 $\frac{Nm}{kg}$ and -1.411 $\frac{Nm}{kg}$ respectively. The normalized torque error of the GSS fluctuates considerably with the arm movement.

The normalized parasitic force ($F_{X_e,norm}$) is shown in Fig. 2.3 A (1PF) and B (99PM) for the SBS, and C (1PF) and D (99PM) for the GSS. The parasitic force is considerably smaller for the SBS with a mean of -0.025 $\frac{N}{kg}$ for 1PF and -0.009 $\frac{N}{kg}$ for 99PM and a maximum value of -1.026 $\frac{N}{kg}$ and -0.325 $\frac{N}{kg}$ respectively ROM on the opposite to 2.922 $\frac{N}{kg}$ (1PF) and -0.187 $\frac{N}{kg}$ (99PM) for the GSS with maximum normalized parasitic forces of 8.184 $\frac{N}{kg}$ (1PF) and -0.677 $\frac{N}{kg}$ (99PM).

Both the normalized torque error ($T_{errV.norm}$) and the normalized parasitic force ($F_{X_e,norm}$) of the GSS show iso-lines oriented parallel to the torso movement, which signifies that the compensation is not notably influenced by lateral movement of the torso but by the arm angle, which changes significantly both the normalized torque error and the normalized parasitic force.

To avoid any singularity problems, the angle between the two segments cannot go out of the -80° to 80° range (0° corresponding to the arm at a right angle). If the mechanism is not constrained in this range, singularities are appearing. As a side note, the ROM of the arm segment (-80° to 80°) is larger than the ROM of the arm (-60° to 5°) as it allows combination of both arm abduction and waist bending.

2.4 Implementation

The built mechanism is shown in Fig. 2.4. The articulation linking both the arm and the torso segments is a revolve joint made of a bearing (3200 A-2RS1TN9/MT33, SKF, Sweden) for less friction. This articulation is sized to sustain a torque (Γ_p) of 10 Nm in the sagittal plane, which
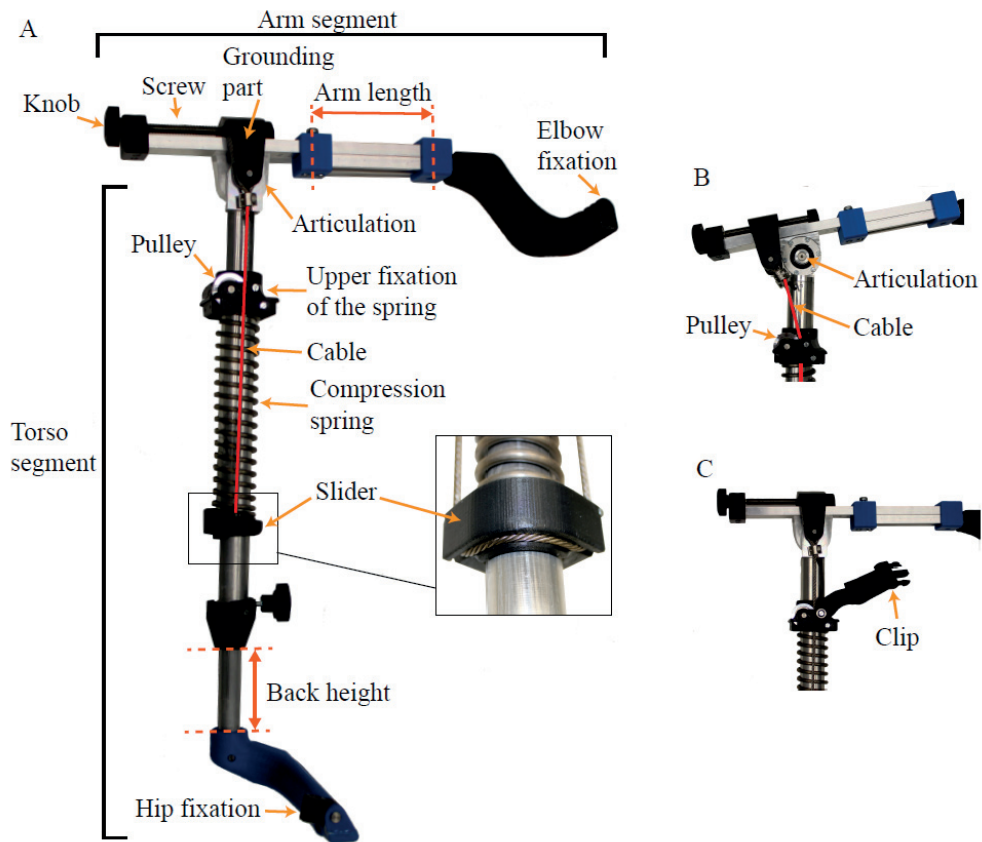
Figure 2.4 – A) Full device with an inset showing the turning point of the cable. B) Grounding part shifted showing the cable angle and the bearing of the articulation. C) Clip to maintain the device close to the torso. Cables are highlighted in red.

happens when the maximal arm mass, i.e. 6.56 kg, is at an out of lateral plane distance of 150 mm. This torque corresponds to the offset of the arm regarding to the device, i.e. the body and the device are not located on the same lateral plane (see Fig. 2.8 E).

A compression spring (Ressorts du Leman Sarl, Switzerland) is generating the balancing force (Fig. 2.4). Compression springs were prefered over tension springs as, in most cases, they produce more force for the same dimensions and they do not need to be preloaded. The compression spring is guided by the torso segment to avoid risk of buckling and is fixed at its upper extremity. The lower extremity of the spring is attached to a slider, which transfers its linear motion to a cable (three millimetres steel, Jakob AG, Switzerland, highlighted in red in Fig. 2.4 A and B). The cable is turning in a groove around the slider (see inset of Fig. 2.4 A), allowing to balance its tension to each side of the spring. The robustness of this slider was assessed by running a finite element simulations using SolidWorks to ensure that it could sustain the full load of the spring (up to 600 N). At its extremities, the cable is attached to a grounding part. This part can be shifted along a screw (M10 x 1.5) with the help of a knob located at the extremity of the arm segment (see Fig. 2.4). Thus, the tension in the cable

can be changed and the force of the gravity compensation can be adapted to each user. Ten millimeters of the grounding part course corresponds to one kg of arm mass compensation for the largest arm length (0.312 m). When the grounding part is aligned with the articulation as in Fig. 2.4 A, the torque compensation of the system is null. The redirection of the cables is done with pulleys mounted on bearings (626-2Z, SKF, Sweden) for less friction. To prevent the unwanted rotation of the grounding part in case of unequal tension in both cables, it is linearly guided by the screw, mounted on plain bearings for less friction, and by the linear profile of the arm segment.

Two distances (arm length and back height) can be adapted regarding the user's morphology (see location in Fig. 2.4 A). The device is fixed to the hip using a plate attached to the waist belt of the FlyJacket (see Fig. 2.8 C). As the entire load of the arm is redirected toward this fixation point, its dimensions (0.11 x 0.07 m) were designed to have a large force distribution area, reducing the risk of pain. The link between the device and this hip plate is made through a three degrees of freedom (DOF) joint made from two plain bearings to insure a low friction in the joint. To remove the arm support from the FlyJacket, it can be disconnected from the hip plate using a pin. The device was linked to the upper arm support using a hinge joint similar as previously used in the Gas Spring Support (GSS) (see Chapter 1). A special care was given in the design of these two fixation points to avoid contact between the device and the body, which would reduce the ROM and may injure the user. An additional attachment point was set to the FlyJacket with a clip between the upper fixation of the spring and the top of the shoulder to maintain the device close to the torso (Fig. 2.4 C and Fig. 2.8 A).

To avoid any injuries due to the compression spring (such as having body part, hairs, or clothes being stuck on it), it was covered by a plastic box, which also creates a protection from the system in case of failure (Fig. 2.8). While the device is not being used, the spring is still under tension. To avoid any device damage or user injuries, the spring can be locked by an insert placed below the spring on the torso segment to prevent an unwanted loading of the spring (Fig. 2.8 D). The insert can not be removed if the spring is compressing it.

The mass of the full device is 1.6 kg per arm support and its collapsed size 0.53 x 0.20 x 0.13 m.

2.5   Experimental Validation

The device was validated with both a mechanical characterization and a user study.

2.5.1   Mechanical Characterization

Experimental Procedure

The torque response of the device was measured when varying the angle of the arm segment using an INSTRON machine (Fig. 2.5). The device was vertically attached to a rigid plate with an alternative hip fixation and the arm segment was vertically pulled down by a wire
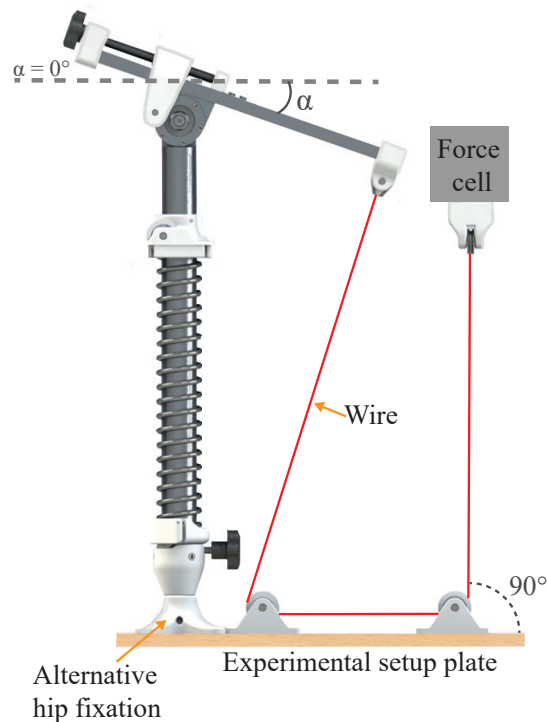
Figure 2.5 – Setup for the mechanical characterization.

(Dyneema 0.4mm, Spiderwire, SC, USA) connected to the force cell of the INSTRON machine. The output force was measured for arm segment angles between -69° and 63° (negative angles corresponding to the arm segment going down). This range was intentionally limited to be smaller than the actual ROM of this segment (-80° to 80°) in order to protect the device against collisions or singularities. In addition, over these angles, due to the rigid connection between the torso segment and the plate, the system undergoes high vertical forces, which may damage the device.

Tests were conducted by changing the grounding part position from 10 mm to 60 mm, with steps of 10 mm, with the arm length sets at its largest distance (0.312 m). This corresponds to weights compensation from one to six kg. The output force for each grounding part position was measured over ten cycles. The corresponding theoretical torque was computed using Eq. A.20 described in the Appendix A.

Results

The torque response over the arm segment angles is shown in Fig. 2.6. Dashed lines represent the theoretical torque, the shaded areas show the theoretical torque uncertainties due to the 10% tolerance on the spring force constant given by the manufacturer, and the solid lines represent the measured torques (see Appendix A for the calculations).
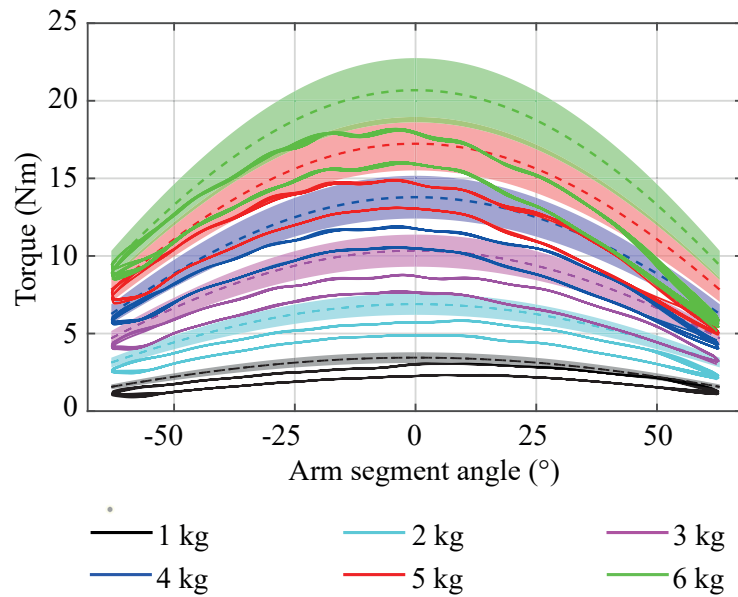
Figure 2.6 – Theoretical torque (dashed lines), theoretical torque uncertainties due to the 10% tolerance on the spring force constant given by the manufacturer (shaded areas), and measured torque (solid line). The legend (weights between one and six kilos) corresponds to the weight that can be lifted when the trimming is done for the greatest arm distance (0.312 m).

We can observe that the measured torques follow the same trend as the theoretical torque; i.e. it has a sinusoidal shape over the ROM of the arm segment and increased proportionally to the arm's weight. However, the measured torques were lower than the theoretical torque. A possible reason could be some friction between the slider and the torso segment. This could be solved by adding a linear bearing between the slider and the segment but this would add complexity to the system. On the other hand, despite the fact that the maximal output torque is below expectation, the tuning range is still fairly large and can adapt a variety of arms' weights and sizes. The maximal output torque of 18 Nm still ensures arm masses going up to 5.87 kg for the maximal arm length (0.312 m) to be fully compensated. It has been shown during the user study (see next section) that the arm weight of all participants could be compensated. We can also observe a shift of the maximum locations for the measured torque from negative angles for the highest weights to positive angles for the lowest weights. This is due to the change in cable length between the pulley and the grounding part (called b in Fig. A.1 B), which slightly increases relatively to the displacement of the grounding part (i.e. when Δs increases). This length has been considered as constant to simplify the theoretical model. As the average of the population has an arm weight between 3 and 4 kg, a maximum at zero angle has been set for these weights.

Fig. 2.6 also shows hysteresis in the torque, which can be due to the friction of the slider against the torso segment or due to the testing setup (i.e. energy loss in the pulleys and bearings, both cable and wire friction and deformation, 3D printed part deformation, etc.). Fig. 2.7 displays
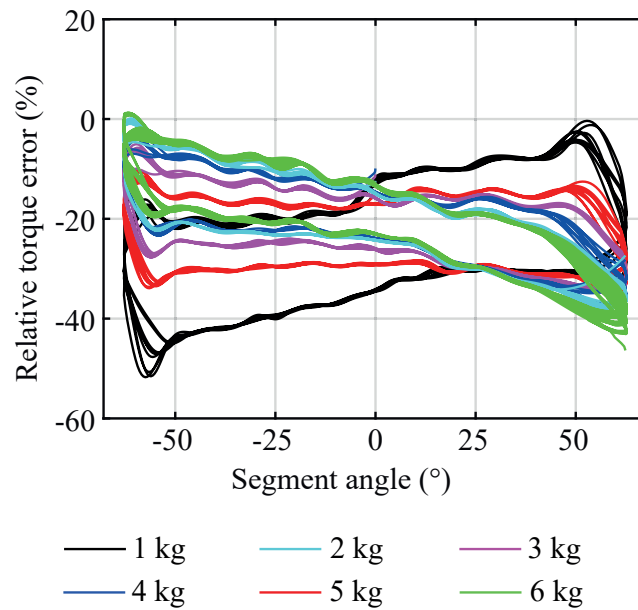
Figure 2.7 – Relative torque error. The legend (weights between one and six kilos) corresponds to the weight that can be lifted when the trimming is done for the greatest arm distance (0.312 m).

the relative torque error; the difference between the theoretical curve and the measured data. We can observe that the relative torque error and the hysteresis tend to be bigger for smaller arm weight (such as the black curve) reaching 50% for an arm segment angle of -60°, meaning when a small output torque needs to be compensated. This higher relative torque error can be explain because of the largest influence of the friction for small torque than for larger torque.

2.5.2 User Study

Experimental Procedure

The aim of this user study was to investigate the static Balancing Support (SBS) performance to prevent arm fatigue and its acceptance by users, and to compare it with both the previously developed Gas Spring Support (GSS) and with No Support (NS) when controlling a simulated fixed-wing drone. To study the devices' efficiency, we recorded the electromyographic (EMG, Desktop DTS, Noraxon, USA) activity of six shoulder muscles: the anterior (DANT), medial (DMED) and posterior deltoid (DPOS), the infraspinatus (INF), and the upper (TRAPU) and middle trapezius (TRAPM), as well as of the biceps (BIC) for every task of the experiment. The muscle activities were measured for both shoulder.

Twelve participants (Ten men and two women, age 32.55 ± 8.87 years; mean ± SD; height min = 1.62 m, max = 1.99 m; weight min = 59 kg, max = 86 kg) took part in this experiment. They began the experiment by completing a questionnaire about their physical traits (height and
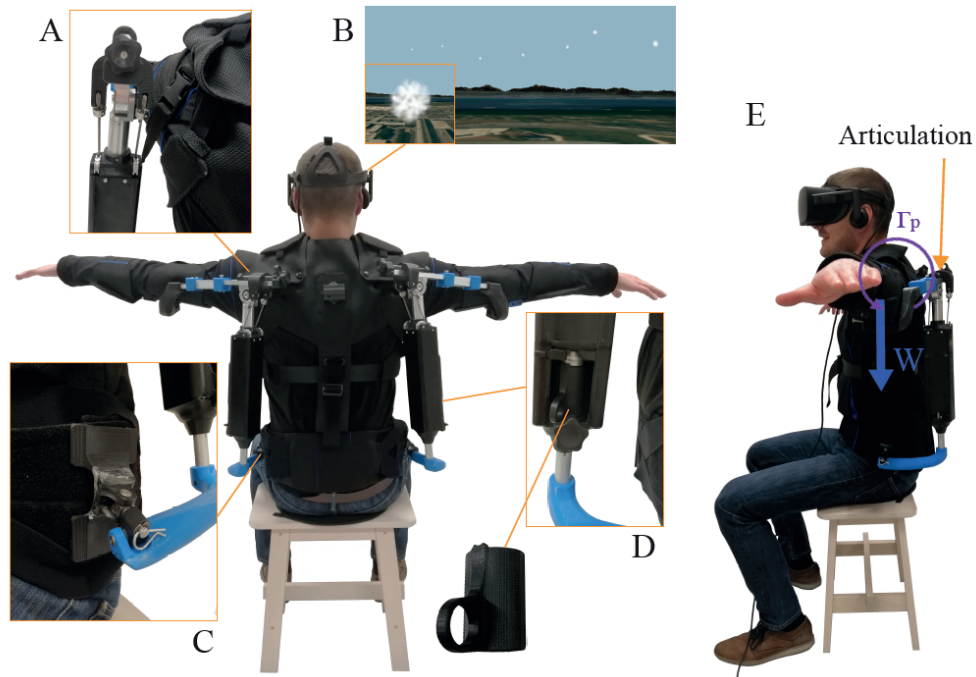
Figure 2.8 – User study setup. A) Insert highlighting the clip to fix the device to the jacket at the shoulder. B) Flight environment with waypoints (symbolized by white clouds) with an inset showing how a waypoint is seen by the participant when they fly towards it. C) Hip fixation point of the device. D) Locker system. E) Side view of the user showing the torque (Γ_p) due to the offset between the device and the arm weight.

weight), handedness (left or right), visual acuity, hours of physical activities, and experience in playing video games and piloting remotely an aircraft. Then, the EMG electrodes were placed and a Maximal Voluntary Contraction (MVC) test was performed. Next, they wore the FlyJacket above the electrodes and sat on a stool (Fig. 2.8). They also wore virtual reality goggles (Oculus Rift) that gave a first person view of the flight and wind sound for more immersion. They flew the same fixed-wing drone in the same environment as used in the user study of Chapter 1. They also started with the same short training. Then, participants had to fly three times through 50 waypoints represented by small clouds (Fig. 2.8 B) once with the SBS, once with the GSS and once with NS. The waypoint characteristics were the same as in Chapter 1. The distance between the drone and the center of each waypoint was recorded. The flight performance was computed as the RMS of these 50 distances. Participants had a five minutes break between each task where the type of arm support was changed and tuned to each body morphology. At the end of the flight tasks, participants had to fill a questionnaire about their appreciation of each flight conditions (i.e. SBS, with GSS and NS).

The EPFL Institutional Review Board procedures approved the study and the participants provided written informed consent. All calculations for the data analysis done in this study were computed in MATLAB (MathWorks, Massachusetts, USA) and R Studio (R Studio Inc.,

Boston, MA, USA). The raw EMG data, acquired at 1500Hz were corrected for linear trends. The signals were then low-pass filtered at 400 Hz, high-pass filtered at 50 Hz, rectified, and low-pass filtered at 5 Hz to remove noise using seventh-order Butterworth filters. Eventually, each channel was normalized to its MVC. Graphs were also plotted in MATLAB and aesthetically enhanced with Adobe Illustrator (Adobe Systems Incorporated, San Jose, CA, USA).

Results
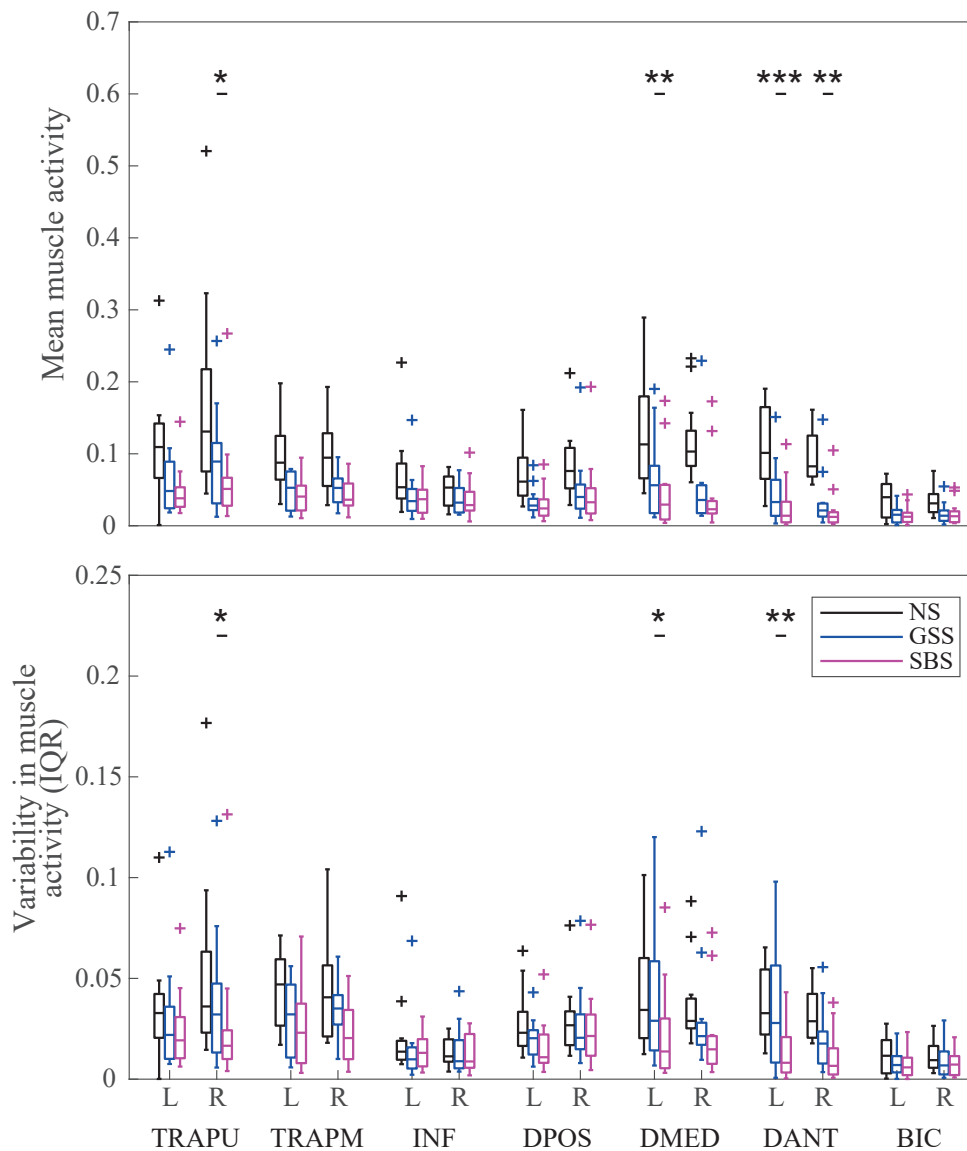
Figure 2.9 – Muscular activities (n=12). A) Mean muscle activity. B) Variability as assessed by the interquartile range (IQR). Significant differences are indicated only between GSS and SBS conditions; $*p < 0.05$, $**p < 0.01$, $***p < 0.001$

They were no significant differences in the flight performance between the three flight conditions (SBS, GSS and NS), which means that the SBS doesn't prevent user's movements and therefore performance.

Fig. 2.9 A shows the mean muscle activity for the six shoulder muscles tested, and for the biceps. Fig. 2.9 B show the variability in the muscle activity between the 25% and 75% quartiles. Regarding the mean muscle activity, repeated measure analyses of variance (ANOVAs) revealed a significant effect of support for all muscles (see Table 2.3 for the statistical analysis values, p-values were corrected for multiple comparisons using the Benjamini-Hochberg procedure). The statistical differences between each type of support (SBS, GSS, and NS) were tested with one-sample t-tests. We can observe that having an arm support, either SBS or GSS, reduces significantly the muscle activity when comparing with NS. The Cohen's d coefficient of the one-sample t-test results were calculated to compare the effect size. They show a large effect for most of the muscles with values higher than 0.8, strengthening the importance of the effect of support. Regarding the variability in muscle activity, the ANOVA results showed significance for eight muscles and one-sample t-tests were significant between SBS and GSS for the same muscles as for the mean muscle activity. The variability displays the mechanical stability of the support whereas the mean muscle activity shows the efficiency of the support in assisting the muscles. No significant difference in the ANOVA results of the variability can either mean that support has no effect or that these muscles were not moving during flight.

Statistically significant differences between the two arm supports (SBS and GSS) were observed in both the mean muscle activity and their variability for the right TRAPU, the left DMED, and both left and right DANT. As a large part of users fly with the elbow bent instead of straight – we observed 9/12 participants of the user study adopting this flight style – they probably use their DANT to support the torque produced by their forearm in this position. The SBS seems to be providing more support for the shoulder rotation than the GSS, consequently reducing the muscle activity and the variability of the DANT. A statistically significant effect was also observed for the right TRAPU and the left TRAPU one-sample t-test shows a p-value relatively close to significance ($p = 0.097$). The TRAPU is playing an active role in the stabilization of the shoulder both in abduction and in rotation. These results reinforce our assumption of the SBS being a more stable device for the shoulder rotation than the GSS. Results for the DMED are surprising as only the left muscle showed a difference in muscle activity and variability between the two arm supports. Indeed, we expected to have a symmetrical effect of the supports. As only one participant was left-handed, we cannot draw conclusion on the possibility of stronger muscles on one side of the body due to handedness. Another explanation could be a difference in the mechanical characteristics between the left and the right arm support (which could exist in either the SBS or the GSS). However, this difference in muscle activity between body side is present only for the DMED.

Regarding the questionnaire results, the participants felt significantly less fatigue when flying with the arm supported by the SBS ($p = 1.2 \cdot 10^{-4}$) or with the GSS ($p = 8.6 \cdot 10^{-4}$) (which corroborates results found in Chapter 1) than with NS (Fig. 2.10 A). There are no significant

Table 2.3 – Statistical Significance of the Different Arm Supports on the Mean Muscle Activity (n=12)

Muscle		ANOVA		NS vs GSS		NS vs SBS		GSS vs SBS	
		p	η^2	p	d	p	d	p	d
TRAPU	L	$5.83 \cdot 10^{-4}$	0.63	0.031	0.83	$3.84 \cdot 10^{-3}$	1.24	0.097	0.52
	R	$5.83 \cdot 10^{-4}$	0.68	$7.40 \cdot 10^{-3}$	1.06	$2.25 \cdot 10^{-3}$	1.33	0.024	0.75
TRAPM	L	$7.05 \cdot 10^{-5}$	0.72	$1.18 \cdot 10^{-3}$	1.37	$8.54 \cdot 10^{-4}$	1.51	0.250	0.35
	R	$1.18 \cdot 10^{-4}$	0.76	$2.76 \cdot 10^{-3}$	1.22	$4.14 \cdot 10^{-4}$	1.65	0.178	0.42
INF	L	0.017	0.67	0.010	1.08	0.055	0.73	0.492	0.21
	R	0.017	0.52	0.019	0.97	0.085	0.66	0.745	-0.10
DPOS	L	$2.60 \cdot 10^{-4}$	0.70	$1.18 \cdot 10^{-3}$	1.45	$1.18 \cdot 10^{-3}$	1.44	0.318	0.30
	R	$9.77 \cdot 10^{-5}$	0.72	$1.60 \cdot 10^{-3}$	1.32	$7.47 \cdot 10^{-4}$	1.53	0.342	0.29
DMED	L	$1.33 \cdot 10^{-4}$	0.77	$1.02 \cdot 10^{-3}$	1.40	$3.44 \cdot 10^{-4}$	1.68	$4.98 \cdot 10^{-3}$	1.01
	R	$2.60 \cdot 10^{-4}$	0.71	$9.21 \cdot 10^{-4}$	1.49	$2.60 \cdot 10^{-3}$	1.24	0.420	0.24
DANT	L	$6.52 \cdot 10^{-5}$	0.83	$2.58 \cdot 10^{-4}$	1.66	$7.50 \cdot 10^{-5}$	2.00	$5.98 \cdot 10^{-4}$	1.37
	R	$7.46 \cdot 10^{-7}$	0.92	$3.31 \cdot 10^{-5}$	2.09	$1.09 \cdot 10^{-6}$	3.10	$9.29 \cdot 10^{-3}$	0.91
BIC	L	$1.61 \cdot 10^{-3}$	0.60	$5.76 \cdot 10^{-3}$	1.15	$5.76 \cdot 10^{-3}$	1.17	0.358	0.28
	R	$6.52 \cdot 10^{-5}$	0.75	$4.98 \cdot 10^{-4}$	1.55	$4.98 \cdot 10^{-4}$	1.61	0.898	-0.04

differences in subjective shoulder fatigue between the two arm supports. Both arm supports did not prevent users to have enjoyable sensations, as the sensation of flying was rated the same for the three flight conditions (Fig. 2.10 B). They felt equally confident with both arm support and did not feel more constraint with one arm support comparing to the other. Some participants reported that they felt more confident flying with an arm support as they did not have to reflect about what to do with their arms.
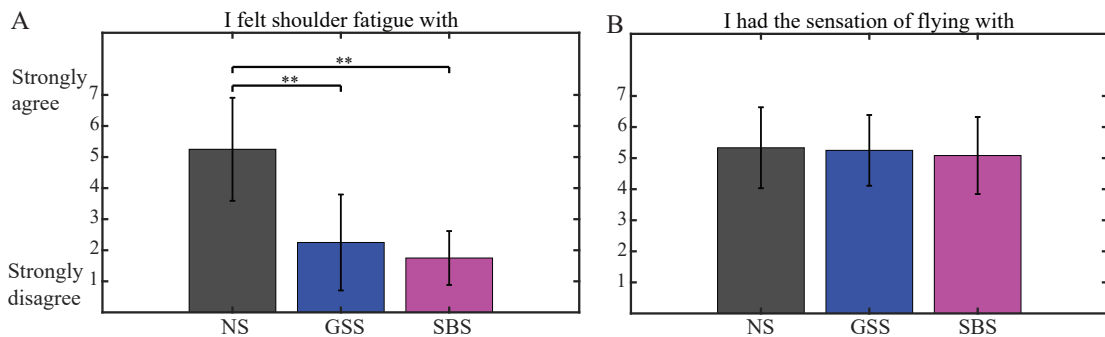

Figure 2.10 – Questionnaire results (n=12). A) for the question "I felt shoulder fatigue". B) for the question "I had the sensation of flying". (**) denotes $p < 0.01$.

Table 2.4 – Statistical Significance of the Different Arm Supports on the Variability (n=12)

Muscle		ANOVA p	η^2	NS vs GSS p	d	NS vs SBS p	d	GSS vs SBS p	d
TRAPU	L	0.165	0.27	-	-	-	-	-	-
	R	$6.38 \cdot 10^{-4}$	0.69	0.014	0.95	$2.00 \cdot 10^{-3}$	1.39	0.028	0.73
TRAPM	L	$7.97 \cdot 10^{-4}$	0.69	0.003	1.20	$3.00 \cdot 10^{-3}$	1.29	0.226	0.37
	R	$9.53 \cdot 10^{-3}$	0.58	0.14	0.55	$9.00 \cdot 10^{-3}$	1.09	0.14	0.58
INF	L	0.266	0.52	-	-	-	-	-	-
	R	0.843	0.04	-	-	-	-	-	-
DPOS	L	0.024	0.42	0.065	0.71	0.052	0.81	0.126	0.48
	R	0.178	0.44	-	-	-	-	-	-
DMED	L	0.019	0.73	0.878	-0.05	$3.00 \cdot 10^{-3}$	1.29	0.015	0.94
	R	0.082	0.33	-	-	-	-	-	-
DANT	L	$3.71 \cdot 10^{-3}$	0.80	0.853	0.06	$3.71 \cdot 10^{-3}$	1.80	0.009	1.04
	R	$6.38 \cdot 10^{-4}$	0.74	0.018	0.80	$1.00 \cdot 10^{-3}$	1.50	0.018	0.91
BIC	L	0.035	0.38	0.103	0.63	0.074	0.75	0.422	0.24
	R	0.066	0.35	-	-	-	-	-	-

2.6 Conclusion

The arm support presented in this chapter addresses the challenges of compensating the torque induced by gravity along the ROM used to fly a drone while remaining portable and adaptable to 98% of the body size and weight of the population. This arm support enables a better torque compensation along a larger ROM than the arm support described in Chapter 1. The parasitic force is also substantially lower across the whole ROM allowing a more comfortable device. The mechanical characterization of the built device validated the feasibility of a torque compensation up to 18 Nm ensuring arm masses going up to 5.87 kg for an arm length of 0.312 m to be fully compensated. The results of the user study validated the usefulness of an arm support during flight as the muscle activity of the shoulder was significantly reduced and the participant felt less shoulder fatigue. In addition, participant reported to have the same flight sensation with arm support than without. In comparison to the previously developed arm support (GSS), results of the muscle activity suggest that the SBS allows more support in shoulder rotation.

Some minor improvements can be done to the SBS. The thread of the screw is 1.5mm. Therefore, screwing the grounding part until the gravity is compensated – on average 40 mm for the participants of the user study – takes time. As such a precise positioning of the grounding part is not required in our systems, this screw could be replaced by one with a larger thread. In the case where a precise positioning of the screw is however required, the tuning of the torque could be motorized. Another issue is that, due to the placement of the knob on the back of the user, the adjustment for the torque compensation cannot be done by the user himself. To solve this issue, again a motorized torque tuning mechanism with, for example, a digital

interface could be implemented.

In a future work, haptic feedback could be transmitted through the arm support in order to render flight sensations (such as air lift or drag) or guidance to the FlyJacket user. Actuators could be added in this arm support to render these forces. However, a special attention needs to be given to keep the device portable.

The arm support presented in this chapter enables a better torque compensation along a larger ROM and provides a better constraint of the arm than the support described in Chapter 1. However, this technology was not yet available when we performed the haptic experiments. Therefore, the user studies of the following chapters are performed using the Gas Spring Support.

3 Kinesthetic Feedback: Guidance with a Soft Exoskeleton to Reduce Error in Drone Teleoperation

3.1 Introduction

This chapter presents the integration and test of a cable-driven kinesthetic guidance in the FlyJacket. This work is motivated by several results showing that haptic feedback improves the task performance in many domains such as for surgery [32], rehabilitation [54] or sports [57, 99]. Haptic feedback has been implemented as a force feedback on joysticks to control flight for obstacles avoidance [29, 73, 100]. In those studies, an attractive or resistive corrective force relative to the distance between the drone position and the obstacle increases users' awareness and reduces collision occurrences. The flight immersion can also be enhanced by including the velocity of the drone in the haptic feedback [74, 75].

When the aim of the kinesthetic feedback is to correct a trajectory, linear feedback control laws (e.g. proportional-derivative control) on the error between the robot position and a reference trajectory are typically used [32, 54, 60, 101, 102]. The stiffness of the guidance is a very important feature because a too soft guidance may not be effective while a too strong guidance may lead to user passivity [60, 101, 103]. Therefore, the force profile and stiffness play an important role and need to be studied in order to optimize the guidance provided by
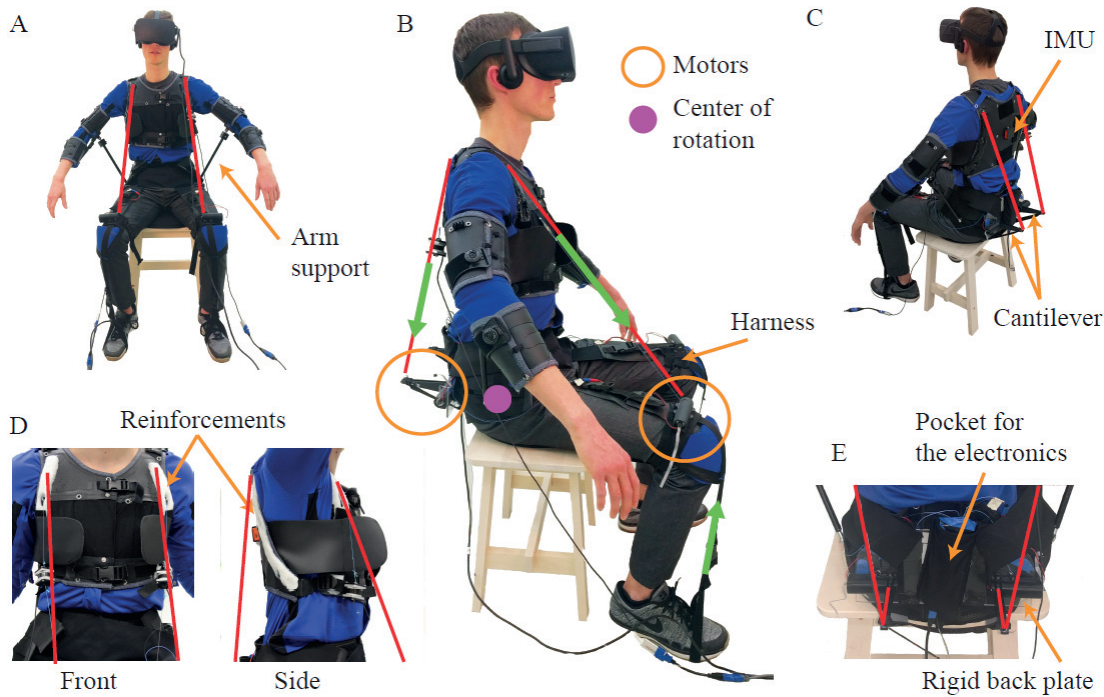
Figure 3.1 – FlyJacket with kinesthetic guidance device. Cables are highlighted in red and the forces shown in green. A) Front view. B) Side view. C) Back view. D) Magnification on the torso part to highlight the reinforcements. E) Magnification of the lower back part to highlight the back motors.

the kinesthetic feedback.

The kinesthetic feedback described in this chapter aims to correct and guide the user toward waypoints when flying a simulated fixed-wing drone using torso gestures. The aim of the guidance is to improve the performances of the user by correcting the torso position. We investigated four different force profiles to determine their contribution on the reduction of the error between the drone and the waypoints. We studied how the addition of kinesthetic guidance acts on the performance and on the workload of the user.

3.2 Kinesthetic Guidance Implementation

3.2.1 FlyJacket Hardware

Kinesthetic guidance to the FlyJacket user is provided by a cable-driven system. With this system, four electrical motors (DC22S, gear ratio 6.6:1, Maxon Motor, Switzerland) pull on cables (Dyneema 0.4mm, Spiderwire, SC, USA, displayed in red in Fig. 3.1) attached to the user's upper torso. In order to pull the torso according to the gestures performed by the user during flight, e.g. bending forward and backward with a center of rotation located on the hip (see Fig. 3.1 B), one motor is positioned on the distal part of each leg and two motors on each

side of the lower back. With this antagonistic configuration, forces bend the user in both the sagittal and frontal planes. Both front motors are fixed to the legs with a harness system. To prevent the motors from sliding along the legs when pulling on the cables, they are maintained by a non-elastic textile band attached at its extremity to the user's feet by the mean of a loop. Padding on the knee avoids user discomfort due to the force routing. The two back motors are located on the lower back and screwed onto a rigid plate to prevent them from moving (Fig. 3.1 E). Cantilevers made of 3D printed ABS create a lever arm to induce forces that pull the user backward, instead of downward. Two non-elastic textile bands attached from the extremities of the cantilevers to the leg harness, passing on the back of the thigh, restrain the cantilever tips from moving when the back motors are pulling on cables. As the cables are attached on the torso part made of leather, reinforcements made of polymorph thermoplastic (Thermoworx Ltd, Ayrshire, Scotland, UK) have been inserted to stiffen the structure in order to prevent force losses and transmission delays (see Fig. 3.1 D).

The range of force of the kinesthetic guidance should induce a torque higher than the passive stiffness of the human torso of around 10 Nm [104], in order to be able to move the torso of a fully compliant human. However, the user should also have full control of their body movements at any time. Therefore, we ensure that the maximal torque applied to the torso is much lower than the maximal torque a human can produce, which is around 150 Nm [105, 106]. As a comparison, the X-Arm 2, a rigid arm exoskeleton used to teleoperate a humanoid robot for extra-vehicular space missions, can produce up to $1/20^{th}$ of the maximum human arm torque to deliver force feedback during manipulation [16]. Each motor of the FlyJacket's kinesthetic system can produce up to 30 N of force, which corresponds to a torque of approximately 20 Nm for a 175 cm tall user when both motors of one body side are pulling together.

The four electrical motors are independently controlled by four transistors activated through a control board (Arduino Uno, Arduino, Italy). Thanks to the low gear ratio (6.6:1), motors are back-drivable. They are only activated when a corrective force is required to pull on the cables.

3.2.2 Guidance Profiles

The kinesthetic guidance is based on the error (Δx) between the drone position and a predetermined trajectory at a predefined time in the future. For ease of visualization, Fig. 3.2 A is showing a 2D schematic of the distances, but the flight trajectories in the tasks are 3D. This error (Δx) is calculated as the scalar product between the vector from the drone to the look ahead point and the vector perpendicular to the direction of flight, pointing to the right for the correction in roll and up for the correction in pitch. The look ahead principle has been shown to enable stable vehicle control using external interfaces (e.g. remote controller) [101, 102]. In this study, participants were asked to follow a trajectory in the sky symbolized by small clouds (see Fig. 3.3 A), called waypoints, spaced apart by approximately 40 meters. The look ahead time was set to 3 seconds, which corresponds to a distance of 36 meters as the drone is flying
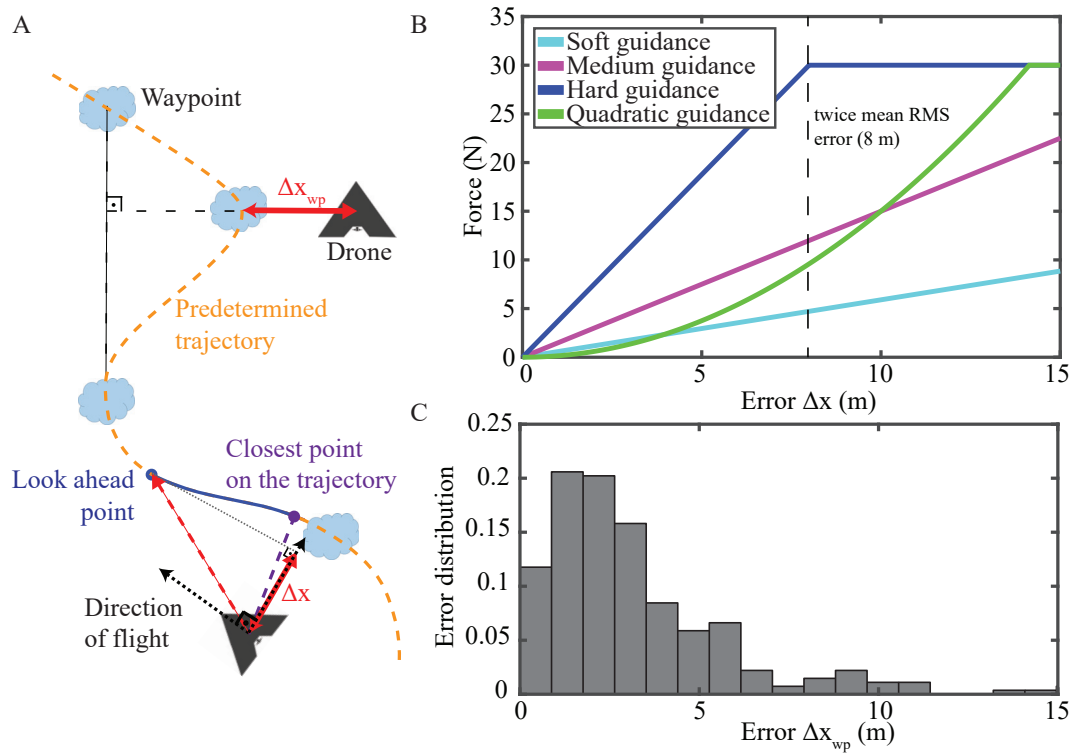
Figure 3.2 – Kinesthetic guidance strategies. A) 2 D schema displaying the error (Δx) for the haptic guidance (measured throughout the task) and the error (Δx_{wp}) to measure the performance at each waypoint. B) Force guidance over the error (Δx). C) Waypoint error distribution (Δx_{wp}) found in Chapter 1.

at a constant speed of $12 \frac{m}{s}$. The user receives an attractive force relative to their error (Δx), which indicates how they should move their torso to correct the drone position. As the four motors can be actuated separately, combination of forces on the front, back, and sides are achievable in order to correct the drone in pitch, roll or a combination of both. For example, as shown in Fig. 3.2 A, if the drone is positioned too far on the left regarding to the predetermined trajectory, front-right and back-right motors will pull on cables to exert a force to bend the user's torso on the right side. With this torso movement, the drone will roll on the right, and the error (Δx) will be reduced.

Four guidance curves were implemented to investigate which type of feedback could best correct torso movements during a flight task (see Fig. 3.2 B). We used three linear profiles with different levels of stiffness (hard, medium, and soft) and one quadratic profile that transitions from soft to hard guidance. These force profiles have been calibrated based on the RMS and standard deviation (std) of the error (Δx_{wp}) measured at each waypoint from the user study described in Chapter 1, which has a similar flight task but without guidance (see Fig. 3.2 A and C). This error was the distance between the center of the waypoint and the point where the trajectory of the drone crosses a plane drawn perpendicular to the line connecting the previous and next waypoint (for more detail see [67]). The participant's performance was

computed as the RMS of these distances over all waypoints of the task. The mean RMS error over all participants was 4.02 ± 1.62 meters (mean ± std).

The hard guidance has the advantage of giving a strong feedback to the user with a stiffness of 3.75 $\frac{N}{m}$. This guidance imparts the maximum force the motor can produce (30 N) at twice the mean RMS error found in previous experiment (Eq. 3.1). At more than 30 N, the motor is not able to produce more force, and it saturates as shown in Fig. 3.2 B. Since more than 90% of the errors (Δx_{wp}) found in the user study of Chapter 1 were smaller than twice the mean RMS error (8 meters), users seldom reach the saturation limit. This guidance strongly pulls the torso toward the orientation that would correct the drone's trajectory and immediately emphases every small error (Δx). However, this strong force may be unpleasant for the user as they may feel less involved in the control.

$$F_{\text{hard}} = \begin{cases} 3.75 \cdot \Delta x, & |\Delta x| \le 8\text{N} \\ 30\text{N}, & |\Delta x| > 8\text{N} \end{cases} \tag{3.1}$$

In contrast, the soft guidance aims to hint which movements the user should perform to correct their orientation as the forces are too weak to influence the torso movement. This guidance has a stiffness of 0.59 $\frac{N}{m}$, which gives the maximal force at the mean error plus 30 times the standard deviation (Eq. 3.2). For small errors, the guidance force is very weak, which allows the user to make some mistakes without being strongly pushed back towards the reference trajectory as the hard guidance does.

$$F_{\text{soft}} = \begin{cases} 0.59 \cdot \Delta x, & |\Delta x| \le 51\text{N} \\ 30\text{N}, & |\Delta x| > 51\text{N} \end{cases} \tag{3.2}$$

The medium guidance aims to be an intermediate guidance between hard and soft guidance and was designed to give half of the maximal force at the mean error plus 10 times the standard deviation, which corresponds to a stiffness of 1.5 $\frac{N}{m}$ (Eq. 3.3).

$$F_{\text{medium}} = \begin{cases} 1.5 \cdot \Delta x, & |\Delta x| \le 20\text{N} \\ 30\text{N}, & |\Delta x| > 20\text{N} \end{cases} \tag{3.3}$$

The fourth proposed guidance has a quadratic shape. It combines the advantages of both the soft and the hard guidance. For small errors, it gives a weak correction force; therefore, the participant avoids being strongly perturbed. When the error becomes more significant, this guidance pulls the user strongly towards the reference trajectory. The force intensity was set to match the error of the medium guidance at half of the maximum motor force (15 N) as display

in Fig. 3.1 B (Eq. 3.4).

$$F_{\text{quadratic}} = \begin{cases} 0.15 \cdot \Delta x^2, & |\Delta x| \leq 14\text{N} \\ 30\text{N}, & |\Delta x| > 14\text{N} \end{cases} \tag{3.4}$$

3.2.3 Flight Experiment

In order to evaluate the effectiveness of kinesthetic guidance of the four different guidance profiles, ten participants (six men and four women, age 28.5 ± 4.5 years; mean ± std) flew a simulated fixed-wing drone using upper body movements. All participants tested the four types of guidance and flew once without guidance. They sat on a stool wearing the FlyJacket with arm support and VR goggles (Oculus Rift) that gave a first person view of the flight and wind sound for more immersion. They flew the same fixed-wing drone in the same environment than the one used in the user study of Chapter 1.

Participants started with the same short training period as described in Chapter 1, without guidance. For the evaluation part, participants were instructed to fly through 42 waypoints represented by small clouds (see Fig. 3.3 A). The waypoint characteristics were the same as in Chapter 1. Each participant completed five trials, once with each guidance condition and once without guidance. They were not told which type of guidance they were to receive or what type they had received. The order of the guidance conditions presented to the participant was arranged so that each condition was placed twice at every position in the task order (see Fig. 3.3 B). The same succession of conditions was avoided as much as possible in order to remove learning effects. Participants' performance was computed as the RMS of the error ($\Delta \mathrm{x}_{wp}$) of all waypoints.
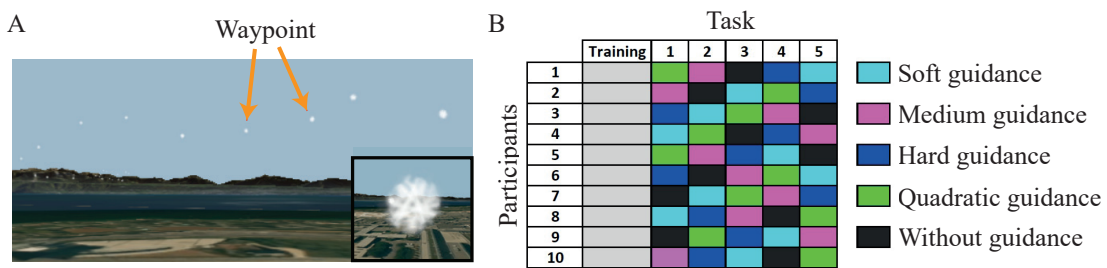
Figure 3.3 – Experimental settings. A) Flight environment with an inset showing how a waypoint is seen by the participant when they fly towards it. B) Task order for each participant.

At the end of each task, participants completed a NASA-TLX questionnaire with pairwise comparison [107], which assessed the workload variation between flight conditions. At the end of the experiment, participants completed a final questionnaire asking which kind of guidance condition they enjoyed the most and the least, and which guidance condition they

found the most and least useful (Table 3.1). The EPFL Institutional Review Board procedures approved the study and the participants provided written informed consent.

3.3 Results

3.3.1 Performance Results

Participant performance was measured as the RMS error reduction obtained by subtracting the RMS error of each task done with kinesthetic guidance from the RMS error in the condition without guidance for each participant. This removes the performance level variation among participants and shows the effect of flying with a kinesthetic guidance with respect to no guidance, i.e. what is the error reduction induced by the kinesthetic guidance comparatively to flying without guidance. Therefore, a positive RMS error reduction means that the kinesthetic guidance increases flight performance.
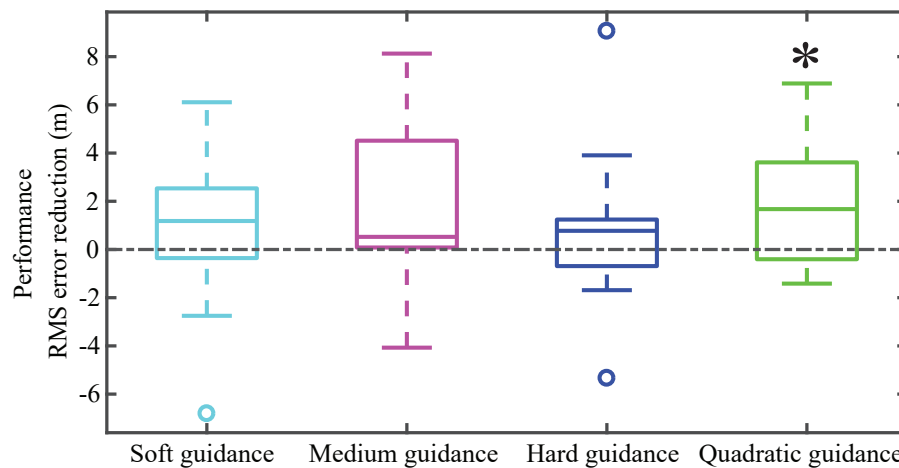
Figure 3.4 – Participant performance measured by RMS error reduction of each haptic guidance relative to without guidance (n=10). The central mark indicates the median, the bottom edge the 25th percentile and the top edge the 75th percentile. The whiskers show the most extreme data points not considered outliers (open circles). Asterisk (*) denotes $p < 0.05$.

Results of Fig. 3.4 show that the median RMS errors for all types of kinesthetic guidance are positive; the RMS error of the task was lower when performing the task with any type of kinesthetic guidance than when flying without guidance. To determine if any of the guidance has a statistically significant effect on the error reduction, we ran a Wilcoxon Signed Rank test using MATLAB. The error reduction was significant for the quadratic guidance with $p = 0.0488$. The three other guidance conditions, i.e. soft guidance ($p = 0.4922$), medium guidance ($p = 0.0840$) and hard guidance ($p = 0.4316$), do not show any statistical significance. However, due to the limited number of samples commonly gathered with human experiments, these results do not have a high statistical power. Therefore, we used a bootstrap metric. This

Table 3.1 – Number of Participants Selecting the Flight Task as the Most or Least Enjoyable and Most or Least Useful in the Final Questionnaire (n=10)

In which task was kinesthetic feedback:	Soft guidance	Medium guidance	Hard guidance	Quadratic guidance	Without guidance
the least enjoyable	1	2	6	0	1
the least useful	0	1	5	1	3
the most enjoyable	3	3	1	3	0
the most useful	3	2	2	3	0

non-parametric method generates the replication of 500 sample means (obtained by sampling with replacement 10 samples from the original dataset), which follow the same distribution as the data recorded during the experiment. This allowed us to obtain the empirical distribution for the sample mean. We then assessed whether the [2.5 ; 97.5] quantile interval covers 0; the negation of the latter implying that the mean is significantly different than 0. We found that the quadratic guidance has a significant $p = 0.0040$, which supports the result found using the Wilcoxon Signed Rank test done on our ten participants. In addition, the medium guidance also has a significant result with $p = 0.0260$. The other two guidance conditions, i.e. soft guidance and hard guidance did not show any statistical significance with $p = 0.2080$ and $p = 0.1860$ respectively.

3.3.2 Subjective Assessment of Kinesthetic Guidance

At the end of the experiment, participants filled a questionnaire specific to kinesthetic guidance. The statement "I found the kinesthetic guidance useful" was rated 6.08 out of 7 on the Likert scale from 1 (Strongly disagree) to 7 (Strongly agree). All participants rated between 5 and 7. They reported that it helped them anticipate maneuvers, particularly roll movements.

In the same questionnaire, they had to state which flight condition they found the most and the least enjoyable and the most and the least useful (Table 3.1). A proportion of 6/10 participants found the hard guidance the least enjoyable versus 0/10 for the quadratic guidance. Also, half of the participants found the hard guidance the least useful versus 1/10 for the quadratic guidance. Notably, no participants found that the soft guidance, which provides the weakest force, was the least useful guidance.

Results for the most enjoyable and the most useful kinesthetic guidance were more mixed (Table 3.1). Proportionally, 3/10 participants found the quadratic guidance the most enjoyable and the most useful and three others the soft guidance versus 0/10 for without guidance. As no participants rated the without guidance condition as the most enjoyable or the most useful, this result corroborates the high score of the guidance usefulness.
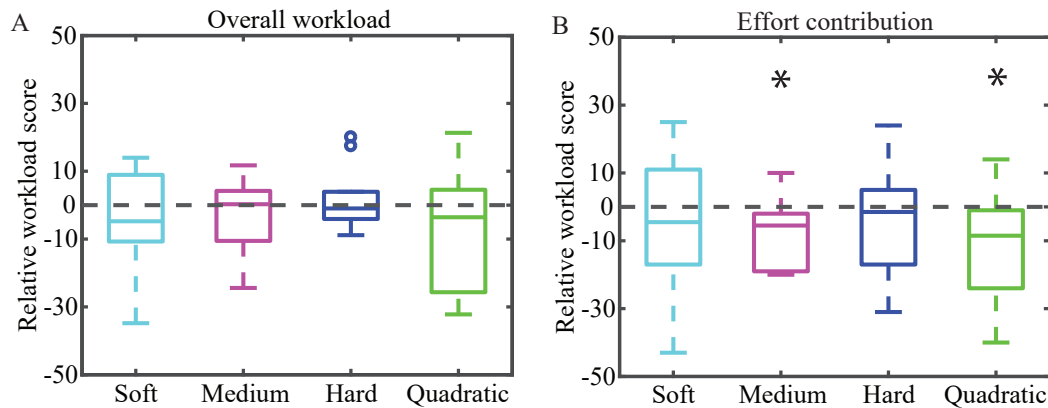
Figure 3.5 – Results of the NASA-TLX test. A) Overall workload, which includes contribution from the effort. See Fig. 3.4 for boxplot explanation. B) Effort contribution. (*) denotes $p < 0.05$ (n=10), (open circles) signify outliers.

Workload Results

As shown in Fig. 3.5 A, there are no statistically significant workload differences between flying with a kinesthetic guidance and flying without guidance. There is also no difference in workload among kinesthetic guidance types. Workload is composed of six different contributions: physical demand, mental demand, effort, temporal demand, frustration and performance, each of which can be analyzed separately [107]. The effort (Fig. 3.5 B) when flying with the medium and the quadratic guidance is significantly lower than when flying without guidance ($p = 0.0488$ and $p = 0.0352$ respectively). The same bootstrap metric used for the performance analysis with a replication of 500 sample means was applied. Both guidance show significance with $p = 0.0080$ for the medium guidance and $p = 0.0040$ for the quadratic guidance. The contribution of the effort on the general workload is 17%. The other workload contributions did not show any significant difference from zero and between guidance conditions.

3.4 Conclusion

This study demonstrated that receiving quadratically shaped kinesthetic guidance when performing a flight task with the FlyJacket helped improve flight accuracy without increasing the workload. Out of the four force profiles tested, the quadratic profile was found to be the best over three linear profiles of different stiffness. In addition, our results showed that all users found kinesthetic guidance useful when flying.

Having a quadratically shaped guidance, which gives weak force when the error is small and strong force when the error becomes large, is the most effective type of feedback to improve precision but also the one that requires the lowest effort. In comparison, the soft guidance was not only more enjoyable than hard guidance, but participants also found it more useful. Hard guidance was rated least enjoyable because participants felt the force

was too strong. This may be because any small deviations from the nominal trajectories trigger large forces from the FlyJacket's kinesthetic system, frequently perturbing the user's body. Consequently, they may not feel fully in control of their torso orientation, leading to the unpleasant feeling of being obstructed or to user passiveness [103]. The medium guidance, which is an intermediate guidance between the hard and soft guidance, had a more meaningful impact on the performance than the two extremes (soft and hard guidance) and significantly reduced user's effort.

Our study had a few limitations. We instructed users to follow waypoints during the evaluation task, and we calculated the performance measure only at these waypoints. However, in order to have a more precise understanding of drone dynamics, error could be measured by assessing the deviation from an overall trajectory, rather than discrete waypoints. To do so, additional experiments should be designed were the participant is able to see, for example by the mean of a line, the full trajectory in between the waypoints. We also restricted our tests to proportional controllers. Additional experiments could be performed to determine if adding a derivative term of the drone position to the quadratic or medium controller (e.g. PD controller) would further improve the performance.

By identifying an effective profile to reduce the error when following waypoints, this study provides the basis for further investigating the learning rate of the user with guidance in comparison to without guidance. The goal will be to understand if kinesthetic guidance can accelerate the flight learning process and if this knowledge can be better retained by users. This could facilitate drone control and, therefore, make their use more accessible to non-expert users.

4 Kinesthetic Feedback: Perception and Learning with Cable-Driven Guidance in Exosuit Teleoperation

4.1 Introduction

In the previous chapter, the kinesthetic feedback implemented in the FlyJacket has been tested in a short flight task of following waypoints in the sky. The aims were to determine the effect of kinesthetic guidance on flight performance and the best force profile to guide the user. We found that a quadratically-shaped kinesthetic guidance increased user performance in comparison to flying without any guidance. Participants also subjectively reported that kinesthetic guidance while flying was useful. However, the long term effects of the guidance, as well as participants' perception of the force applied, remained unclear. If the user could learn to fly better with kinesthetic guidance, such a device could be used for training, and the guidance could be removed once the user reached a sufficient level of performance. In order to design the training task and the type of guidance provided during this period, it is important to understand how users perceive this type of kinesthetic feedback, in particular the minimal force difference they can discern and the force magnitude they perceive on the front and on the back of their torso. Moreover, it is imperative to determine the threshold of human force perception as previous work has shown that the provision of sub-threshold force feedback can be detrimental to user performance in haptic-enabled virtual environments [108].

The study of human force perception was intensively carried out by G.T. Fechner and E.H.

Weber [109]. They developed the Just Noticeable Difference (JND) test which study the difference required by human to perceive changes in stimuli [110]. S. S. Stevens extended this work and demonstrated that stimuli perceptions do not follow a logarithmic law but a power law [109, 111, 112]. Stevens' work on tactile sensations through vibrations demonstrated a linear correspondence between a stimulus and the perceived magnitude [113]. It is uncertain if a similar linear relationship holds for kinesthetic stimulus on the torso.

In this chapter, we investigated what would be the most effective way to transmit the information to the user and the retention of this information with the same cable-driven device as presented in Chapter 3. To address these questions, we conducted two studies. First, psychophysical experiments were performed to determine how the user perceived the force applied to their body through determining the Just Noticeable Difference [110] and the coefficients for the Stevens' power law [111]. Second, flight experiments were conducted to determine the influence of the kinesthetic guidance on user performance for an extensive flight task and the level of short term information retention when the kinesthetic guidance was removed. All participants to these two studies provided written informed consent prior to the study in accordance with the EPFL Institutional Review Board procedures.

4.2 Kinesthetic Feedback Perception

The first phase of research investigated the sensitivity of FlyJacket users to a given force to understand how applied forces are perceived and to improve the control of the drone. It is therefore important to measure the minimal force amplitude the user can perceive and their ability to discern differences in amplitude. In this phase, two sets of tests were conducted on 10 participants. The first set investigated the Just Noticeable Difference (JND), which is the minimal force difference the user can perceive at different force amplitudes. The second set aimed at determining whether perception of kinesthetic feedback to the torso by motor-driven cables followed a linear law between a given stimulus and the participant perception, based on the Stevens' power law.

4.2.1 Description of the Experiment

These two studies were performed on healthy adult participants (n=10, five males, five females, age 23.1 ± 4.46 years; mean ± SD). The participants sat on a stool, wearing the FlyJacket with the arm supports and earmuffs to block external noises, such as from the motors (see Fig. 4.1 A). Participants were asked to close their eyes during the trials. The kinesthetic feedback perception tests measure the force perception on static limbs. Therefore, participants were instructed to stay in an upright position and resist the force applied to their torso (i.e. by keeping their torso aligned with gravity) during all the trials.

The first experiment determined the Just Noticeable Difference — the minimal force difference a participant can perceive for various force amplitude — for four standard force amplitudes (5,
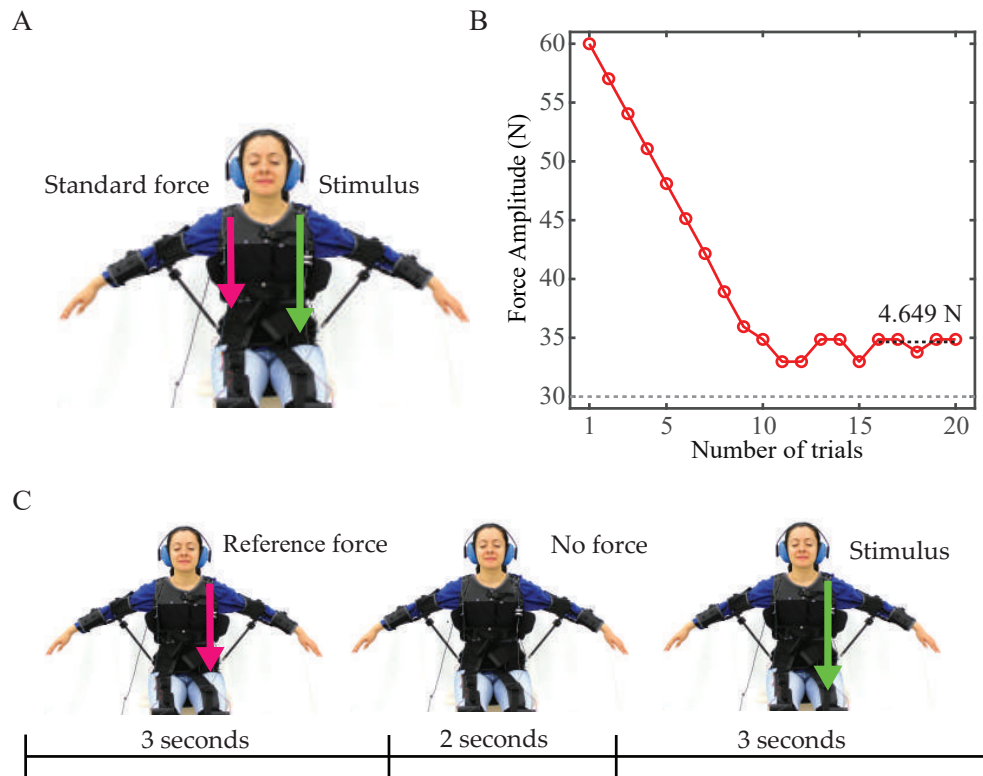
Figure 4.1 – kinesthetic feedback perception experimental flow. A) Experimental setup and schema of the application of the force for the Just Noticeable Difference experiment with the standard force (pink) and the stimulus (green). B) Exemplar results of the staircase method from one participant using the standard force of 30 N on the front torso. The dashed black line represents the average over the last five trials C) Testing procedure for the Steven's power law experiment with a schema of the reference force (pink) and the stimulus (green), here applied on the left side, and timing. The reference force and the stimulus were applied on the same side, alternatively between right and left.

10, 20 and 30 N). The standard force was applied on one side of the torso, and on the other side, a proposed stimulus was given simultaneously (see Fig. 4.1 A). The standard force and the proposed stimulus were applied simultaneously on either side of the upper torso for three seconds. The proposed stimulus amplitude started at twice the amplitude of the standard force. After the standard force and the proposed stimulus were applied, the participant then verbally stated on which side they felt the stronger force. Depending on the participants' answer, the amplitude of the proposed stimulus was adjusted by a step corresponded to 10% of the standard force amplitude going down in a staircase method "two up, one down" for 20 trials for each standard force (see Fig. 4.1 B) [114]. If the answer was correct, the proposed stimulus amplitude was reduced by 10% of the standard force for the 10 first trials. For trials 11 to 20, the participant needed to give two successive correct answers for the proposed force to be reduced. The JND of each of the standard force amplitudes was calculated as the average force of the amplitudes from the last five trials [115]. Averaging among the two to eight last

trials did not influence the results. The forces were applied pseudo-randomly on the right and the left of the torso to ensure an equal number of pulls of the proposed stimulus on both sides. This experimental procedure was performed for first the front and then the back of the torso. A linear fit of the JND data was performed using *polyfit* function in MATLAB and the coefficient of determination was computed using the *rsquare* function.

The second experiment aimed at understanding the relationship between a given stimulus and what the user perceives. The objective was to find the coefficients of the Stevens' power law (*a* in Eq. 4.1) to determine if receiving kinesthetic feedback with the FlyJacket followed a linear progression over the proposed amplitudes and therefore matched with results previously found for vibrations [113]. For this test, the experimental setup remained the same as for the JND experiment. However, this time the participants received first a reference force of 15 N randomly on either the left or the right of their torso and then, after a two seconds break, a stimulus at the same place (see Fig. 4.1 C). The proposed stimuli *S* were 5, 10, 15, 20, 25 and 30 N. The reference force was applied for 3 seconds, followed by a 2 second break, and then the stimulus was applied for 3 seconds. The participant then verbally stated their estimate of the perceived force intensity *P* (N). They were told that the stimulus force could range from 0 N to 30 N, inclusive. Each stimulus was presented three times for a total of 18 trials. This experiment was performed both for the front and the back of the torso.

A linear fit for each participant in the log space was performed. The exponent *a* of the Stevens' power law (Eq. 4.1) was calculated as the slope of a linear fit of the logarithm of participant data (Eq. 4.2) [110]. The multiplier λ was calculated as the exponential of the y-intercept of the linear fitting in the logarithm scale.

$$P(s) = \lambda S^a (N) \tag{4.1}$$

$$\log P(S) = a \log S + \log \lambda \tag{4.2}$$

The significance of fit parameters *a* and λ were tested using Wilcoxon signed rank test. The detection threshold was computed as the y-intercept ($\log \lambda$) of the linear interpolation for the front and the back [116].

4.2.2 Results for the Just Noticeable Difference

The results of the JND experiment showed a linear trend of the perception over the standard force tested (5, 10, 20, 30 N) for both the front and back of the torso (Fig. 4.2). Results for the front and the back are comparable, and both are strongly correlated with a linear law. From a fit to all participants' data, the coefficient of determination of R^2=0.765 for the front and R^2=0.991 for the back of the torso. If the data point from one participant at standard force
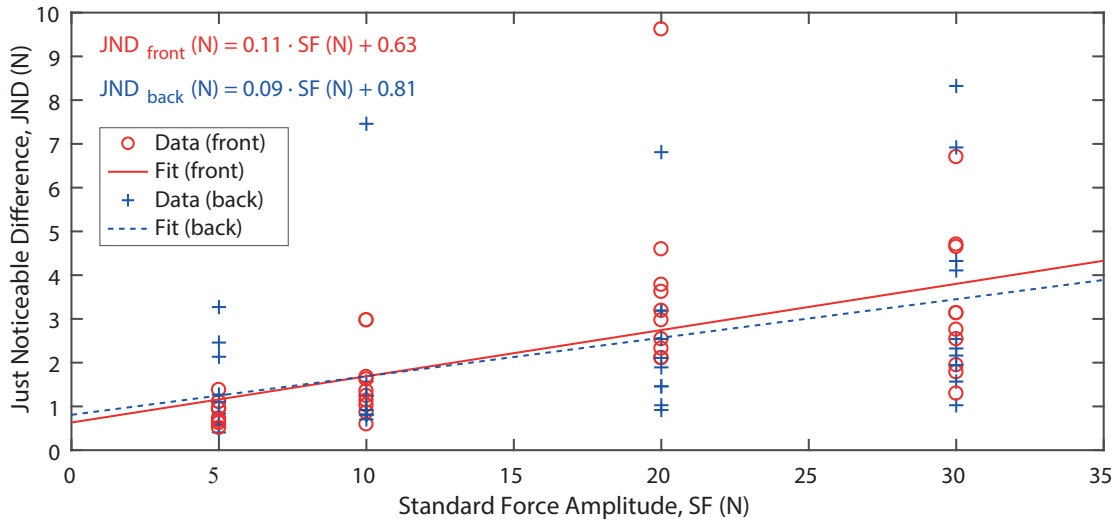
Figure 4.2 – Just Noticeable Difference as a function of Standard Force Amplitude (n=10). All participants' data for each standard force amplitude are presented for the front of the torso (red circles) and for the back (blue crosses). The mean of participants' linear fit of the data are shown for the front (solid line) and for the back (dashed line) of the torso.

amplitude of 20 N and JND of 9.62 N (see red circle sign in Fig. 4.2) is considered as an outlier — as its JND is greater than the mean of all participants (3.03 N) plus twice the standard deviation (0.85 N) – and is removed from the regression, the R^2 of the front becomes R^2=0.916. The extrapolation of the linear fit for each participant to the y-intercept predicts that the detection threshold should be 0.63 N ± 0.70 (mean ± SD) for the front and 0.81 N ± 0.81 for the back. However, further tests should be performed to confirm this predicted threshold difference between front and back. Following the linear law, the JND for any standard amplitude can be predicted as this threshold plus 10% of the standard force, SF (the slope of the linear fitting is 0.11 ± 0.08 for the front and 0.09 ± 0.060 for the back of the torso). This linear fitting over all the participants has a significant trend for both the front ($p = 0.0020$) and the back ($p = 0.0039$). With the exception of the 5 N and 10 N standard force applied to the back, the standard deviation among participants was small (6% of the standard force amplitude). For the two exceptions, the standard deviation across participants was approximately 20% of the standard force amplitude.

4.2.3 Results for Stevens' Power Law

The results of the Stevens' power law experiment (Fig. 4.3) show that participants' magnitude perception for proposed stimulus followed a linear law for stimuli applied to the front and the back of the torso. The computed fits for both the front and the back of the torso demonstrated that the perceived magnitudes follow a linear law with Stevens' exponents close to one (a_{front}= 0.97 ± 0.24 and a_{back} = 1.16 ± 0.36, mean ± SD). The correlation with a linear law is strong as the coefficient of determinations of the linear fit are close to one (R^2=1.000 for the front and
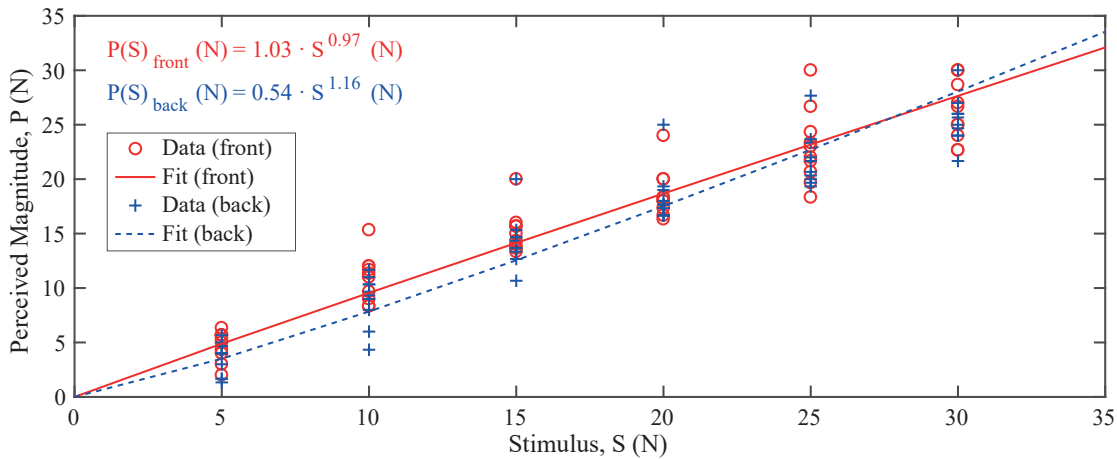
Figure 4.3 – Perceived magnitude as a function of stimulus from the Stevens' power law experiments (n=10). All participants' data for each stimulus are presented for the front of the torso (red circles) and for the back (blue crosses). The computed Steven's power equations obtained from the average of participants' fit parameters are shown for the front (solid line) and for the back (dashed line).

R^2=0.999 for the back). However, the multiplier λ doubles between the front (λ_{front}=1.03) and the back (λ_{back}=0.54) of the torso. Therefore, for the front, users perceived the increase in force linearly and at the same amplitude as intended. In contrast, the measured slope was steeper for the back than the front, with the two lines crossing at 27 N. Therefore, users perceived a lower force for lower stimuli (less than 27 N) and a higher perceived force for high stimuli (greater than 27 N) on the back.

4.2.4   Discussion

Our perception studies demonstrate that the information transmitted to the user's torso by the kinesthetic force feedback will be perceived as intended by the command. The kinesthetic feedback perception also follows a linear tendency for both the JND and the perceived magnitude, which corroborates with similar research on vibrotactile feedback [113, 115, 116]. The JND results show that the minimum force difference a user of the FlyJacket can perceive scales linearly with the amplitude of the given forces. Users will not perceive differences in force lower than 10% of the stimulus. Therefore, force feedback indications should have a difference in amplitude larger than this threshold. The perceptions for the front and the back of the torso are comparable with a slightly higher detection threshold for the back. The perception of force on the back of the torso is also more variable among participants at lower amplitudes than greater ones. The results of the experiment to determine the coefficients of the Stevens' power law showed that users perceive forces at an intensity similar to the given stimulus, nevertheless, similarly to the JND results, at a slightly lower intensity for the back than the front.

The differences between front and back for both perception experiments could be due to a difference in sensitivity between the front and the back of the torso [117]. Another possibility is that the lever arm of the back cables is smaller than for the front cable, resulting in a smaller applied torque for the same force stimulus. However, it is unclear how much influence this torque difference has on perception.

We used the results of these experiments to validate the parameters of the quadratically-shaped force guidance curve (see Eq. 3.4 from Chapter 3) that will be used in the flight task. As a reminder, this force guidance curve gives a weak force when the error is small and a strong force when the error is large and is perceived as designed according to the results of the perception experiments. The perception of the minimal force difference is 10% of the stimulus. The slope of the quadratic term was set at 30%. Therefore, the current guidance force is compelling enough to affect the user, and its changes over time can be perceived by the user. The minimal force threshold that participants could feel was approximately 0.7 N, which is the force they would receive with an error of 2.2 m. This corresponds to approximately the half of the mean RMS error over all participants that took part to the user study presented in Chapter 1. Both the JND experiment and the Stevens' power law experiment showed no significant difference in perception between the front and the back of the torso. Therefore, the command can be set identically for the front and the back motors. As the experimental results of the perception experiment justify the parameters of the quadratically-shaped curve, which was found to have improved the performance during a short flight task, we retained the same parameters for our longer flight task on training.

4.3 Performance Improvement during a Flight Task

In Chapter 3, we demonstrated that having kinesthetic guidance, by correcting the torso position when flying, increases the user's performance in comparison to flying without any guidance. The best type of force profile was found to be quadratically shaped as it provided a weak guidance when the error was small (< 4 meters; for reference, the wingspan of the drone is 0.96 meter) and a strong guidance when the error was large (> 10 meters). Having a kinesthetic guidance was also valued by participants. With this user study, we sought to determine how kinesthetic guidance influenced performance over an extended period of time (9 minutes of flight instead of 2.5 minutes for the previous study) and if the user retained the control skills when the kinesthetic guidance was removed. Results would determine if the training time could be reduced using kinesthetic guidance, what the appropriate amount of training required would be, and whether the user retained the skill acquired with the kinesthetic guidance when the guidance was removed. To evaluate these questions, a user study was performed on participants in which they were asked to perform a flight task of following a trajectory composed of waypoints (wp) similar as the one described in Chapter 1.
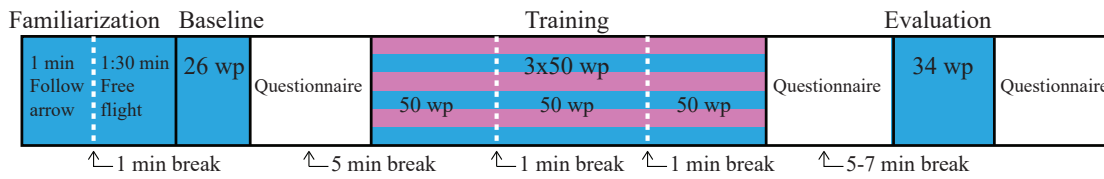
Figure 4.4 – Flight experiment protocol, indicating the tasks performed without guidance (blue) and with guidance (magenta). During the training, eleven participants flew with guidance and nine participants flew without guidance. wp: waypoint

4.3.1 Description of the Experiment

In total, 27 participants took part in this study, out of which data from 20 participants were used (12 males, 8 females, age 25.85 ± 4.17 years; mean ± SD). Of the 20 participants, eleven received kinesthetic guidance during the training task and nine flew without any kinesthetic guidance. Nine of these 20 participants also took part in the kinesthetic feedback perception experiment. Of the seven participants excluded from this study, five participants could not finish the experiment due to feelings of dizziness, one participant had to stop because of technical problems with sensors, and one participant stopped the experiment after the training as he was unable to control the drone. The standard deviation of the performance of this last excluded participant over the 150 waypoints of the training task was 24.40 m, which is six times greater than the mean of the standard deviation of the other participants flying without feedback (4.55 m).

Participants began the study by completing a questionnaire about their physical traits (height and weight), handedness (left or right), visual acuity, hours of physical activities, and experience in playing video games and piloting remotely an aircraft. Then, the participants wore the FlyJacket with the passive arm support and sat on a stool (as in Fig. 3.1 in Chapter 3). They wore VR goggles (Oculus Rift), which provided the visual feedback of the simulated environment. The movements to control the drone were demonstrated to them by the experimenter, and the experimental protocol was explained (see Fig. 4.4). Participants began with a short familiarization of the flight movements and simulator without any kinesthetic guidance by performing the same training session described in Chapter 1.

After this short familiarization phase, participants started the next phase of following waypoints spaced apart by approximately 30 meters (Fig. 3.3). Experimenters explained to the participants that the distance between the drone and the center of each cloud was recorded and that their goal was to minimize their error over all the waypoints. The order of the maneuvers to reach the waypoints (up, down, left, right) was randomized between trials, but the number of maneuvers was always the same between participants. Participants had to perform three types of tasks named "Baseline", "Training", and "Evaluation" (see Fig. 4.4). Their first task "Baseline" was to fly through 26 waypoints, which took approximately a minute and a half, without any kinesthetic guidance. This task was used to calculate their baseline performance. Next, the participants completed a questionnaire to rate on a Likert scale (from 1 to 7) how

strongly they agreed with the following statements concerning their subjective control ability and flight sensations (1 being strongly disagree and 7 strongly agree):

1. "I felt as if I was flying,"

2. "I had the feeling of controlling the flight trajectory,"

3. "The training was clear and sufficient,"

4. "I enjoyed the experiment,"

5. "I felt dizzy,"

6. "I felt some physical discomfort,"

7. "The setup was comfortable,"

8. "My movement did not feel constrained during the flight."

The second part was the training phase. It was composed of three sessions of 50 waypoints each (around 3 minutes per session), with approximately a one minute break in between each session where the participant could remove the VR goggles and rest. These short breaks were enforced to reduce the probability of motion sickness due to the VR goggles [87]. participants either flew with kinesthetic guidance (n=11) or without kinesthetic guidance (n=9). The kinesthetic guidance setup of the FlyJacket was the same as the one described in Chapter 3. The kinesthetic guidance corrected the user's torso position by pulling it toward a position that would allow them to fly a pre-calculated trajectory passing through the waypoints. The force rendered to the torso, F_{quad} was quadratically proportional to the distance between the center of the waypoint and the drone, Δx (see Eq. 3.4). The same force command was given for the front and the back of the torso.

After finishing these training tasks, both groups (with and without the kinesthetic guidance) again filled out a questionnaire about their flight experience. The questionnaire was the same as the one given after the baseline task, but additional questions about the kinesthetic guidance were given to the group that had received it. The additional statements were the following:

9. "Apart from the haptic feedback, my movements did not feel constrained during the flight,"

10. "The haptic feedback helped me to correct my trajectory,"

11. "The haptic feedback was on time with the flight."

In addition, they had to rate on a Likert scale from 1 (too weak) to 7 (too strong) the overall force intensity and for each body side (front, back, right, left). Participants also completed

a NASA-TLX test, which measures the perceived amount of workload during this flight task [107].

The third and last task of this study was the evaluation task — a flight through 34 waypoints without participant guidance for both groups. The aim of this part was to determine how well participants performed when the participant guidance was removed in comparison to participants that did not receive any participant guidance. At the end of this task, the participant had to fill the questionnaire about the flight sensations once more.

The baseline score of each participant was calculated as the RMS of this error over the 26 waypoints of this task. The flight performance for the training and the evaluation task was evaluated as an error reduction relative to the performance achieved during the baseline task. This error reduction was computed by subtracting the error at each waypoint of the training task or the evaluation task from the RMS error of the baseline task. A larger error reduction means a greater improvement in performance. The data of the training and the evaluation tasks was fit with a linear curve (using the *polyfit* function in MATLAB) to determine the learning curve for these two tasks. The difference between the groups and their statistical significance were evaluated with a Wilcoxon Rank Sum test and Wilcoxon Signed Rank test.

4.3.2   Results of the Flight Experiment

The error reduction during training and evaluation tasks was evaluated for each participants' flight through 150 wp during the training task and through 34 wp for the evaluation task (Fig. 4.5). The slope of the linear fitting of the data was similar for both group with 0.0040 ± 0.0124 m/wp (mean $\pm$ SD) for the group flying with guidance and 0.0062 ± 0.0221 m/wp for the group flying without guidance ($p = 0.970$). Both groups show no statistically significant improvement over time ($p = 0.365$ for the group flying with participant guidance and $p = 0.570$ for the group flying without guidance). The performance improvement of the training task is immediate with an offset of the linear fitting of 5.43 ± 6.40 m for the participants training with participant feedback and 3.58 ± 3.48 m for the participants training without participant feedback. Both improvements are statistically significant ($p = 0.0010$ and $p = 0.0039$ respectively), but the difference between the offset of both groups was not significant ($p = 0.880$).

After the training, both groups completed an evaluation task without guidance to assess whether they retained the skills acquired during the training. The participants that trained without guidance continued to improve their performance at, surprisingly, a faster rate of 0.0296 ± 0.0994 m/wp than during training. Comparatively, participants that trained with guidance started the evaluation task with a better error reduction on average than at the end of the training with an offset of error reduction of 7.24 ± 6.48 m. They started also with a better mean performance than participants that trained without feedback (4.89 ± 6.08 m). However, over time their performance degraded without participant guidance with a rate of -0.0416 ± 0.0778 m. The difference between the trend and offset for the two curves are not significant ($p = 0.197$ for the slopes and $p = 0.0965$ for the offsets) and their performance tended towards
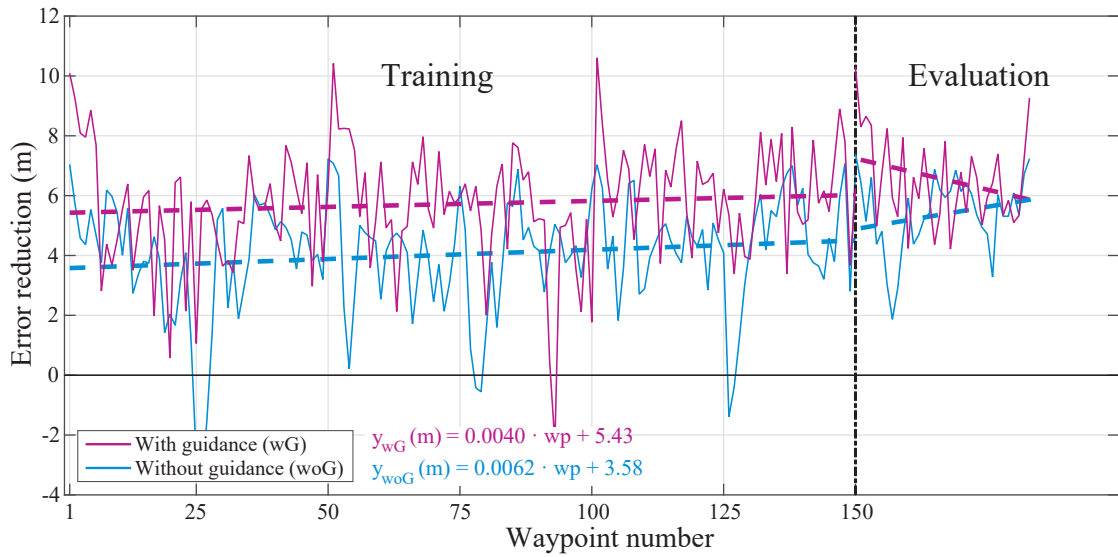
Figure 4.5 – The error reduction for both the training and evaluation flight tasks, relative to the RMS error of the baseline task, for participants that trained with guidance (n=11, magenta) and without guidance (n=9, blue). Participants also had a five to seven minute break (dashed line) to fill a questionnaire between the end of the training task and the beginning of the evaluation task.

the same level of performance as the participants trained without guidance at the end of the evaluation task.

When flying with the participant guidance, the same force was given to the front and back of the torso for the same level of error. The results of the experiment on the participant perception described earlier on this chapter demonstrated a slightly lower perception of the magnitude of a given force applied to the back in comparison to the front. Therefore, we compared mean performance during training between "up" and "down" maneuvers (Fig. 4.6). For participants that trained with guidance, the error reduction was statistically higher ($p = 0.049$) for the "down" maneuvers (7.45 ± 2.30 m) — when the participant guidance is pulling on the front of the torso — than for the "up" maneuvers (4.51 ± 3.62 m) — when the participant guidance is pulling on the back of the torso — during the training task (Fig. 4.6). There is no significant difference in error reduction in any directions for the participants that trained without guidance (Fig. 4.6). This corroborates the results found with the participant perception experiment that the participants feel the participant feedback applied on the front of their torso with a higher magnitude than on the back.

The questionnaires completed by the participants after each task assessed their subjective feeling on their ability to control the trajectory and the comfort of the flight. No significant differences were found between the group training with guidance and the group without guidance. Adding participant guidance to the flight did not physically constrain the user or prevent them from enjoying the flight tasks. There were also no significant differences in
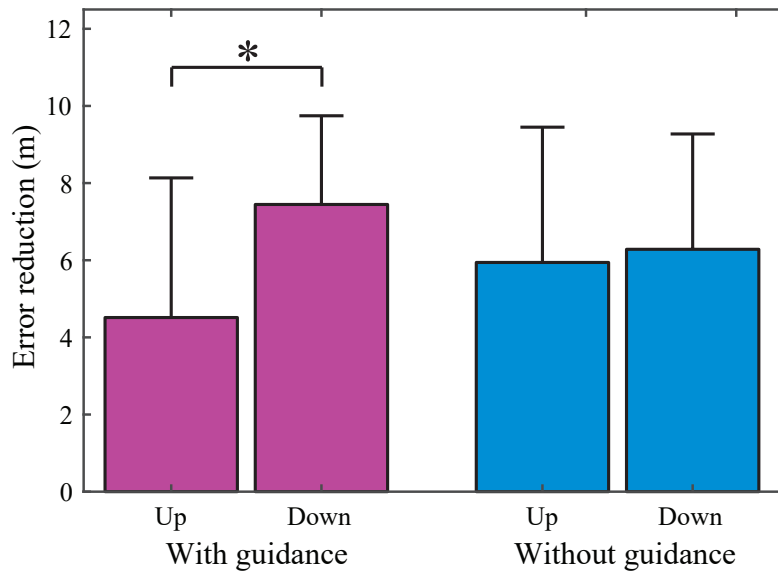
Figure 4.6 – Mean and standard deviation of the error reduction for "up" and "down" maneuvers during the training task for participants training with participant guidance (n=11) and without participant guidance (n=9). With participant guidance, an "up" maneuvers corresponds to a pull on the back of the torso, and a "down" for a pull on the front of the torso. Asterisk (*) denotes p < 0.05.

participant responses on the questionnaire's statements 1 to 8 among the baseline, training and evaluation tasks. From responses on the NASA-TLX questionnaire, there were no significant differences in workload between the group flying with the participant guidance and the group flying without guidance with a workload of 54.96 ± 19.19 (on a scale from 1 to 100) for the people flying with feedback and 51.25 ± 19.26 for people flying without feedback. The participant guidance does not alleviate or aggravate the subjective workload. There was no significant correlation between the physical characteristics (e.g. age, BMI, vision, handedness, gender, hours of physical activities per week) or their experience with VR goggles, piloting remotely an aircraft, or computer gaming of the participants and their performance of piloting the drone independently than if they receive an participant guidance during their training or not.

4.3.3   Discussion

During a training period of approximately nine minutes, participant guidance did not seem to help users learn the flying task faster than without guidance. However, participant guidance improved performance instantaneously without increasing the workload on the user or degrading the sensation of flight. Therefore, flying with the participant guidance could be a useful assistance mostly for naive users as they can immediately start flying with more precision. By averaging the performance of the participants, data show a trend of improvement over time with a better performance for the group training with the participant feedback and

also a better average performance during the evaluation. However, significant effects of the training over time were hard to assess because of the large variance of performance among participants. This large variance was present for both groups and is therefore independent of the participant guidance.

One surprising behavior is the higher learning rate of the participants that were trained without the guidance during the evaluation task. One hypothesis is that they still had room for improvement and therefore continued to learn. Their faster learning rate, regarding the training task, may be because flying during a long period is tiring and the five to seven minutes break between the training and the evaluation tasks allowed them to recover. A step in the error reduction is also seen between the baseline task and the training task, where participants had a five minutes break to fill the questionnaire. Apparently, a few minutes break may have influenced the error reduction during the next flight task and seemed to have a positive effect on the performance of both groups. However, the effect of these breaks is unknown, and specific experiments should be performed to understand precisely their influence on the learning process of participant, which is out of the scope of this article.

The perception of the participant feedback had an influence on the error reduction. Indeed, from the perception experiments described earlier on this article, the minimum force difference is slightly but not significantly smaller for the front than for the back of the torso. Also, the magnitude of a given stimulus is perceived slightly larger on the front than on the back. These differences of perception were observed on the performance of the participants training with the participant feedback as the error reduction was significantly higher when the haptic cue was given on the front of the torso than on the back. This difference was not observed in the group of participants flying without the participant feedback. As apparently even non-significant variations on the perception lead to changes in performance in the flight task, quantification of the minimal force that the user can perceive is important. It was observed in the perception experiment that participants could not discern guidance forces below an error of 2.2 m (see section 4.2.4). Although it has been demonstrated in the previous chapter that having a weak guidance force for small error prevents the user to be too frequently perturbed by the force and results in better performance than a hard guidance, possibly the force curve could be slightly tuned to still give light but perceivable guidance below this threshold.

Additional points should be considered to explain how participants had the same learning rate with and without guidance. The tuning of the guidance force was set on static perception experiment. Perhaps dynamic torso behavior somehow influenced force perception and should be taken into account in the force profile.

As the performance of the participants that trained with guidance decreases over time during the evaluation task, we hypothesize that participant got dependent on the feedback and relied on it to flight instead of learning. In addition, the results showed a large variation in performance between the participants. To tackle both of these issues, a possibility to improve the flight performance is to implement a personalized participant guidance i.e. the

stimulus intensity and frequency would be adapted to each user and could also adjust over time regarding the performance and confidence of the user in the flight. This implementation could improve the performance of individuals that were less responsive to the participant guidance and reduce the variance of the overall performance. For each of these proposed approaches, subject experiments should be conducted to determine how they individually affect the learning rate and skill retention over an extended period of time.

4.4 Conclusion

The work presented in this chapter shows that a cable-driven force feedback to the human torso is perceived linearly with the applied stimulus. These results corroborate with previous experiments on the perception of vibrotactile feedback [113]. The force perception was observed to be slightly lower on the back of the torso, both during the perception studies as well as during the flight experiments. This imbalance can have repercussions in the flight performance and can be addressed by appropriately modulating the magnitude of the applied force with larger control gains for the back motors. We also demonstrated that a guidance-based kinesthetic feedback provided through the FlyJacket boosts user performance during the training phase of a path-following task. However, this improvement in performance was not significantly greater than training without feedback, and these gains might subsequently be lost when this feedback is taken away. This could be indicative of poor skill retention, possibly due to users developing a dependence on the guidance or "slacking" [118]. More thorough retention tests need to be conducted to assess and distinguish the short-term and long-term effects of the flight training.

In this chapter, a kinesthetic feedback guidance was explored to understand its effect on user performance, motor learning, and skill retention. The perception test performed investigated stimuli in static positions. As a follow-up, we are currently carrying out a participant study to examine the dynamic response of a human torso when it is subjected to a continuous sinusoidal kinesthetic stimulus. The stimulus is provided to the torso via the same motorized cable driven system used in the perception and motor learning studies shown in this chapter. More specifically, we are interested in establishing relationships among torso movement, the applied stimulus frequency, the location of the cable attachment points on the torso, and inter-subject anthropometry. Furthermore, we are developing a neuromechanical model to capture the dynamical torso response to input stimulus and quantify cognitive alertness and mechanical passivity as model parameters for each participant. Separately, we will be investigating dynamic torso perceptiveness i.e., the dependence of threshold perceptible force on velocity for subjects in motion. Our aim is to use the model to predict the response of each individual participant in a flight teleoperation task and the dynamic perception tests to ascertain the type of feedback that should be provided to them to augment the rate of their motor skill acquisition.

The FlyJacket with kinesthetic guidance can be used to test different approaches to target

improved human-robot interaction. One of the methods by which augmented feedback can be provided, without the learner developing dependency effects, is error amplification [119]. The merits of this approach are supported by studies which show that learning through the modification of movement patterns, is an error informed process [120, 121]. Compared to guidance-based feedback, amplifying errors results in relatively permanent retention of skilled performance for certain types of tasks [122] due to the users active participation in error-detection. Error amplification can be implemented using different strategies such as negative impedance [123], where the user would be pulled away from the trajectory. Alternatively, an offset could be implemented equal to the average initial error of each subject to remove eventual direction bias, e.g. if users have a tendency to be positioned too far on one side with respect to the trajectory [124]. The benefits of each of these strategies would need to be tested with a user study comparing the different techniques. Nevertheless, following [122], as flying following a trajectory is a continuous, non-rhythmic, spatial task, the recommended strategy to adopt is a fixed guidance.

Still using the same hardware setup, any type of guidance discussed above can be implemented to prevent the drone from colliding with an obstacle or from performing dangerous maneuvers that are outside the flight envelope, such as flying at a too high angle of attack. In these critical conditions, the movements of the user can be restricted using kinesthetic guidance.

Alternatively, one could employ passive kinesthetic feedback, a type of feedback that combines certain favourable attributes of guidance and error amplification to hinder erroneous joint movement. Here, a system of brakes and clutches can be embedded into the existing FlyJacket to have a more body-conforming design [39, 125]. When using passive kinesthetic feedback, users are forced to identify their error to correct it rather than the error being corrected by the active haptic feedback. Studies have shown that if a user has a heightened awareness of their mistakes, this awareness could aid the motor learning process, particularly as it related to skill retention.

5 Tactile Feedback: Soft Haptic Device to Render the Sensation of Flying like a Drone

5.1   Introduction

In the two previous chapters, kinesthetic guidance was implemented in the FlyJacket. We demonstrated that having guidance while flying improves the flight performance and is perceived favorably by the users. In the next two chapters, we are exploring the implementation of tactile feedback to render the flight sensation instead of providing guidance. The aim was to study the effect of tactile feedback on the human perception, immersion into the flight and performance. To render the adequate flight sensations while remaining a portable exoskeleton, a new type of tactile actuator needed to be developed.

Haptic devices that provide tactile feedback to the fingers and hands to render grasping sensations have proven to be a compelling way of transmitting information and enhancing training and performance of a variety of tasks. However, many applications require the hands to be available for manipulation or interaction. This motivates the study of tactile feedback to other parts of the body, such as the arms and torso. Another potential benefit of tactile feedback located on parts of the body other than the fingers and hands is that it could increase user state awareness in a virtual or teleoperated task in which relevant sensations should
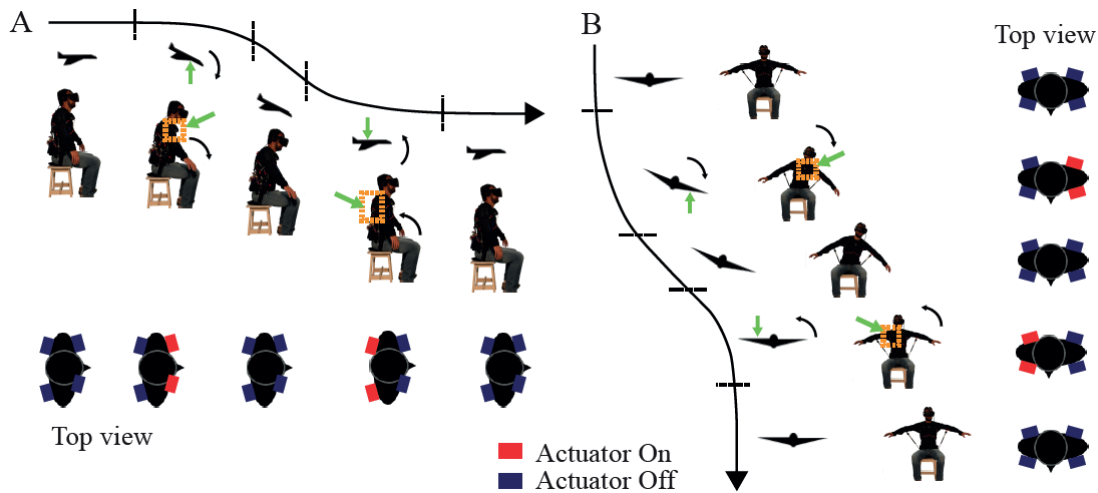
Figure 5.1 – Forces rendered on the torso relating to the drone orientation and schema of the actuated tactile devices. The actuated devices are highlighted in red on the top view of the user. A) During pitch maneuvers. B) During roll maneuvers.

occur on those parts of the body. For example, it has been shown that immersion in a virtual world can be improved with a tactile feedback vest using vibrations [126, 127] or pneumatic actuators [47].

In this chapter, we include in the FlyJacket tactile feedback on the torso to enhance realism and increase the flight awareness. In prior work, vibrotactile vests have been used to communicate information to pilots, e.g. [128]. Tactile feedback on the torso has also been used to connect between humans located remotely from each other [129, 130, 131] and enhance emotions [132, 133]. Various actuators have been used to achieve tactile feedback on the upper body. Shape memory alloy actuators [134] and vibrotactile actuators [135] have been used for navigation tasks. Pneumatic actuators located on the torso [136] and vibrators located on the limbs [137, 138] were used in rehabilitation, as well as for motor learning tasks [139]. Products dedicated for gaming have also used pneumatics (e.g. Tactsuit from bHaptics Inc., Daejeon, Republic of Korea) and vibration (e.g. TN game vest from Phantomsense, WA, USA). A whole-body haptic system used blowing air to create the sensation of navigating a windy environment [140].

In order to enhance flight awareness, sensations of the air pressure during drone movements could provide valuable feedback to help the user perceive the drone state. In most prior work, tactile feedback was provided using vibrotactile actuators. These have the advantage of being small and lightweight, which makes them easy to integrate into wearable devices. However, the vibration sensation cannot realistically transmit the sensation of skin compression as is required to recreate the air pressure felt by the drone. Another approach is using active pneumatics. Such device could transmit compressive force normal to the skin. However, pneumatic actuation requires valves and an air source, which is currently cumbersome and complex to integrate in a portable system.

The FlyJacket aims to be used for drone rescue missions or inspection and therefore should be portable to be deployable in the field. We present a novel approach to render tactile feedback on the torso in order to improve the control of a drone and increase the flight awareness. The tactile device presented in this chapter combines the advantages of a soft device that is conformable and safe to interface with the human body, while being actuated by motors in order to be responsive and portable. The device gives cues on the drone orientation by rendering air pressure on the torso proportional the centripetal acceleration of the drone via a soft air pouch pressed against the skin. The forces rendered on the user are shown in Fig. 5.1 A for pitch maneuvers and in Fig. 5.1 B for roll maneuvers.

5.2 Device Design
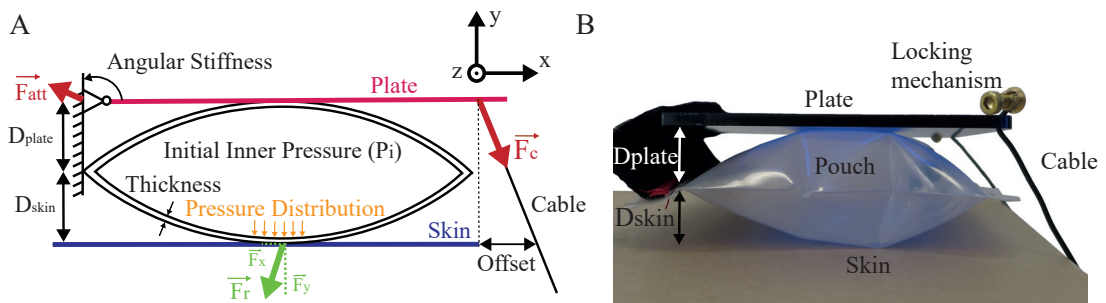
Figure 5.2 – Tactile device. A) Analytical model of the soft air-filled pouch being compressed by the plate onto the skin. B) Image of the mechanism.

To render the sensation of distributed pressure against the body, we developed a tactile device composed of soft, closed air pouches that are compressed against the skin by cables driven by electric motors (Fig. 5.2).

The portable actuation via motors is less cumbersome than a pneumatically actuated device. The inner pressure of the pouch can be varied for different applications using more or less inflation, which gives this technique an advantage over other soft material approaches such as foam. In addition, pouches can be deflated during transportation to gain space. Furthermore, the holding structure, in this case the soft exoskeleton, does not need to be tightly attached to the body; the cables allow a large range of motion to generate compression. In order to make the compression of the pouch against the skin relatively uniform, the cables do not pull directly on a pouch's corner or edge, but rather on a rigid plate situated on top of it as shown in Fig. 5.2. If the cables were directly attached to the pouch, the pouch would deform, and the force transmission efficiency would decrease. One end of both the pouch and the plate are attached to the exoskeleton, and on the other end the plate is attached to the cables.

In order to design the force transmission from the actuator to the skin and make the sensation as realistic as possible, two output variables are considered: the force vector (magnitude and

direction), and the pressure distribution. First, we optimize the change in the force vector that occurs between the uncompressed and compressed state. The aim is to effectively minimize the motor torque and limit losses on the exoskeleton, to avoid applying unnecessary reaction forces to other parts of the body. The direction of the force is an important component. Force in the y direction (according to Fig. 5.2) applies normal pressure on the skin, triggering Merkel mechanoreceptors [141]. Forces in x and z directions induce shear forces, which trigger Ruffini mechanoreceptors. Stimulating multiple types of mechanoreceptors raises the awareness of the user. The force magnitude and pressure distribution are related; humans are sensitive to magnitudes of forces as well as the contact area [142]. Ideally, no pressure should be applied by the pouch on the skin before compression, and the area in contact with the skin once the pouch is fully compressed should be as large as possible to have the largest spreading possible and therefore maximizing the change of sensations.

5.3 Modeling and Simulation

5.3.1 Model and Simulation Procedure

In order to study the influence of the tactile device parameters on both outputs (the force vector and the pressure distribution) and determine the best parameters, a simulation of the device was implemented using SOFA (Simulation Open Framework Architecture) software [143] as shown in Fig. 5.3.

The pouch is represented by two rectangular thin shells sealed together at the four sides. These two layers are defined by a mesh of 10×8 triangles (Fig. 5.3 A). The number of triangles for the mesh was chosen as a compromise between precision and simulation duration. Refining the mesh further did not substantially change the results, while greatly increasing the time required for each simulation.

The pouch is attached on one side to a rigid fixation point. The distance between the pouch fixation and the skin is D_{skin} (see Fig. 5.3 B); this represents how closely the jacket is tightened to the body. Due to the comparatively high compliance of the pouch, the skin is represented by a non-deformable and flat plane. It consists of two gridded planes: a reference plane that does not move and a second plane of very high stiffness ($10^5 \frac{N}{m}$). The small displacements between these two planes, due to the force applied by the pouch, are used to calculate the force on each grid element. The upper plate used to compress the pouch is also non-deformable and attached at a distance D_{plate} from the fixation point of the pouch. Opposite these attachment points, two cables, one attached at each corner, pull on the plate. The interaction between the upper plate and the pouch, and the skin and the pouch is modeled as Coulomb friction with μ = 0.5.

At the start of the simulation, the pouch is inflated to an initial inner pressure with no force on the cables. For the remainder of the simulation, the amount of air in the pouch remains constant, and the pressure in the pouch depends on the volume of the pouch according to
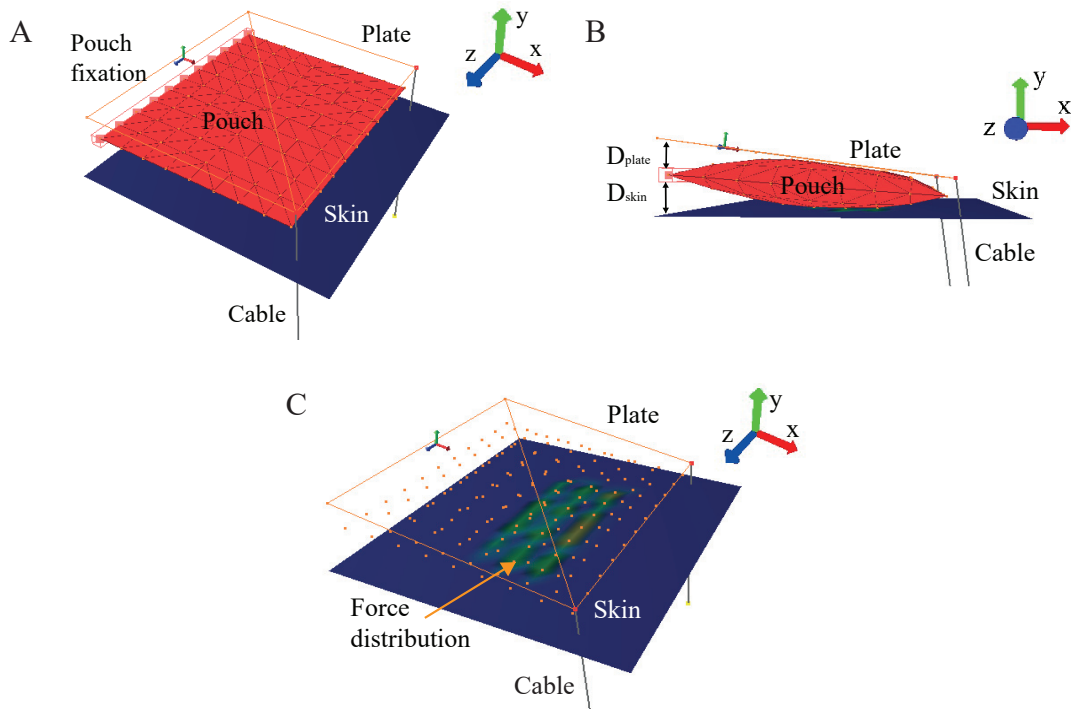
Figure 5.3 – Simulation of the air pouch being compressed against the skin by a plate, using SOFA software. A) Top perspective view of the pouch, with the triangular meshing of the pouch (in red). B) Side view of the inflated air pouch (in red) being compressed by the plate. C) Top perspective view of the force distribution on the skin during compression. Only the meshing points of the pouch are visible (orange dots) to enable visualization.

Boyle's law (i.e., the product of pressure and volume remains constant). The compression of the pouch is simulated as a cycle that starts from no force (0 N) on the cables, increases gradually to 14 N, and then decreases to 0 N at the same rate. The cables pull from a fixed pull point, which is assumed to be the location of the cable routing on the jacket. The forces on the skin in x, y, and z directions are recorded during the simulation. The pressure distribution on the skin is recorded using the normal force on each element of the grid divided by its area.

5.3.2 Simulation Parameters and Results

The parameters are described in Table 5.1, and the effects of varying these parameters on simulation results are shown in Fig. 5.4. The parameters were varied independently, and the resulting force vectors and pressure distributions were obtained using the simulation in SOFA. Parameters were tested in a range of value that were physically possible to be used when building the hardware. The simulation was done quasi-statically, so dynamic forces are not reflected in the results. The physical characteristics of the pouch – the Young's modulus of the material and the thickness – where also tested but did not have a major influence on either the force vector or the pressure distribution, for a realistic range of parameters.

Table 5.1 – Parameters of the Air Pouch

Parameters	Range tested	Device parameters
Thickness (m)	0.0005 - 0.005	0.0005
Young modulus (GPa)	0.05 - 4	0.3
Initial Inner Pressure, P_i (kPa)	1 - 10	6
Angular Stiffness, AS ($\frac{\text{Nm}}{\text{rad}}$)	0.5 - 10.5	2
Cable offset in X (m)	0 - 0.32	0
Cable offset in Z (m)	0 - 0.2	0
D_{skin} (m)	0.005 - 0.021	0.0011
D_{plate} (m)	0.002 - 0.018	0.01

The plate can be thought of as a lever. The torque applied by the cables is balanced predominately by the pressure of the pouch but also by the small angular stiffness at the attachment point. The distribution of contact of the pouch on the plate, which is influenced by the pouch internal pressure and the mounting distances, D_{skin} and D_{plate}, determines the effective radius of the force and contact area between the pouch and the plate. Given a particular cable force, the torque on the plate from the cables and therefore the reaction force required from the pouch, is maximized when the cables are perpendicular to the plate. All of these variables influence the force vector and pressure distribution on the skin.

The initial inner pressure of the pouch P_i influences both the resulting force and the pressure distribution (Fig. 5.4 A and C). When the initial inner pressure increases, the amount of air in the pouch increases, leading to different contact conditions between the pouch and the plate, as well as between the pouch and the skin. The torque applied by the cables is the same for these tests, but the change in contact conditions results in different force distributions on the skin. As the pouch internal pressure increases, the force applied to the skin increases (Fig. 5.4 C). On the other hand, as the initial inner pressure increases, the pressure distribution decreases; less of the surface of the pouch is in contact with the skin (Fig. 5.4 A) but the maximum pressure on one cell increases; the pressure is less distributed. Depending on the application and the desired tactile sensations, more weight can be given to the resulting force or the pressure distribution by varying this initial inner pressure.

The angular stiffness of the plate should be as small as possible in order to have the force produced by the cables be used to compress the pouch and not to rotate the plate. Both the resulting force and the pressure distribution decrease when the angular stiffness of the plate increases.

As in the case of increasing the initial inner pressure, both distances – between the pouch and the skin (D_{skin}) and the plate (D_{plate}) – have a trade-off between the resulting force and the pressure distribution; the force decreases when the distance increases (when the jacket is less tightly attached to the body) but the change in pressure distribution increases. These three parameters (P_i, D_{skin} and D_{plate}) can be set according to the desired sensations.
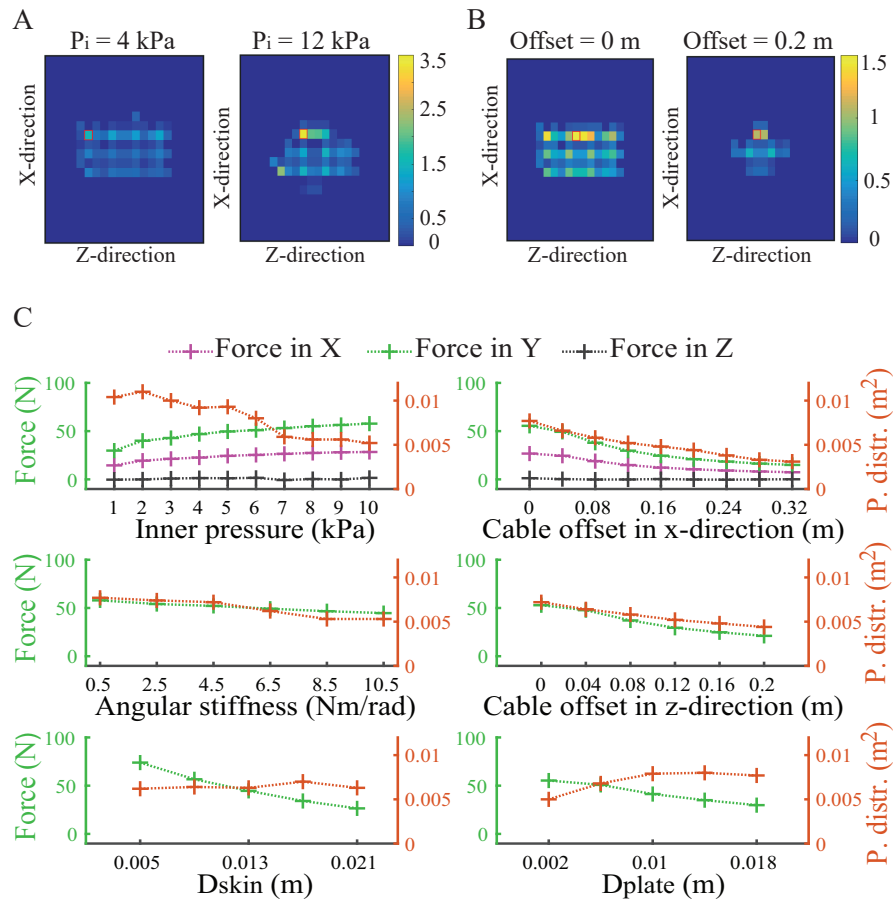
Figure 5.4 – Results of parameter variation in simulation. A) Pressure distribution (kPa) normal to the skin (in y direction) at maximum cable force for an inner pressure (P_i) of 4 kPa (left) and 12 kPa (right). B) Pressure distribution (kPa) normal to the skin (in y direction) at maximum cable force for no cable offset (left) and 0.2 m offset in x direction (right). C) Influence on the two outputs (force in y and pressure distribution) when varying each device parameters over their tested range. The first two graphs include the force component in x and z.

The offsets of the cables in the x and z directions influence the resulting force and the pressure distribution (Fig. 5.4 B and C). As the cables become more perpendicular to the top plate, more force is transmitted to the pouch because less force is lost to reaction forces from the fixation point of the plate. Angling the cables away from the perpendicular does not greatly increase the shear force (x and z directions), but it does decrease the normal force substantially, which is more critical to our application. Nevertheless, the current configuration already gives a substantial shear force in x direction because the compression of the plate is not vertical, but rather is done by rotating the plate.
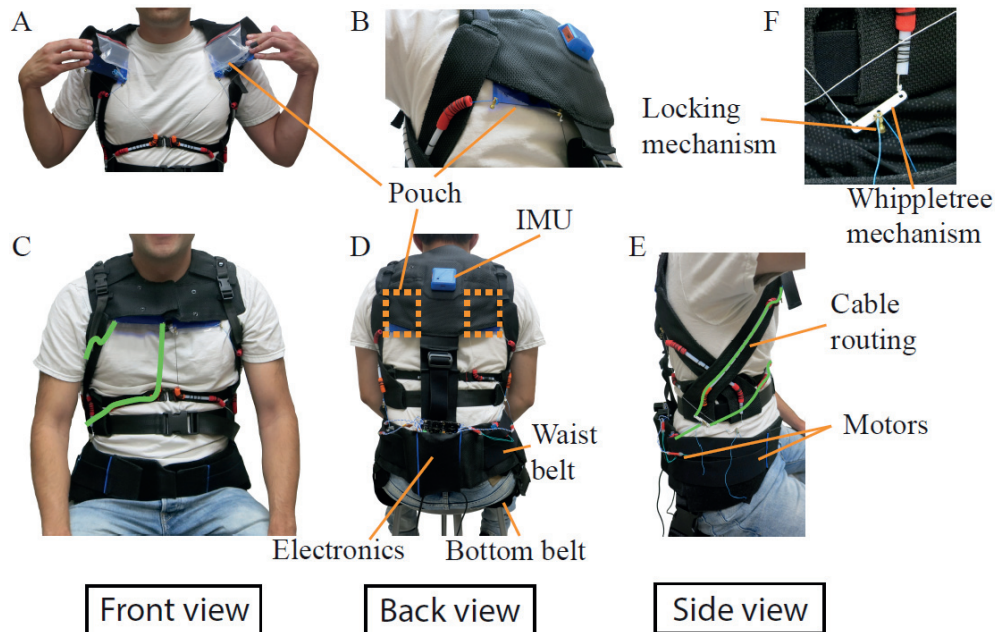
Figure 5.5 – Hardware implementation of the device in the FlyJacket. A) View of the front pouches. B) View of the left back pouch. C) Front view of the device. The cables of the left side are highlighted in green. D) Back view of the device highlighting the pouch placement. E) Side view highlighting the front cable routing in green. F) Whippletree mechanism to distribute the tension equally on both cables, and the locking mechanism.

5.4 Hardware

5.4.1 Implementation

The aim of the tactile device is to render the sensation of the centripetal acceleration of the drone to the FlyJacket user. Therefore, in order to give compressive forces on the torso when "pitching up", "pitching down", "rolling left", and "rolling right", four pouches are included in the soft exoskeleton.

The dimensions of the pouch need to be as large as possible in order to have the largest surface in contact with the body. However, this characteristic is limited by the space available in the soft exoskeleton. To determine the optimal size of the pouches, additional perceptional user studies would be required. Pouches were located on the torso so that the tactile feedback was collocated with the point of actuation on the user's body. They were placed on the upper torso as these parts remain more stable during torso movements compared to the lower part of the torso. Four pouches were used, as this is the minimal number which can render the sensation in all the flight directions. More pouches could give finer sensations, but would also increase the complexity and the weight of the device. Still, looking at the results of the user study described in Chapter 6, the pouch is sufficiently large (100 mm × 80 mm) to be clearly perceived by the user and transmit a noticeable sensation.

Two pouches are placed on the front part of the jacket (Figs. 5.5 A and 5.5 C). They are located on each side of the upper chest with the cables pulling against the torso to give the sensation of being compressed when the drone is pitching down. The other two pouches are placed on each side of the back as shown in Fig. 5.5 B and highlighted in Fig. 5.5 D to give the sensation of being pushed forward when the drone is pitching up.

Using the simulation results to inform the design, the following parameters for the device were selected and are summarized in Table 5.1. The pouch is made of Low-Density Polyethylene (LDPE) with a thickness of 0.5 mm and a Young's Modulus of 0.3 GPa, and it can be inflated and deflated easily via tubing closed with a removable cap. The compressive plate is made of acrylic in order to be both rigid and lightweight, and it has the same dimensions as the pouch. Both the pouch and the plate are connected to the soft exoskeleton with a piece of fabric (Fig. 5.2 B), which provides a low angular stiffness ($2 \frac{\text{Nm}}{\text{rad}}$) at the fixation point of the plate.

In cases where the force and pressure distribution response were the same with the variation of the parameter (such as cable offset in the x and z directions and the angular stiffness of the plate), the parameter was made small as possible within feasible manufacturing constraints. In other cases, the tradeoff between force and pressure distribution, as well as the manufacturing, was considered. An inner pressure of 6 kPa was used as a compromise between high force and large pressure distribution. D_{skin} and D_{plate} were also set in the middle of the tested range, to 0.0011 m and 0.01 m respectively, for the same reason. The cables should be oriented as perpendicular to the skin as possible to optimize the force transmission. However, as the cable cannot go through the torso, a perfectly perpendicular angle is not possible. Adding an extra band of material to the exoskeleton and a pulley below the pouch was tested as a way to achieve a more perpendicular angle, but due to the compliance of the textile, the pulley was pulled upwards toward the plate and off the skin, rather than pulling the plate down and applying force to the user. Thus, this modification did not show significant improvement for the force transmission. Instead, a wedge can be inserted between the compressive plate and the pouch in order to decrease the angle of the cable pulling on the plate and therefore increase the force applied on the skin (Fig. 5.6 C). The angle of the wedge influences proportionally the output force. An angle of 20 degrees was chosen for the hardware measurement as a proof of concept. The wedge is made of 3D-printed Polylactic Acid (PLA) plastic of the same dimension as the pouch and the acrylic plate.

In order to apply forces on the torso in the directions described in Fig. 5.1, the four electrical motors (DC22S, gear ratio 6.6:1, Maxon Motor, Switzerland) that pull on the cables are placed on the waist belt of the exoskeleton (Fig. 5.5 D). The cables, made of Dyneema (diameter 0.4mm, Spiderwire, SC, USA), are routed along the structure of the soft exoskeleton through Polytetrafluoroethylene (PTFE) tubes in order to limit losses due to friction (Fig. 5.5 E). The four motors can be actuated separately, and the control is performed by an Arduino Mega 2560 (Arduino, Italy) with a shield including two double H-bridge drivers (DRV8412, Texas Instruments, TX, USA). In order to be used in the field, the communication with the com-

puter is wireless using Bluetooth (module RN-42N, Microchip, AZ, USA). These electronic components are located in a pocket on the lower back of the exoskeleton (Fig. 5.5 D). In order to prevent the belt from moving when the motors pull on the cables, an extra bottom belt, passing under the person, was added to the exoskeleton. Because only one motor pulls on both cables connected to each compressive plate, a whippletree mechanism was inserted between the output of the motor and the separation of the cables on their routing tubes (see Fig. 5.5 F). This mechanism is used to distribute equal tension on the two cables. To reduce as much as possible the parasitic reaction forces felt at the mounting location of the motors and along the cable routing, padding made of foam was added to the waist belt and the side panels of the jacket. Each motor actuates the pouch located on the same side of the body, so any parasitic forces due to the motors or the cable tension should still be perceived on the correct side. A locking mechanism made of a screw and a bolt was used to quickly change the nominal length of the cables to adapt the device between different users' morphologies. It is placed at the end of each cable on the plate (see Fig. 5.2 B) and on the whippletree mechanism (Fig. 5.5 F).

5.4.2   Comparison with Simulation

In order to compare the performance of the hardware device to the results found from simulation, the compression force on the skin (the pressure distribution and the maximum pressure) were measured by placing a capacitive pressure sensor array (Conformable TactArray, Pressure Profile Systems, Los Angeles, CA, USA) between the pouch and the skin as shown in Fig. 5.6. The pressure sensor is made of an array of 8×6 pressure cells of 25.4 mm $\times$ 25.4 mm. The resulting pressure values were recorded with Pressure Profile System's Chameleon visualization software with a resolution of 0.0276 ± 0.0069 kPa and a scan rate of 20 Hz. The resulting force was calculated by multiplying the recorded pressure by the area of the cell and summing the values of all the cells. Only the normal force (in the y direction) is measured with this pressure sensor array.

A force sensor (ELFS-T3E-25N, Entran Sensors and Electronics, NJ, USA) was placed in series with the cable in order to measure the applied force (Fig. 5.6 D) at a rate of 100 Hz. During the test, the cable was pulled gradually until the force on the cable reached 15 N and then released (this explains the non-symmetric profile of Fig. 5.7 B in comparison to the results of the simulation in Fig. 5.7 A). Recorded forces were low-pass filtered using a Butterworth filter with a cut-off frequency of 10 Hz. Fig. 5.7 B shows the effect of the filtering. Four comparison tests were done: (1) using the device parameters displayed in Table 5.1, (2,3) when lowering the initial internal pressure of the pouch to 1 kPa and then increasing it to 20 kPa in order to investigate the effect of the change of the initial inner pressure, and (4) adding a wedge of 20 degrees between the pouch and the plate. The wedge makes the cables more perpendicular to the plate within the physical constraints of the jacket. The tests were performed on a plastic mannequin as shown in Fig. 5.6 to avoid the variability between individuals.
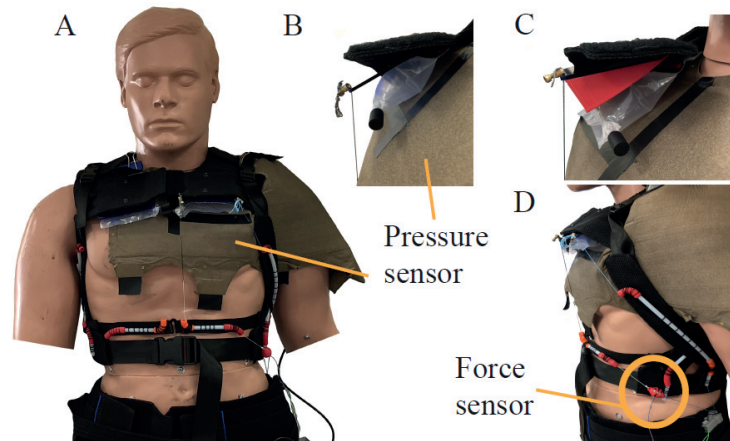
Figure 5.6 – Testing setup to measure the force transmitted by the hardware on the skin using a mannequin. A) Front view. B) Close up view of the pouch. C) Close up view of the pouch with the wedge. D) Side view highlighting the force sensor.

Table 5.2 – Comparison Between Simulation and Hardware Measurements

	Maximum Normal Force in Simulation (N)	Maximum Normal Force of the Hardware (N) (mean ± std)	Maximum Pressure in Simulation (kPa)	Maximum Pressure of the Hardware (kPa) (mean ± std)
Normal	20.82	20.29 ± 2.11	7.1	5.78 ± 0.52
Initial Inner Pressure: 1 kPa	4.12	4.10 ± 0.88	1.89	0.92 ± 0.20
Initial Inner Pressure: 20 kPa	39.86	37.18 ± 1.62	13.65	14.85 ± 0.52
Wedge	31.01	34.10 ± 4.92	9.77	9.17 ± 0.65

Results for the four experiments are listed in Table 5.2, and the data recorded for the device parameters condition are shown in Fig. 5.7. For the normal device parameters, the mean maximum normal force output is over 20N. The measurements with the hardware are close to the results of the simulation for the four tests; the force in y direction and the maximum pressure in a cell increase both when the initial inner pressure of the pouch increases and with the addition of a wedge between the pouch and the plate. The maximum pressure in a cell is slightly higher in simulation than for the measurement with the hardware. This can be due to the alignment between the surface of the pouch and the cells in the pressure sensing array. With the hardware measurement, the pouch was likely located in between three columns of cells instead of the two used in the simulation. This effect can be seen when comparing the pressure distribution between Figs. 5.7 C and 5.7 D. The pressure distribution is similar between the simulation (Fig. 5.7 C) and the hardware measurement (Fig. 5.7 D). However, it is difficult to quantify because of the lower resolution of the pressure sensor array – only 4×4 instead of 20×20 in the previous results of the simulation (Fig. 5.4).
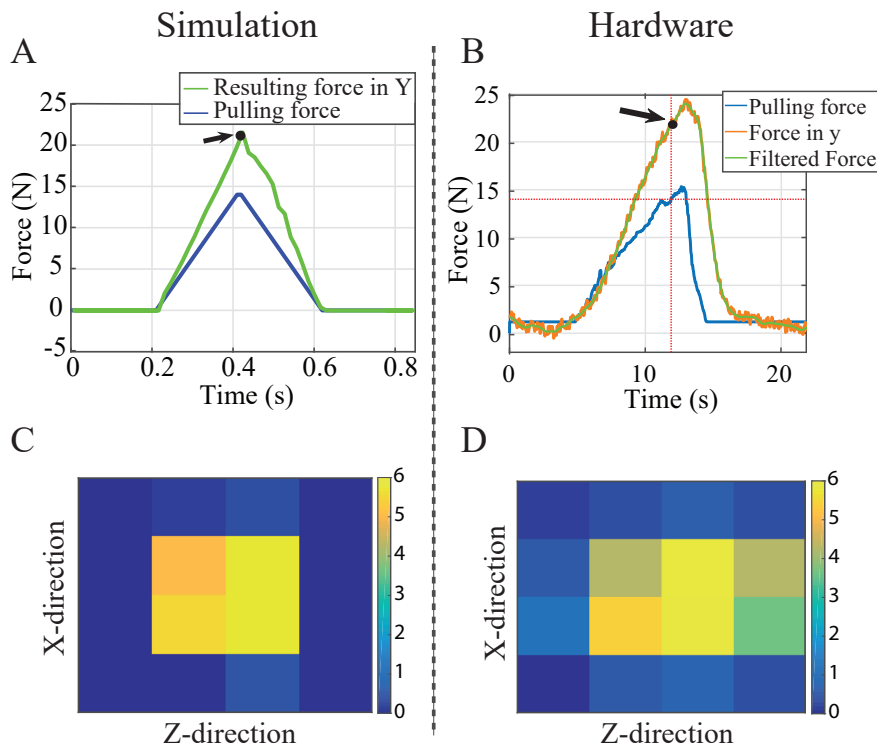
Figure 5.7 – Comparison of the forces and pressures transmitted to the skin between the simulation and the hardware, with a force of 14 N pulling on the cables. A) Resulting force (N) in y direction in simulation. The simulation is quasi-static so its rate is not significant. B) The evolution of the resulting force (N) in y direction measured with the hardware. The resulting force is dependent on the applied pulling force, and the arrow points to the data at a compression of 14 N. C) Pressure distribution (kPa) normal to the skin in simulation. D) Pressure distribution (kPa) measured with the hardware. (·) denotes the value of the force at 14 N.

5.5 Conclusion

The presented tactile feedback device addresses the challenges of rendering forces relative to the centripetal acceleration of a drone on the torso of a human teleoperator, while maintaining compliance and portability. Its parameters were studied with a simulated model of the device. The hardware built based on the results of the simulation showed performance close to the simulation. Also, the construction of the device is simple and its components are inexpensive, which makes this tactile feedback device widely accessible.

During the development of the tactile actuator, we investigated different pouch materials such as airtight textile or rubber. The given tactile sensations were not significantly different then when using LDPE but the mechanical process to build them was much more complicated. However, additional work could explore a change in the texture of the pouch surface as changing the friction coefficient between the pouch and the skin may produce other types

of sensations. We also considered the possibility to reduce the height of the actuator by combining multiple smaller pouches but this decreased the amount of surface in contact with the skin and considerably complicated the manufacturing process.

Due to its simplicity, this tactile feedback approach can be used for many different applications such as the teleoperation of underwater robots, the transmission of emotion between remote humans, and for gaming applications.

In the next chapter, we assess quantitatively with a user study the tactile feedback accuracy, the time to recognize cues, the influence on flight control and stabilization, and the sense of realism.

6 Tactile Feedback: Perception of a Wearable Haptic Feedback Device to Render the Sensation of Flight

6.1 Introduction

In the previous chapter, we described a soft wearable tactile feedback device embedded in the FlyJacket which can render the sensations of flying by recreating the centripetal forces that a fixed-wing drone undergoes during its change in attitude. These actuators aim to produce the sensation of air being compressed against the body. Realistic tactile feedback requires not only to render the appropriate type of sensations but also to enable the user to correctly interpret the cues with high accuracy and a rapid response time. In this chapter, we investigate the perception of this tactile feedback, the accuracy of the information transmitted to the user, the impact of this feedback on the flight realism, and its effect on a flight stabilization task.

To test the performance of the tactile feedback, we performed four user experiments. First, the types of sensations perceived by the user were investigated with an open response experiment. Then, the accuracy and reaction time to recognize a directional cue was evaluated. Third, the performance and sense of flight realism was quantified by flying a simulated fixed-wing drone

both with and without the tactile feedback. Finally, the effectiveness of the tactile feedback was evaluated in a task in which users stabilized the drone following a perturbation. The aim of this last experiment was to investigate how the tactile feedback could improve the user's awareness of the drone attitude and whether it could reduce the workload of the user during flight.

Twelve participants (four women and eight men, age 27 ± 4.9 years; mean ± SD) took part to the four experiments. Six of the participants already had experience flying with the FlyJacket, but none of them had experience with the soft tactile device. During the experiment, they sat on a stool and wore the FlyJacket with the embedded actuators over a single layer of clothing. For participant comfort, the maximum compression force produced by the actuator was set to 10 N , though the motor voltage could be increased to produce a stronger force. All participants provided written informed consent prior to the study in accordance with the EPFL Institutional Review Board procedures.

6.2 Open Response Experiment

6.2.1 Methods

The first part of the user study was a perceptual experiment where the twelve participants were asked to describe the sensations they experienced from the tactile device without wording restriction or suggestion. Four tactile sensations were presented in a pseudo-random order to the participants: the two front pouches, the two back pouches, the two pouches on the right (one on the front and one on the back), and the two pouches on the left. The force of the tactile cues was set at the middle of the possible range of force of the actuator (5 N).

Participants were asked to describe the sensations for each stimulus verbally to the experimenter and to draw on a body map where they felt these sensations. The participants were allowed to experience each stimulus as many times as desired.

6.2.2 Results

All the participants reported that it was easy to distinguish where on the body the cues were given. The sensations were described as both pulling the torso and compressive forces against the skin on the side corresponding to the cue. Seven participants commented that the sensations were pleasant. Front and back cues were harder to describe due to a larger range of sensations on the torso and because the sensations were sensitive to torso posture (e.g., if the participant bent forward slightly versus kept their torso strictly straight).

When applying the front cue (compressing the two front pouches), nine out of twelve participants described being pulled down and forward. In addition to being pulled forward, three participants reported having the impression of being moved forward. Six participants described feeling compressed. Three of these also reported feeling pulled down and forward.

When triggering the two actuators on the back of the jacket, seven participants described being pulled backwards. Four others related feeling a compression. In addition to other sensations, four participants described that this feedback helped them to straighten their back. Only two participants reported the back cue to feel symmetric to the front cue.

Eleven participants described the sensations for the right and the left cues as symmetric. Half of them (six out of twelve) described a sensation of being pulled down on the side while the other six described it as being bent laterally. In addition to these two sensations, five participants described feeling compressed and five of them described having their shoulder pulled down. Only two of them described sensations on the hip at the waist level (where the motors are located).

6.2.3 Discussion

All participants correctly recognized the side on which the cues were given and reported force on their body almost exclusively on this side, which indicates that the device has very little parasitic force or reaction force at another location of the jacket. Only a few participants reported feeling a force at the waist level, where the motors are placed. Therefore, padding the waist belt and the cable routing was an effective strategy to localize the sensation. The participants could express the sensations provided by the tactile cues without prompting, and the type of sensation was relatively consistent between the participants, with a clear pattern of compression and pulling force on the corresponding side of the body for all given cues.

6.3 Haptic Perception Experiment

6.3.1 Methods

The twelve participants were asked to identify four directional cues (front, back, right, and left) given by the compression of two of the four air pouches located on their torso. During this experiment, the same type of actuation as for the first experiment was used. The participant could choose when the force started by pressing on a key. The force continued until the participant pressed a key to answer. They entered their response by selecting a labeled key on a computer keyboard. They were asked to use only one finger to perform this task. Participants started with a short training block composed of eight directional cues (two in each direction). They received feedback after identifying each cue, indicating which cue had been displayed and whether they had answered correctly. Then, participants completed an evaluation block of 40 trials where no feedback on the correctness of their answer was given. The evaluation was composed of ten instances of each directional cue. Each participant received unique pseudo-random training and evaluation blocks. At the end of the task, they were asked verbally if one directional cue was easier to recognize than the others.

6.3.2 Results for Accuracy

Table 6.1 – Confusion Table Showing Accuracy for Four Directions (n=12)

	Displayed Direction			
Response	Front	Back	Right	Left
Front	98.33	0.83	0	0
Back	1.67	98.33	0	0
Right	0	0	100	0
Left	0	0.83	0	100

Table 6.1 shows the results for accuracy. Participants were almost always able to identify the directional cues. Over 480 total evaluation trials, participants correctly identified direction cues with an accuracy of 99.2%. All of the errors except one were between the front and the back of the torso. The four errors (over the 480 trials) were made by three participants (P3, P8 and P9). Participant (P9) made two errors. He reported to be confused between the front and the back cues and could not identify them correctly at the end of the training period.

6.3.3 Results for Identification Time
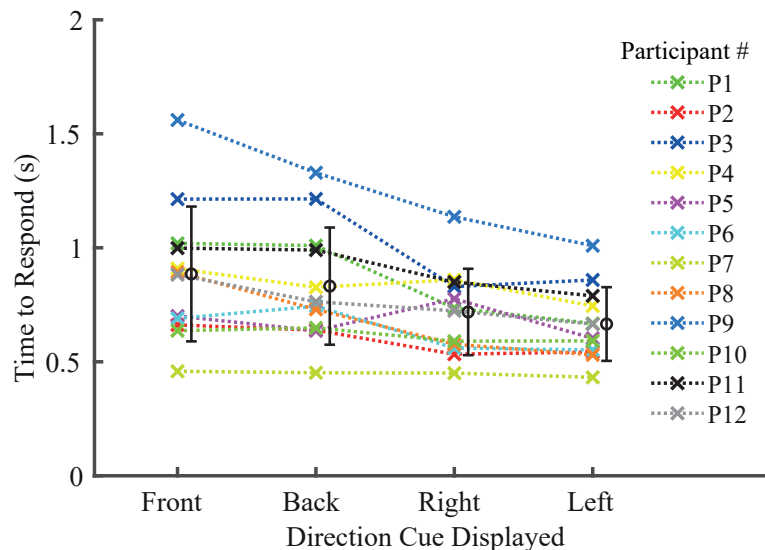
Figure 6.1 – Time to respond for the four direction cues displayed to the participants (n=12). Crosses (×) show the mean time to respond for each participant. Circles (o) display the group mean and the error bars the standard deviations.

Fig. 6.1 shows the response time for each directional cue. The mean time to respond for the front (0.83 s) and the back (0.83 s) are slightly higher than for the right (0.72 s) and left (0.67 s).

Also, the standard deviation is larger for the front (0.30 s) and the back (0.26 s) than the right (0.19 s) or the left (0.16). However, there is only a statistically significant difference (based on a Wilcoxon Rank Sum test) between the time to respond for the front and the left cues ($p = 0.0351$). There are no statistical differences between the other directional cues.

All cues have a mean response time lower than one second. This comprises the system delay (control loop and actuation), human reaction time [144, 145], and the time to perform the movement on the keyboard to answer. To determine precisely how much reducing system delay would improve overall performance requires a more thorough system identification, but would likely not substantially reduce the overall response time considering the proportion of human response. Indeed, as the fastest participants had on average a response time lower than 0.5 seconds and considering the typical human reaction type and movement time, we can deduce than the system delay is only a fraction of the observed variability in human response.

After the experiment, nine participants (out of twelve) reported that the right and left directional cues were easier to recognize than the front and back cues. Among these nine participants, four of them added that the front and back cues were still easy to recognize. Two other participants found all the cues equally easy to recognize (P7 and P11). Finally, participant (P5) found the back cue easiest to recognize, which correlates with her lower time to respond for this direction. These post-experimental subjective reports correspond to the higher average and standard deviation time to respond for the front and back cues recorded during the experiment.

The time to respond shows more variance between individuals than across the different directional cues for a single individual. Participant (P9), who made the highest number of mistakes, had the highest time to respond for all cues while participant (P7) had the fastest time to respond for all cues.

6.3.4 Discussion

The low number of errors in identifying the direction of the cues demonstrates that the tactile devices embedded into the FlyJacket were able to clearly display directional information. Although all the directional cues were easily identifiable, right and left cues were slightly easier to discern than the front and back cues, and it also took slightly less time to identify them. This is consistent with the impression of the participants. The speed at which the tactile cue is understood by the user is a critical aspect of the device's performance. The mean response times, also including the hand displacement between keyboard keys, for all the cues are lower than one second. This time to respond is meaningfully faster than comparable tests done for pneumatic haptic devices [146, 147] or a vibrotactile device [148]. The high accuracy and short time to respond make this device efficient and intuitive to transmit directional information to the user.
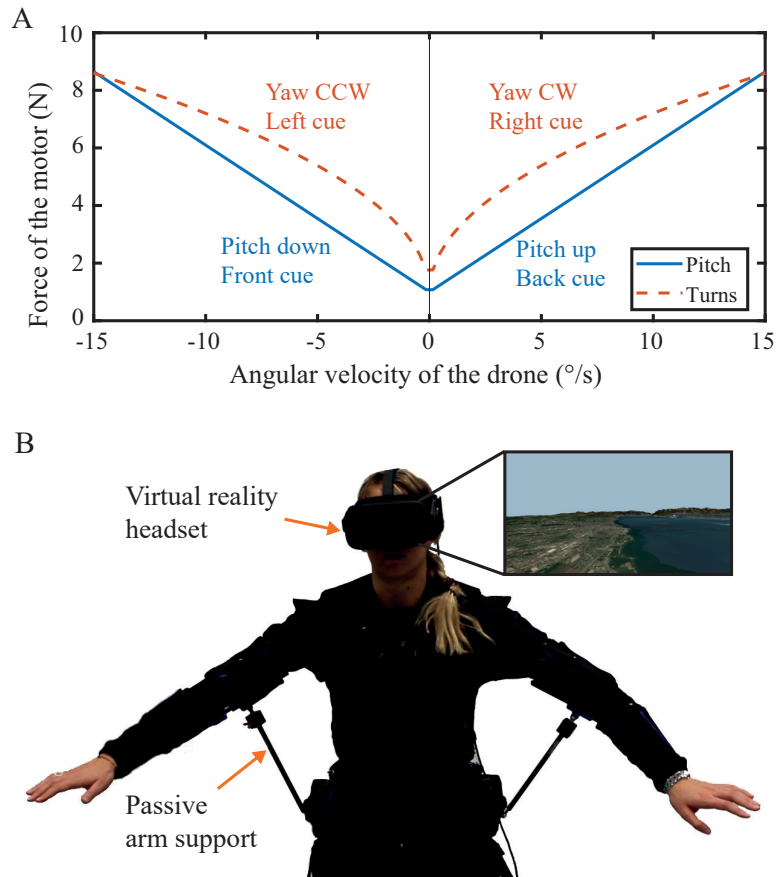
Figure 6.2 – Flight experiment setup. A) Relation between the angular velocities of the drone and the force of the motors for the pitch angular velocity (blue solid line) and the yaw angular velocity (orange dashed line). B) Setup for flight with inset showing the virtual environment.

6.4   Flight Experiment: Performance and Realism

6.4.1   Methods

The tactile feedback is used to render the centripetal forces of the drone, making the user aware of the drone rotation and its inertia (Eq. 6.1). Therefore, the participants felt forces on their torso corresponding to their maneuvers only during drone rotation (i.e. if the drone is going straight, no force is rendered).

$$F = ma = mv\omega \tag{6.1}$$

In the simulator, the drone is modeled as a rigid body with a constant mass (m) and constant forward speed (v). The force therefore varies with the angular velocity of the drone (ω). We made the assumption that the earth is a flat and non-rotating, which is considered as a valid assumption for UAVs [149]. The inertial coordinate system used is earth-fixed with its origin at the defined home location (NED system). In this coordinate system, Newton's equations of

motion are derived relative to a fixed, inertial reference frame. Therefore, the Coriolis terms are not needed. We approximated the angular velocities in the inertial frame with the pitch and the roll rate which are usually expressed with respect to the body frame.

Each angular velocities of the drone are individually converted to compressive forces on the torso (see Eq. 6.1). The pitch angular velocity is translated to a force rendered either in the front or the back of the torso while the yaw angular velocity is translated to a force on the left or on the right (i.e. during turns). The yaw angular velocity was rendered on the user's torso instead of the roll angular velocity in order to render a more realistic sensation of flying. Indeed, during turns to the side, the drone experience a centripetal acceleration while the roll angular velocity is null after the first rolling that initiates the turns. Additive combinations of pitch and yaw cues are possible because the four motors can be independently actuated. In this case, the computed forces derivated from the pitch and yaw angular velocities are summed as output of the motor.

The relationship between angular velocity and the force rendered during the flight was given by the curve shown in Fig. 6.2 A. Preliminary flight tests showed that the force feedback was hard to detect during small turns to the side. Therefore, the force profile for the left and right cues is based on the square root of the yaw angular velocity, in contrast to the linear curve used for the front and back cues. This quadratic curve aims to give more noticeable change in force for small changes in angle while remaining within the maximum force capabilities of the device.

To avoid slack in the cables, the motors are controlled to act as a bias spring. A force of 1 N is always applied to the cables (which corresponds to the offset in the graph of Fig. 6.2 A). When the user bends toward one of the motors, the motor winds the cable onto the motor pulley. Since this bias force is very small and the motor is backdriveable, the user is still easily able to move (and thereby unwind the cable from the pulley).

Participants were in the same setup as for the two previous experiments, with the addition of the VR headset (Oculus Rift), which provided the visual feedback of the simulated environment and the sound of the wind. They flew in the same simulator described in Chapter 1.

At first, participants performed two one-minute free flights in the simulated environment, once with the tactile feedback and once without the feedback. Then, they performed two more flights (one with feedback and one without) which consisted of following 34 waypoints in the sky symbolized by white clouds forming a trajectory. This task is similar to the one described in Chapter 1. The goal of this second task was to force participants to perform each of the flight maneuvers (pitch up, pitch down, turn left, and turn right) eight times (randomly ordered, with two additional waypoints at the beginning and the end of the trajectory). While the primary purpose of this task was to measure the realism of the flight, the task performance was also evaluated by recording the distance from the drone trajectory to the center of each waypoint and computing the RMS error for all the waypoints. For both tasks (free flight and the waypoint following) half of the participants (P1, P2, P6, P8, P10, P12) flew with tactile

feedback first, while the other half first flew without tactile feedback to account for learning effects and potential bias based on the order of presentation.

After each waypoint following task, participants filled out a questionnaire regarding the sensations they experienced during the flight. Using a Likert scale from 1 to 7 (1 being "Not at all" and 7 "Very much"), the participants rated their appreciation of the flight for both conditions (i.e. with and without feedback) on a variety of criteria. Questions are displayed in Table 6.2. Four themes — realism (Q1 and Q2), immersion (Q3 to Q5), performance (Q6 to Q9), and force perception (Q10 and Q11) — were assessed. For Q1 to Q9, the relative performance (the difference in rating) between the flights with and without feedback was calculated. A positive value means that the tactile feedback improved the perception. Q10 and Q11, which concerned only the experience of feeling the tactile feedback during the flight, were asked only after the task with feedback. The statistical significance of the groups were evaluated with a one-sample t-test.

Table 6.2 – List of Questions Presented to the Participants

	Index	Questions
Realism	Q1	I felt as if I was flying.
	Q2	How realistic was the flight?
Immersion	Q3	How well do the sensations match your expectation?
	Q4	How immersive was the flight?
	Q5	I enjoyed the experience of virtual flying.
Performance	Q6	How intuitive was the flight?
	Q7	How confident performing the flight were you?
	Q8	How easy was the task?
	Q9	How well were you able to control the flight?
Perception	Q10	The haptic feedback improved my flight performance.
	Q11	How much did you feel the haptic feedback during the flight?

6.4.2 Results

The tactile feedback had on average no influence on the flight performance with a relative improvement of performance of 3.7 ± 12.3 meters; mean $\pm$ SD. The order of flight conditions appears to have more effect than the tactile feedback, because ten participants performed better during their second task regardless of the feedback condition. The performance of one participant (P6) was much better with the tactile feedback even though she started with

this condition. She reported feeling disoriented and having motion sickness during the flight without the feedback.

Results from the questionnaire are shown in Fig. 6.3. All the participants except participant (P9) (who had trouble recognizing the directional cues in the previous experiment) thought that the tactile feedback improved their performance (Q10) with eight of the participants rating this question with a score of five (out of seven) or higher. The amplitude of the force feedback (Q11) was sufficient according to the participants as ten of them rated a score of four or more and only two participants reported post-experiment that they would like to have a stronger force.

The relative ratings for the questions regarding the performance (Q6-9) is quite diverse. Participants with generally negative relative scores reported that the tactile feedback "reduced their reactivity" (P7), "prevented them from doing what they wanted" (P12), or "had too much time delay" (P8). On the other hand, participants who gave the tactile feedback an overall positive rating reported that they were more aware of their position and their movements when flying (P1, P3, P6, P10, P11, P12) or felt more stable (P5).

Participants rated the flight more realistic with the tactile feedback with Q1 significantly different from zero ($p = 0.0463$) and Q2 almost significantly different from zero ($p = 0.058$). Mostly, participants described the flight with feedback as being more natural, more comfortable, and less weird than without the feedback. On the other hand, the results for the immersion are more disparate. For half of the participants, the sensations given by the tactile device did not match their expectations, and they reported that they expected to feel sensations on the whole body to feel totally immersed. The same participants who rated negatively for this set of questions also rated negatively for the questions about performance.

6.4.3 Discussion

From the results of Fig. 6.3, two clusters of user perception of the tactile feedback can be seen; half of the participants were very optimistic about the feedback and had a good acceptance of it while the other half were more skeptical of the feedback, rating the flight experience with feedback either the same or one grade lower than the flight without feedback. The main comments of the skeptic group were that the tactile feedback prevented them from moving and reduced their reactivity. This is a reasonable response given that the tactile feedback was designed to render the centripetal forces and therefore the inertia of the drone. These participants were not convinced by the rendered sensations. On the other hand, half of the participants found that the tactile feedback improved the realism of the flight, their immersion in the flight control task, and their performance of the task. With regard to the disparate views on whether the sensation matches the user's expectation, it should be noted that people are generally not familiar with the actual sensation of flying, and the users had widely variable expectations. Participant (P3) has extensive experience remotely piloting an aircraft (~500 hours), one other participant (P12) has 10 hours of experience, and all other participants have

at most 2 hours of experience. P3's rating for all questions was positive except for Q5 and Q9, which were rated the same for with and without tactile feedback. He reported that having the inertia of the flight rendered made the flight more realistic. Half of the participants reported that the flight was more realistic with the addition of the tactile feedback. Three participants (P5, P6 and P11) reported feeling less motion sickness when flying with the tactile feedback, and none of the participants reported feeling motion sickness during the flight with feedback.
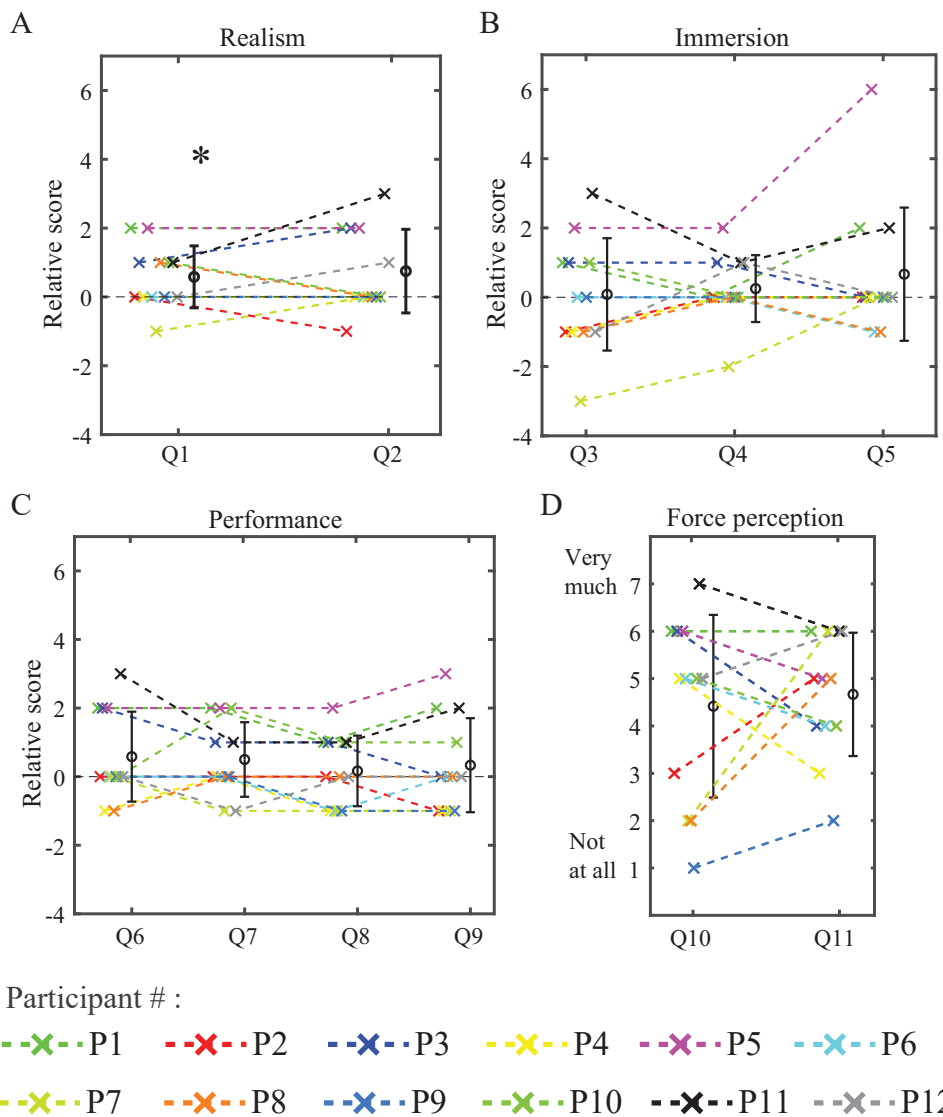
Figure 6.3 – Results of the questionnaire (n=12). Crosses (×) show the mean time to respond for each participant. Circles (o) display the group mean and the error bars the standard deviations. Responses to questions concerning: A) the realism of the flight. Asterisks (*) denotes p < 0.05, B) the immersion into the flight, C) the participant's subjective perception of their performance, and D) the force perception.

6.5 Flight Experiment: Stabilization and Workload

6.5.1 Methods

Participants were in the same setup as for the previous experiment. They had to perform two sessions of stabilizing a drone after perturbations coming from the side. One session was performed with the tactile feedback, and the other session without. The order of these two sessions was pseudo-randomized among participants. A cross in the middle of the field of view indicated the drone's attitude (see Fig. 6.4 A). Each session was composed of 36 perturbations in which the roll angle of the drone was shifted by -30, -20, -10, 10, 20 or 30 degrees (a negative angle corresponds to a counter-clockwise roll and a positive to a clockwise roll). After each perturbation, the participants had to re-align the cross with the horizon as fast as possible (Fig. 6.4 B). An example of perturbation is shown in Fig. 6.4 C. Most of the time, due to its slow dynamics, the drone did not reach the whole shift of angle because the user reaction to straighten the position was faster than the drone to reach its new commanded angle. The perturbations were pseudo-randomly ordered and separated by either seven, eight, nine or ten seconds. During this experiment, participants had control on only the roll of the drone by bending their torso laterally. Participants were free to move their torso in any direction, but other movements had no influence on the control. Stability criteria were to maintain the roll angle within a stabilization zone defined as a range of -3 to 3 degrees, which corresponds to the static noise of the IMU, for a stability period of three seconds (Fig. 6.4 C). The stabilization time (the time between the perturbation and the end of the stability period) and the number of overshoots (defined as crossing outside the stabilization zone) were computed.

At the end of each session, participants completed a NASA-TLX questionnaire, in which participants had to assess the workload for the two flight stabilization tasks on a scale from 1 to 100. As described in Chapter 3, the workload is composed of six components: physical demand, mental demand, effort, temporal demand, frustration, and performance. For stabilization time, overshoot, and workload metrics, on a per participant basis, relative results were computed as the results from the task with feedback subtracted from the results from the task without feedback. Therefore, a positive relative result signifies an improvement in the task with tactile feedback.

6.5.2 Results

While the stabilization time was not influenced by the tactile feedback (-0.17 ± 0.39 seconds), the absence of tactile feedback led to slightly larger number of control overshoots (2.33 ± 3.94 more overshoots, $p = 0.065$). As shown in Fig.6.4 D, there is no difference in the overall workload between the two tasks, but some of the components of workload are reduced with tactile feedback. Statistically significant differences (based on Wilcoxon Signed Rank test) were found for the relative mental workload ($p = 0.0112$), physical workload ($p = 0.0356$) and temporal workload ($p = 0.0132$). There is no statistical difference for the other contributions

(effort, frustration, and performance).
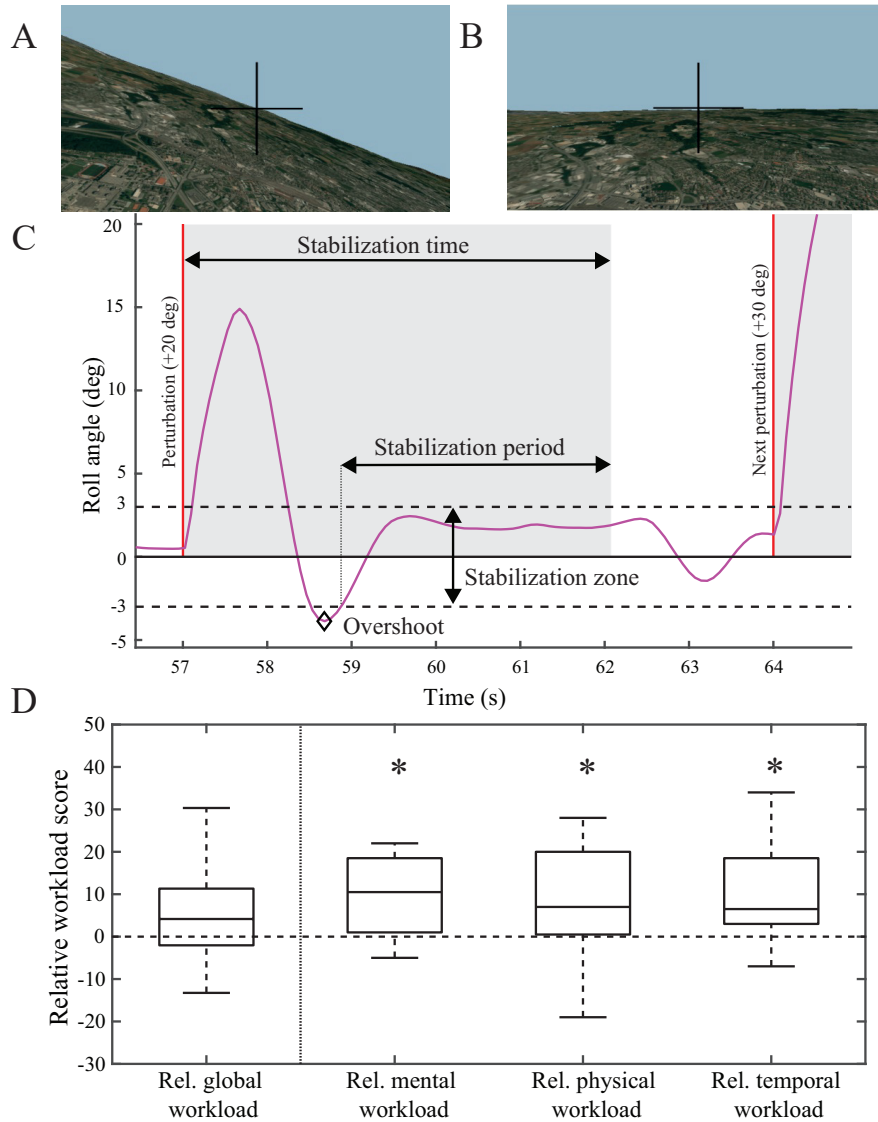
Figure 6.4 – Flight task of stabilization (n=12). A) Environment after a perturbation of 30 degrees. B) Environment in a stabilized condition. C) Example of the drone roll angle for a perturbation of 20 deg with feedback (P7). D) Results of the workload questionnaire, where the relative score is the difference between the score with tactile feedback and the score without tactile feedback. Asterisks (*) denote $p < 0.05$.

6.5.3 Discussion

This last experiment showed that the tactile feedback slightly reduced the amount of overshoot during the stabilization of the drone. With the help of the feedback, participants could better estimate the torso displacement necessary for the stabilization than when they had to rely

only on vision. This quantitative results are correlated with the impression of the participants as they reported that the feedback helped them to know how to stabilize the drone – in which direction and with what intensity – and was a good complement to the visual feedback. Results of the workload measurement also supported this result. No difference was observed for the stabilization time. Changing the force profile to have a more dynamic force feedback or by giving cues indicating in which directions the user should move their body to counteract the perturbations, could maybe reduce the stabilization time.

6.6   Conclusion

In this paper, we presented a user study to evaluate the effectiveness of a soft tactile feedback device that is embedded in the FlyJacket and provides feedback to the torso. The device was able to transmit directional cues to the user with very high accuracy, and the response time is meaningfully lower than for comparable devices. These features show that this device could be used for guidance, which could be tested with the same type of experiment as performed in Chapters 3 and 4. This device has the advantage to be more compact than the one presented in this previous work.

When applying this feedback during a simulated flight, the realism increases significantly, but the performance did not improve, which is not surprising since the users are already receiving good visual feedback. To test the influence of the feedback on the performance, the device could be further tested in situations with increased visual or cognitive load.

The perception of immersion was less consistent between the users with half of the participants enthusiastic about the feedback while the other half was more skeptical. Some participants disliked the impression of having an inertia while flying, which is the sensation recreated by the device, because it prevented them from moving while other participants emphasized that this same sensation of inertia made the flight more immersive and realistic.

Modifications to the hardware could be done in order to improve the user's immersion in the flight. The size, number, and location of the pouches is not limited to the current configuration, so different arrangements and combinations may provide a better experience or render more complex sensations such as force propagation along the torso. Pouch actuators could also be added on the arms to increase the surface receiving the tactile feedback. However, adding more pouches increases the jacket complexity and weight. The reactivity of the feedback could be increased by changing the command of the motors to make the force profile more aggressive and reducing the time delay between the motor actuation and the point at which the sensation is detected on the skin. The aerodynamic forces (lift, drag, external disturbances such as wind gusts, etc.) could be implemented with the same hardware by changing the actuator control. It would be interesting to test if users can still understand the tactile cues in this more complex scenario.

The realism of the sensation provided by the device could be further improved by consulting

experts in free fall and wingsuits in order to compare these sensations with what would be the closest to reality. Since the actual sensation of flying has been experienced by very few people, the expectation of the sensation varied widely among participants.

The tactile device was assessed with a virtual drone stabilization task. The tactile feedback increased the state awareness of the user by giving them information about the direction and intensity of the perturbation while reducing their mental, physical and temporal work-load. However, the stabilization time was not reduced when having tactile feedback. One assumption is that the task was not challenging enough to demonstrate the usefulness of haptic feedback. A flight experiment on users, where they would fly in a more challenging environment, such as in between buildings as implemented in Chapter 1, would maybe show some improvements due to the haptic feedback on the stabilization time as the user would have more workload to avoid buildings and deal with the perturbations at the same time. Another change to exploit the benefit of haptic feedback to help stabilizing the flight would be to test a more reactive setup, by playing with the slopes of the mapping between the angular velocities and the given forces.

An interesting phenomenon was observed during the experiment; some participants reported feeling less motion sickness when flying with the tactile feedback. These results warrant further study and quantification, as motion sickness is a well-known problem when performing VR tasks [87].

7 Conclusion

Robots have taken a non-negligible place in our society for multiple purposes, including industries, medical applications, ensuring our safety, and personal leisure. More intuitive human-robot interfaces can expand the use of robots to a wider range of the population.

In this PhD thesis, we developed a whole interface that enables the natural and intuitive bidirectional interaction with a fixed-wing drone. This device allows to control the drone with upper body gestures and receive feedback from the drone. The first step of this project was to identify design principles to build an upper body soft exoskeleton to record body movements. This exoskeleton had to be versatile to easily include other devices such as movement recording devices, haptic feedback devices, and electronics, or to interchange different types of arm supports, in order to test new types of technologies developed during the project. The anchoring points of the exoskeleton to the human body were carefully studied to allow proper force transmission and a comfortable fit. An important aspect was the adaptation to many body morphologies to allow accessibility to a wide range of people. These criteria shaped the exoskeleton and were proven to be effective for the additional devices that were then embedded in the initial jacket. In order to reduce the fatigue when flying with the arms spread out, a lightweight and passive arm support has been developed and integrated in the FlyJacket. We demonstrated that both a simulated and a real fixed-wing drone can be controlled with intuitive body gestures recorded by this soft exoskeleton. The performance improvement when having the arm spread out instead of along the body was validated by the user study conducted with this first version of the FlyJacket. The necessity of an arm support to reduce the sensation of arm fatigue was also shown in this user study.

In order to further reduce arm fatigue, we developed an advanced passive arm support that can cover more than 97% of the ROM required to fly with the FlyJacket while being adaptable to 98% of the population and remaining portable. The arm support used a gravity compensation mechanism composed of a spring. The amount of compensation and the device size can be adjusted to adapt to the user morphology. Again, a user study was performed to test the efficiency of this new arm support by recording the flight performance, the shoulder muscles activity and the device appreciation by the participants. Results showed that this gravity

compensation arm support further reduces the shoulder fatigue compared to the previously developed arm support made of gas springs.

As the FlyJacket is an adaptable platform, it allowed us to explore the two types of haptic feedback; kinesthetic and tactile. Kinesthetic feedback was implemented with a cable-driven system to give haptic guidance to the user's torso position. During the two user studies conducted to test the efficiency of the device, we investigated this kinesthetic feedback by studying the best force profile, the force perception and the learning effect. We determined that haptic guidance improved flight performance and that a quadratically shaped force feedback curve was the most adequate profile to guide the user. Indeed, this profile gives a weak force when the error is small and a strong force when the error becomes significant. We also established the minimal force difference and the perceived magnitude of this system. This data helped us to design the learning experiment. This experiment gave us mixed results as it validated over a longer period of time the performance improvement when having haptic guidance but it did not enhance the learning rate and the performance was not retained by the user once the haptic guidance was removed.

We also explored tactile feedback to render the sensation of flying. As no current devices were able to render the sensation of air compression while remaining portable, we designed and embedded in the FlyJacket a new type of tactile actuator composed of closed air pouches compressed against the skin with cables driven by electrical motors. During the design process, we modeled the actuator to study its behavior during compression cycles when varying the parameters. Once the most adequate parameters were established, we built four devices and implemented them in the FlyJacket. The main challenges of the tactile feedback were to measure the subjective concept of immersion, embodiment and expectation of sensation of flying as few people have already experienced flying like a drone. However, the results of our user study showed that this tactile feedback significantly improved the sensation of flight realism. As with this actuator the accuracy to display directional cues was very high and the reaction time short, we believe that this new tactile actuator can be use for multiple other purposes including to give haptic guidance in the same frame of experiment as the one performed in our kinesthetic feedback studies.

Along with this thesis, the various versions of the FlyJacket have been demonstrated at multiple events with diverse audiences such as users with scientific backgrounds (Cybathlon [2016] and World Haptics [2017]), industrial experience (NCCR Industry Days [2016, 2017 and 2018] and CES Las Vegas [2019]), political backgrounds (World Economic Forum [2019]), artistic backgrounds (Future of Story Telling [2018]) and also at general public events (EPFL Open days [2016], London Science museum Lates [2017], Drone Days [2017] and Boston HUBweek [2018]). We evaluated to around 400 the number of people that used the FlyJacket. Of course, this includes many different morphologies and a large age range, estimated to be between twelve to eighty years old. The main result of these demonstrations was always a great fascination for this new technology and a surprise at how easy was the control of the drone. Sometimes, people even asked us where they could buy this technology. We rarely encountered people

that were afraid of wearing the jacket. Considering the scientific results and looking back at all these events, we can conclude that the FlyJacket fulfilled the requirement of being adaptable to many morphologies, easy to put on and take off, and intuitive to use. Also the reliability and portability of the device were validated with all the travels done for these demonstrations.

7.1 Extension of Raised Concepts

Before concluding this thesis, several aspects of the described research could be furthered by future considerations.

The haptic guidance instantaneously improved the performance in the first user study on kinesthetic feedback. Yet, despite validating the performance increase over time when using the haptic feedback, the second user study did not show that participant's performance improves at a faster rate or that they retain their flight skills once the guidance was removed. We hypothesize that when flying with haptic guidance, the participants already reached a proficient performance and the provided guidance was no longer assisting. In order to counteract this phenomenon, the guidance strategy should be redesigned. The amount of force feedback should be constantly adapted to be proportional to the user's instantaneous performance. When they become more confident in their flight skills, the amount of guidance should be reduced to always keep them in challenging conditions. In addition, an important difference of initial skills and learning rate was observed between the participants of the user study, which prevented us from drawing any statistically significant conclusion about the results. To overcome this, individualized feedback could be designed by either tuning the amount or the profile of force feedback for each participant, or by changing the feedback strategy according to the participant's skill level. Haptic guidance has been shown to be helpful for initially less-skilled participants, while a feedback strategy exploiting error amplification is more beneficial for skilled ones [59]. In the same study, it was observed that participants which undergo the training with haptic guidance had their performance degrading overtime when they were flying again without guidance. This may be explained because they relied too much on the haptic guidance during the training phase and were passively following the guidance instead of actively training. Therefore, the training session should be redesign as described earlier in this paragraph with an amount of force feedback set proportionally to their instantaneous performance. If this redesign of the training session does not show skill improvement, it would be interesting to investigate if a training with guidance over several days to train muscle memory would enhance faster the flight skills than without guidance.

In both the kinesthetic and tactile feedback user studies, the perception of the force and directional cues were assessed under static conditions i.e., the users were not moving when the cues were provided. However, during the evaluation of the feedback in flight tests, the conditions were dynamic with the participants moving their torso. It would be interesting to study the differences in perception under static and dynamic conditions to reveal any effect the respective conditions might have on the perceived amplitude, direction or frequency of the

force. A new set of experiments similar to the one described in Chapter 6 could be designed. As an example, participants could perform the same task of directional cues reconnaissance twice, under static and dynamic conditions respectively. On the same research topic, to further understand our cable-driven kinesthetic feedback method, we are currently investigating how it is perceived by participants under dynamic conditions. The aim of this study is to develop a model of the torso behavior and gain insight to user response when they are dynamically subjected to kinesthetic feedback. A more detailed explanation of our study is provided in the conclusion section of Chapter 4.

During the user study assessing the realism and immersion of the tactile feedback (Chapter 6), some participants reported to feel less motion sickness when flying with than without the tactile feedback. Motion sickness in virtual reality (VR) is a well-known problem [87] and solutions to reduce it would allow to expend its use to further applications such as performing longer or more turbulent training. Unfortunately, as it was not the topic of this user study, no specific data were recorded and we can only make an assumption on the benefit of haptic feedback on preventing motion sickness in VR. In order to verify this assumption, a set of more specific experiments should be designed. Some parameters to investigate for the cause of motion sickness would be longer or more turbulent flights, a worse refreshment rate of the VR goggles, or performing test on participants that are known to be sensitive. However, deliberately inducing motion sickness to participants is not pleasant. In addition, the probability of having participants suffering of motion sickness is not guaranteed even when a sensitivity to VR goggles is a criterion of selection [150]. Another way would be to test a fairly large number of participants using the current setup in order to get a significant number of participants suffering of motion sickness.

One of the envisaged application of the FlyJacket is search-and-rescue, where the device could be used to fly drones to gather information in the field. Currently, drones are used during these missions to generate a map of the surrounding which helps the rescuers to plan the mission and distribute efficiently their resources. Using the map provided by drones helps them to know where to deploy the rescuers, what kind of material they should take with, and which ways are the safest to reach their destination (which can be for example a person stuck under a collapse building with a broken leg). Preliminary work has been done in this direction (see Chapter 1). In depth evaluation is however recommended to extensively test our interface for this scenario. As we are convinced that it can really bring huge benefits, we are hoping to have the occasion to demonstrate the capability of the interface in such situation.

7.2 Future Directions of Research

The FlyJacket was designed to be easily adaptable for experiments testing a variety of hypotheses about human-robot interaction. As a result, our interface still provides a large space to develop new devices and verify assumptions. In this section, we would like to propose few examples of future directions of research.

During our user studies on rendering the sensation of flying, some participants reported that they wished to have a more distributed feedback on the entire upper body. Giving the sensation of air flow on the arm using the arm support could be an additional modality of haptic feedback to enhance immersion. This could be done by motorizing the displacement of the grounding part of the gravity compensation arm support presented in Chapter 2. Shifting the position of this grounding part would give more or less gravity compensation. The user could receive kinesthetic feedback on their arm representing the air flow experienced by the drone. Nevertheless, the design of this motorization have to be carefully studied as the arm support should remain small and lightweight to be portable.

Another type of kinesthetic feedback device that uses electrostatic adhesive clutches could be integrated in the FlyJacket to have a fully textile-based exoskeleton with haptic feedback [39]. As this technology can be worn close to the body and directly at joint locations, it allows to embed multiple actuators on complex joints such as the shoulder joint. Such a technology would enable feedback provision along multiple DOFs while remaining compact. Using clutches introduces another feedback strategy not yet discussed in this thesis; a feedback that prevents motion. This type of kinesthetic feedback does not move a body part either toward or away from a target position as is the case for the kinesthetic feedback methods described in this thesis. Rather, feedback technologies employing these types of wearable clutches can prevent joint movement. As an illustration, the FlyJacket user could move freely within a predetermined envelope but if they perform a movement out of this range, specific clutches would be activated and the movement stopped. One of the key challenges that remains to be addressed is to change the user's perception about the safety of the high voltage required for powering these clutches.

A relevant feature to be implemented on the control of the drone is management of the drone's speed. In the current system, the speed is fixed in the simulator and can be modified thanks to a hand-held potentiometer when flying a real drone. Data-driven experiments similar to what have been achieved in [72], could be performed to investigate what type of intuitive movements could be used to control the drone speed. We would suggest to focus on the arm as they are currently not actively used in the control.

The current pattern of movement used to control the drone has been determined to be intuitively used by 60 % of the tested population [72]. The remaining 40 % of people would not necessarily use exactly the same pattern of movements and some short explanations should be provided to them. Even if the amount of people that were not able to understand the drone control was insignificant, it would be enjoyable to have an adaptive control able to be personalized to the natural gesture of each user. This could be implemented by having a machine learning algorithm which studies our body movement during the first short period of our flight and personalize the drone control strategy to each user. This may enable an even more intuitive interaction with the drone, deepen the immersion, increase the flight performance and reduce the task workload.

Along this thesis, we developed one instance of human-drone embodiment by linking body movements and haptic sensations with drone motion. This concept of embodiment can be further explored by exploiting the concepts of self-location – the sense of where the self is perceived to be located in space – and out-of-body experiences. These illusions can be manipulated experimentally by imposing multi-sensory conflicts [151]. The congruence between visual and tactile stimulation can induce change in self-location perception and lead to out-of-body experiences. By altering these two sensorial feedback mechanisms, a person can experience the sensation to be present at a remote location regarding their body position. Applying this concept in the interaction with a drone could deepen the sensation of being the robot and not controlling it from the ground. An investigation assessing flight control performance of a drone when wearing first person view VR goggles reported that their users felt "the sensation of flying and out-of-body experiences" [150], which further encourages what can be achieve with our interface.

Opportunities

In this thesis, we demonstrated that our interface could control a fixed-wing drone by recording torso movement and render either guidance to improve the fight performance or tactile feedback to render the sensation of flying. Similar interfaces, based on the same principle of bidirectional interaction between the human and the robot, could be applied to different type of robots and benefit other applications.

As briefly discussed in this thesis, an intuitive interaction between human and robots can enhance the performance of complex mission and reduce the operator workload. In this scenario, operators can control robots with natural gestures, allowing them to pay more attention to their mission than to the control of the robot. Robots are shown to be also useful in many other more common environments such as in industry as they can perform physically demanding, monotonous, or dangerous tasks. However, in most industries, they are completely separated from the human workers and in case of problem a specific operator needs to intervene. Because of this separation and isolation, part of our society is getting concerned that robots will take over human's jobs, leaving us unemployed. We do not believe in this vision. Robots can bring great assistance to human physical capacities by providing more force, more safety, and reducing the time to perform a task. In some fields, they exceed human capability thanks to their high computational power. However, imparting human cognitive skills such as innovation, creativity and critical thinking to a robot is difficult. Thus, human-robot teams can achieve great outcomes together by combining the mechanical strength of the robot under the guidance of human cognitive skills.

Looking at the aging of the population, robots can assist the elderly to keep them active in the society by reading instructions, reaching a object, providing basic care, or reminding them of meetings, among other tasks. They can also act as companions to reduce the social isolation and loneliness, and keep training their mental activities. However, due to the generation gap,

most of elderly do not feel confident to interact with robots. Therefore, here again, the need of intuitive interaction with robot is imperative.

During our demonstrations, in addition to the great perspective in the gaming world, multiple users pointed out the potential of the FlyJacket for rehabilitation. After a stroke or an injury, patients undergo a long and usually monotonous physical therapy based on movement repetition. Research has correlated therapy outcome with the motivation of the patient [152]. In order to promote patient motivation, some therapies propose to couple the physical training with a game. VR has been of great interest to keep the patient motivated as the level of the game can be adapted to the patient skills and tailored to the patient's progress. As our system uses upper body movements to control the drone, it could be easily adapted for trunk and back rehabilitation. In order to have the task difficulty adapted to the patient's skills, the gains between the torso movements and the drone angles can be varied, changing the movement's amplitude. Or the distance between the waypoints or their size can be changed, adapting the task's difficulty. A score could be displayed when passing through the waypoints, keeping the participant stimulated.

Robots have also demonstrated encouraging results in therapy and education with children suffering from autism spectrum disorders (ASD) [153]. ASD is a developmental disorder that affects communication and behavior. People with ASD have difficulty to communicate and interact with other people due to their high sensitivity to emotions and difficulty remaining focused on a conversation. Investigations showed that people with ASD enjoyed interacting with computers. They can focus their attention and motivate an individual to speak, read or share achievements with other people, which can greatly facilitate communication. Similar results have been found with robots [153]. Indeed, robots are ideal conversation partners as they never gets angry, their interactions are limited and predictable, their voice is metallic and not very nuanced, and their mimicry is stereotyped. Therefore, they can act as a mediator between people suffering from ASD and people who support them. However, in order to ensure a fluid interaction, the control of the robot should be intuitive and natural.

The benefits in other fields of application briefly discussed in this section emphasize the necessity of having intuitive human-robot interfaces. On a medium to long term vision, robots will certainly not take over the world as science fiction dystopias propose but, thanks to their extended physical capabilities, they will become our companions, helping us during our daily life. However, in order to have more meaningful connections, we need more intuitive interactions with them. We believe that the contributions of this thesis provide insights to the design of intuitive interfaces for human-robot interaction, promoting their accessibility to a wider range of the population. The concepts described in this thesis represent an incremental step towards this goal, and show a high potential for real-world applications, which we sincerely hope to see in the near future.

A Computation of the Torque to Compensate the Arm Weight

Chapter 2 of this thesis presents an advanced arm support fitting 98% of the US population that can compensate the torque produced by the arm weight along 97% of the flight ROM. This Appendix includes the calculations and describes the computation process used to determine the torque compensation and to design the device.

The torque required to compensate the arm weight can be computed depending on the arm position.

At first, the output positions of the elbow joint can be calculated using the parameters described in Fig. A.1.

$$d_1 = \sqrt{u_{th}^2 + c_w^2} \tag{A.1}$$

$$\gamma_1 = \arctan(\frac{c_w}{u_{th}}) \tag{A.2}$$

$$d_2 = \sqrt{L_a^2 + d_1^2 - 2 \cdot L_a \cdot d_1 \cdot \cos(\frac{\pi}{2} + \gamma_1 + \alpha)} \tag{A.3}$$

$$\gamma_2 = \arccos(\frac{d_1^2 + d_2^2 - L_a^2}{2 \cdot d_1 \cdot d_2}) \tag{A.4}$$

$$x = d_2^2 \cdot \sin(\alpha + \gamma_1 + \gamma_2) - H_w \tag{A.5}$$
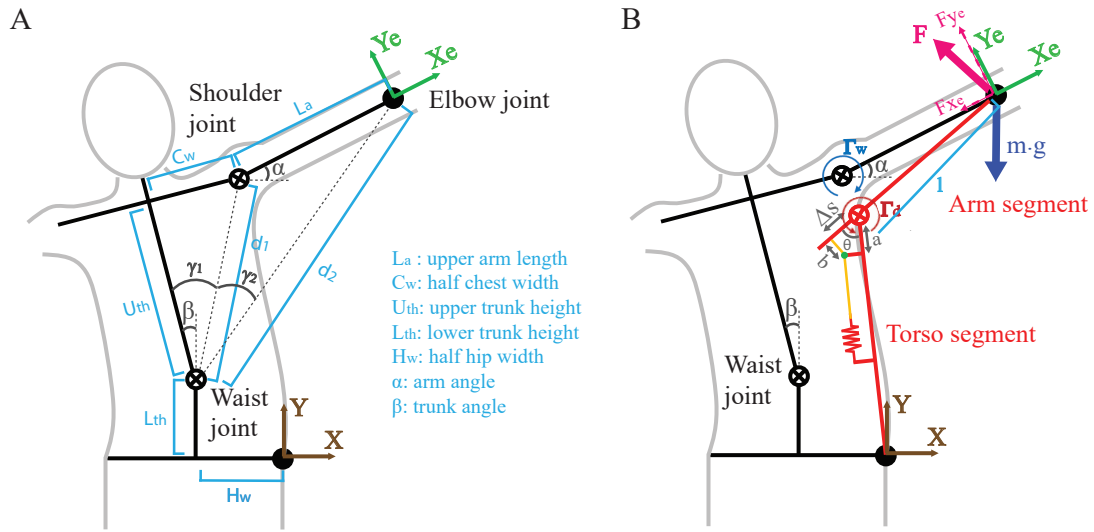
Figure A.1 – Schema of the upper body. A) Body dimensions. B) Schema of the device, and forces and torques induced.

$$y = d_2^2 \cdot \cos(\alpha + \gamma_1 + \gamma_2) + L_{th} \tag{A.6}$$

Upon the output positions, the gravity force values can be calculated. In the current model, two different coordinate systems are used: The XY coordinate system (braun in Fig. A.1) for the positions and the $XeYe$ coordinate system (green in Fig. A.1) for the force projections. This allows to decompose the force generated by the mechanism in two components: the gravity compensation contribution on Ye and the parasitic forces in the arm on Xe (see Fig. A.1 B). The forces on Xe are parasitic and unwanted, even if the gravity also has a component in that direction. Unlike the Ye-projected force that counterbalance the arm weight, the Xe-projected forces act on the interface with the skin. This will lead the interface to create shear stress on the skin and therefore discomfort for the subject.

Both forces can be computed as in Eq. A.7 and A.8.

$$F_{Ye,ref} = \cos(\alpha + \beta) \cdot m \cdot g \tag{A.7}$$

$$F_{Xe,ref} = \sin(\alpha + \beta) \cdot m \cdot g \tag{A.8}$$

with m the mass of the arm (see Table 2.2) and g the gravity. The error of the arm weight

compensation can be calculated as in Eq. A.9.

$$F_{errY_e} = F_{Y_e} - F_{Y_e,ref} \tag{A.9}$$

This force error has to be minimize over the whole domain, which will characterize the performance (p_e) of the device.

$$p_e = \min \| \sum_{\alpha,\beta \in ROM} F_{errY_e}(\alpha, \beta, k, l_s, l_o)^2 \| \tag{A.10}$$

with k the spring constant, l_s the spring length, and l_o the initial spring length.

The spring is making the gravity compensation mechanism and is ruled by Eq. A.11.

$$F_s = k \cdot \Delta x + F_0 \tag{A.11}$$

With k the spring constant ($\frac{N}{m}$), Δx the deformation of the spring (m), F_0 the force at initial length (N).

In a gravity compensation device, the torque induced by the arm weight Γ_w has to be compensated at the shoulder by the torque produced by the device Γ_d.

$$\sum^{\Gamma} = \Gamma_d - \Gamma_w \tag{A.12}$$

The device's torque is:

$$\Gamma_d = a \cdot F_s \cdot \sqrt{1 - (\frac{a^2 + b^2 - \Delta s^2}{2 \cdot a \cdot b})^2} \tag{A.13}$$

with b being:

$$b = \sqrt{a^2 + \Delta s^2 - 2 \cdot a \cdot \Delta s \cdot \cos\theta} \tag{A.14}$$

After combining Eq. A.13 and A.14, we obtain:

$$\Gamma_d = a \cdot F_s \cdot \frac{\Delta s \cdot \sin\theta}{b} \tag{A.15}$$

The torque induced by the arm weight is:

$$\Gamma_w = l \cdot m \cdot g \cdot \sin\theta \tag{A.16}$$

Appendix A. Computation of the Torque to Compensate the Arm Weight

As the equilibrium is required, Eq. A.17 must be satisfied:

$$a \cdot F_s \cdot \frac{\Delta s}{b} = l \cdot m \cdot g \tag{A.17}$$

Therefore, taking into account Eq. A.11, we get a gravity compensation when:

$$a \cdot \Delta s \cdot \frac{k \cdot (b - l_0) + F_0}{l \cdot b} = m \cdot g \tag{A.18}$$

b being dependant on θ, perfect gravity compensation does not occur. To perform perfect gravity compensation, we can simulate a zero free-length spring by adding a pretension b_0 on the spring:

$$k \cdot (b - l_0 + b_0) + F_0 = k \cdot b \longleftrightarrow b_0 = l_0 - \frac{F_0}{k} \tag{A.19}$$

In our device, the distance a is constant, leaving us with one optimization parameter Δs. In that case, the analytical solution for the torque is:

$$\Gamma = m \cdot g \cdot l = a \cdot \Delta s \cdot k \tag{A.20}$$

Bibliography

[1] D. Floreano and R. J. Wood, "Science, technology and the future of small autonomous drones," *Nature*, vol. 521, no. 7553, p. 460, 2015.

[2] R. R. Murphy, S. Tadokoro, D. Nardi, A. Jacoff, P. Fiorini, H. Choset, and A. M. Erkmen, "Search and rescue robotics," *Springer handbook of robotics*, pp. 1151–1173, 2008.

[3] G. Hirzinger, J. Bals, M. Otter, and J. Stelter, "The dlr-kuka success story: robotics research improves industrial robots," *IEEE Robotics & Automation Magazine*, vol. 12, no. 3, pp. 16–23, 2005.

[4] J. Casper and R. R. Murphy, "Human-robot interactions during the robot-assisted urban search and rescue response at the world trade center," *IEEE Transactions on Systems, Man, and Cybernetics, Part B (Cybernetics)*, vol. 33, no. 3, pp. 367–385, 2003.

[5] M. A. Diftler, J. Mehling, M. E. Abdallah, N. A. Radford, L. B. Bridgwater, A. M. Sanders, R. S. Askew, D. M. Linn, J. D. Yamokoski, F. Permenter *et al.*, "Robonaut 2-the first humanoid robot in space," in *2011 IEEE international conference on robotics and automation*. IEEE, 2011, pp. 2178–2183.

[6] O. Khatib, X. Yeh, G. Brantner, B. Soe, B. Kim, S. Ganguly, H. Stuart, S. Wang, M. Cutkosky, A. Edsinger *et al.*, "Ocean one: A robotic avatar for oceanic discovery," *IEEE Robotics & Automation Magazine*, vol. 23, no. 4, pp. 20–29, 2016.

[7] X.-Z. Chen, B. Jang, D. Ahmed, C. Hu, C. De Marco, M. Hoop, F. Mushtaq, B. J. Nelson, and S. Pané, "Small-scale machines driven by external power sources," *Advanced Materials*, vol. 30, no. 15, p. 1705061, 2018.

[8] J. Bodner, H. Wykypiel, G. Wetscher, and T. Schmid, "First experiences with the da vinci™ operating robot in thoracic surgery," *European Journal of Cardio-thoracic surgery*, vol. 25, no. 5, pp. 844–851, 2004.

[9] G. Niemeyer, C. Preusche, S. Stramigioli, and D. Lee, "Telerobotics," in *Springer handbook of robotics*. Springer, 2016, pp. 1085–1108.

[10] J. L. Herder, N. Vrijlandt, T. Antonides, M. Cloosterman, and P. L. Mastenbroek, "Principle and design of a mobile arm support for people with muscular weakness," *Journal of Rehabilitation Research & Development*, vol. 43, no. 5, pp. 591–605, 2006.

Bibliography

[11] M. A. Goodrich, A. C. Schultz *et al.*, "Human–robot interaction: a survey," *Foundations and Trends® in Human–Computer Interaction*, vol. 1, no. 3, pp. 203–275, 2008.

[12] J. Y. Chen, M. J. Barnes, and M. Harper-Sciarini, "Supervisory control of multiple robots: Human-performance issues and user-interface design," *IEEE Transactions on Systems, Man, and Cybernetics, Part C (Applications and Reviews)*, vol. 41, no. 4, pp. 435–454, 2011.

[13] A. Wang, J. Ramos, J. Mayo, W. Ubellacker, J. Cheung, and S. Kim, "The hermes humanoid system: A platform for full-body teleoperation with balance feedback," in *Humanoid Robots, IEEE-RAS 15th International Conference on*, 2015, pp. 730–737.

[14] K. Kim and J. E. Colgate, "Haptic feedback enhances grip force control of semg-controlled prosthetic hands in targeted reinnervation amputees," *IEEE Transactions on Neural Systems and Rehabilitation Engineering*, vol. 20, no. 6, pp. 798–805, 2012.

[15] C. L. Fernando, M. Furukawa, T. Kurogi, S. Kamuro, K. Minamizawa, S. Tachi *et al.*, "Design of telesar v for transferring bodily consciousness in telexistence," in *2012 IEEE/RSJ International Conference on Intelligent Robots and Systems.* IEEE, 2012, pp. 5112–5118.

[16] J. Rebelo, T. Sednaoui, E. B. den Exter, T. Krueger, and A. Schiele, "Bilateral robot teleoperation: A wearable arm exoskeleton featuring an intuitive user interface," *IEEE Robotics & Automation Magazine*, vol. 21, no. 4, pp. 62–69, 2014.

[17] L. N. Awad, J. Bae, K. O'Donnell, S. M. De Rossi, K. Hendron, L. H. Sloot, P. Kudzia, S. Allen, K. G. Holt, T. D. Ellis *et al.*, "A soft robotic exosuit improves walking in patients after stroke," *Science translational medicine*, vol. 9, no. 400, p. eaai9084, 2017.

[18] H. In, B. B. Kang, M. Sin, and K.-J. Cho, "Exo-glove: A wearable robot for the hand with a soft tendon routing system," *IEEE Robotics & Automation Magazine*, vol. 22, no. 1, pp. 97–105, 2015.

[19] I. Koo, C. Yun, M. V. Costa, J. V. Scognamiglio, T. A. Yangali, D. Park, and K.-J. Cho, "Development of a meal assistive exoskeleton made of soft materials for polymyositis patients," in *2014 IEEE/RSJ International Conference on Intelligent Robots and Systems.* IEEE, 2014, pp. 542–547.

[20] C. S. Simpson, A. M. Okamura, and E. W. Hawkes, "Exomuscle: An inflatable device for shoulder abduction support," in *2017 IEEE International Conference on Robotics and Automation (ICRA).* IEEE, 2017, pp. 6651–6657.

[21] P. Polygerinos, Z. Wang, K. C. Galloway, R. J. Wood, and C. J. Walsh, "Soft robotic glove for combined assistance and at-home rehabilitation," *Robotics and Autonomous Systems*, vol. 73, pp. 135–143, 2015.

[22] J. Arata, K. Ohmoto, R. Gassert, O. Lambercy, H. Fujimoto, and I. Wada, "A new hand exoskeleton device for rehabilitation using a three-layered sliding spring mechanism,"

in *2013 IEEE International Conference on Robotics and Automation.* IEEE, 2013, pp. 3902–3907.

[23] F. Scribano, M. Burns, and E. Barron, "Design, development and fabrication of a personnel armor load profile analyzer," IIT RESEARCH INST CHICAGO IL, Tech. Rep., 1970.

[24] A. S. Iberall, "The use of lines of nonextension to improve mobility in full-pressure suits," RAND DEVELOPMENT CORP CLEVELAND OH, Tech. Rep., 1964.

[25] M. Kim, S. Kang, S. Lee, W. Chung, K. Cho, and C.-W. Lee, "Development of a humanoid robot centaur-design, human interface, planning and control of its upper-body," in *IEEE SMC'99 Conference Proceedings. 1999 IEEE International Conference on Systems, Man, and Cybernetics (Cat. No. 99CH37028)*, vol. 4. IEEE, 1999, pp. 948–953.

[26] J. L. Pons, *Wearable robots: biomechatronic exoskeletons.* John Wiley & Sons, 2008.

[27] C. Zhu and W. Sheng, "Wearable sensor-based hand gesture and daily activity recognition for robot-assisted living," *IEEE Transactions on Systems, Man, and Cybernetics-Part A: Systems and Humans*, vol. 41, no. 3, pp. 569–573, 2011.

[28] C. A. Cifuentes, A. Frizera, R. Carelli, and T. Bastos, "Human–robot interaction based on wearable imu sensor and laser range finder," *Robotics and Autonomous Systems*, vol. 62, no. 10, pp. 1425–1439, 2014.

[29] H. I. Son, J. Kim, L. Chuang, A. Franchi, P. R. Giordano, D. Lee, and H. H. Bülthoff, "An evaluation of haptic cues on the tele-operator's perceptual awareness of multiple uavs' environments," in *2011 IEEE World Haptics Conference.* IEEE, 2011, pp. 149–154.

[30] S. Tachi, "Telexistence," in *Virtual Realities.* Springer, 2015, pp. 229–259.

[31] G. Hirzinger, B. Brunner, J. Dietrich, and J. Heindl, "Sensor-based space robotics-rotex and its telerobotic features," *IEEE Transactions on robotics and automation*, vol. 9, no. 5, pp. 649–663, 1993.

[32] M. M. Coad, A. M. Okamura, S. Wren, Y. Mintz, T. S. Lendvay, A. M. Jarc, and I. Nisky, "Training in divergent and convergent force fields during 6-dof teleoperation with a robot-assisted surgical system," in *2017 IEEE World Haptics Conference (WHC).* IEEE, 2017, pp. 195–200.

[33] L. Santos-Carreras, R. Beira, A. Sengül, R. Gassert, and H. Bleuler, "Influence of force and torque feedback on operator performance in a vr-based suturing task," *Applied Bionics and Biomechanics*, vol. 7, no. 3, pp. 217–230, 2010.

[34] M. Diana and J. Marescaux, "Robotic surgery," *British Journal of Surgery*, vol. 102, no. 2, pp. e15–e28, 2015.

Bibliography

[35] S. Lee and G. J. Kim, "Effects of haptic feedback, stereoscopy, and image resolution on performance and presence in remote navigation," *International Journal of Human-Computer Studies*, vol. 66, no. 10, pp. 701–717, 2008.

[36] M. Olivari, F. M. Nieuwenhuizen, H. H. Bülthoff, and L. Pollini, "Pilot adaptation to different classes of haptic aids in tracking tasks," *Journal of Guidance, Control, and Dynamics*, vol. 37, no. 6, pp. 1741–1753, 2014.

[37] N. Diolaiti and C. Melchiorri, "Teleoperation of a mobile robot through haptic feedback," in *Haptic Virtual Environments and Their Applications, IEEE International Workshop*, 2002, pp. 67–72.

[38] H. Culbertson, S. B. Schorr, and A. M. Okamura, "Haptics: The present and future of artificial touch sensation," *Annual Review of Control, Robotics, and Autonomous Systems*, vol. 1, pp. 385–409, 2018.

[39] V. Ramachandran, J. Shintake, and D. Floreano, "All-fabric wearable electroadhesive clutch," *Advanced Materials Technologies*, vol. 4, no. 2, p. 1800313, 2019.

[40] R. Hinchet, V. Vechev, H. Shea, and O. Hilliges, "Dextres: Wearable haptic feedback for grasping in vr via a thin form-factor electrostatic brake," in *The 31st Annual ACM Symposium on User Interface Software and Technology*. ACM, 2018, pp. 901–912.

[41] H. Ando, K. Obana, M. Sugimoto, and T. Maeda, "A wearable force display based on brake change in angular momentum," *Proc Artificial Reality and Telexistence 2002*, pp. 16–21, 2002.

[42] D. Li and H. Vallery, "Gyroscopic assistance for human balance," in *2012 12th IEEE International Workshop on Advanced Motion Control (AMC)*. IEEE, 2012, pp. 1–6.

[43] M. Murer, B. Maurer, H. Huber, I. Aslan, and M. Tscheligi, "Torquescreen: Actuated flywheels for ungrounded kinaesthetic feedback in handheld devices," in *Proceedings of the Ninth International Conference on Tangible, Embedded, and Embodied Interaction*. ACM, 2015, pp. 161–164.

[44] R. S. Johansson, "Tactile sensibility in the human hand: receptive field characteristics of mechanoreceptive units in the glabrous skin area." *The Journal of physiology*, vol. 281, no. 1, pp. 101–125, 1978.

[45] A. M. Okamura, J. T. Dennerlein, and R. D. Howe, "Vibration feedback models for virtual environments," in *Proceedings. 1998 IEEE International Conference on Robotics and Automation (Cat. No. 98CH36146)*, vol. 1. IEEE, 1998, pp. 674–679.

[46] H. A. Sonar and J. Paik, "Soft pneumatic actuator skin with piezoelectric sensors for vibrotactile feedback," *Frontiers in Robotics and AI*, vol. 2, p. 38, 2016.

112

[47] A. Delazio, K. Nakagaki, R. L. Klatzky, S. E. Hudson, J. F. Lehman, and A. P. Sample, "Force jacket: Pneumatically-actuated jacket for embodied haptic experiences," in *Proc. CHI Conference on Human Factors in Computing Systems*, 2018, p. 320.

[48] K. A. Kaczmarek, J. G. Webster, P. Bach-y Rita, and W. J. Tompkins, "Electrotactile and vibrotactile displays for sensory substitution systems," *IEEE Transactions on Biomedical Engineering*, vol. 38, no. 1, pp. 1–16, 1991.

[49] M. Pfeiffer and M. Rohs, "Haptic feedback for wearables and textiles based on electrical muscle stimulation," in *Smart Textiles*. Springer, 2017, pp. 103–137.

[50] M. Nakamura and L. Jones, "An actuator for the tactile vest-a torso-based haptic device," in *11th Symposium on Haptic Interfaces for Virtual Environment and Teleoperator Systems, 2003. HAPTICS 2003. Proceedings*. IEEE, 2003, pp. 333–339.

[51] H. S. Lee, H. Phung, D.-H. Lee, U. K. Kim, C. T. Nguyen, H. Moon, J. C. Koo, H. R. Choi *et al.*, "Design analysis and fabrication of arrayed tactile display based on dielectric elastomer actuator," *Sensors and Actuators A: Physical*, vol. 205, pp. 191–198, 2014.

[52] J. Wheeler, K. Bark, J. Savall, and M. Cutkosky, "Investigation of rotational skin stretch for proprioceptive feedback with application to myoelectric systems," *IEEE Transactions on Neural Systems and Rehabilitation Engineering*, vol. 18, no. 1, pp. 58–66, 2010.

[53] F. Chinello, C. Pacchierotti, N. G. Tsagarakis, and D. Prattichizzo, "Design of a wearable skin stretch cutaneous device for the upper limb," in *2016 IEEE Haptics Symposium (HAPTICS)*. IEEE, 2016, pp. 14–20.

[54] T. Nef, M. Mihelj, and R. Riener, "Armin: a robot for patient-cooperative arm therapy," *Medical & biological engineering & computing*, vol. 45, no. 9, pp. 887–900, 2007.

[55] L. Dovat, O. Lambercy, R. Gassert, T. Maeder, T. Milner, T. C. Leong, and E. Burdet, "Handcare: a cable-actuated rehabilitation system to train hand function after stroke," *IEEE Transactions on Neural Systems and Rehabilitation Engineering*, vol. 16, no. 6, pp. 582–591, 2008.

[56] G. Rauter, R. Sigrist, R. Riener, and P. Wolf, "Learning of temporal and spatial movement aspects: A comparison of four types of haptic control and concurrent visual feedback," *IEEE transactions on haptics*, vol. 8, no. 4, pp. 421–433, 2015.

[57] R. Sigrist, G. Rauter, R. Riener, and P. Wolf, "Augmented visual, auditory, haptic, and multimodal feedback in motor learning: a review," *Psychonomic bulletin & review*, vol. 20, no. 1, pp. 21–53, 2013.

[58] K. Bark, P. Khanna, R. Irwin, P. Kapur, S. A. Jax, L. J. Buxbaum, and K. J. Kuchenbecker, "Lessons in using vibrotactile feedback to guide fast arm motions," in *2011 IEEE World Haptics Conference*. IEEE, 2011, pp. 355–360.

Bibliography

[59] L. Marchal-Crespo, M. Bannwart, R. Riener, and H. Vallery, "The effect of haptic guidance on learning a hybrid rhythmic-discrete motor task," *IEEE transactions on haptics*, vol. 8, no. 2, pp. 222–234, 2015.

[60] E. H. van Asseldonk, M. Wessels, A. H. Stienen, F. C. van der Helm, and H. van der Kooij, "Influence of haptic guidance in learning a novel visuomotor task," *Journal of Physiology-Paris*, vol. 103, no. 3-5, pp. 276–285, 2009.

[61] G. Rauter, R. Sigrist, L. Marchal-Crespo, H. Vallery, R. Riener, and P. Wolf, "Assistance or challenge? filling a gap in user-cooperative control," in *2011 IEEE/RSJ International Conference on Intelligent Robots and Systems*. IEEE, 2011, pp. 3068–3073.

[62] C. C. Berger, M. Gonzalez-Franco, E. Ofek, and K. Hinckley, "The uncanny valley of haptics," *Science Robotics*, vol. 3, no. 17, pp. Art–No, 2018.

[63] S. Rosati, K. Krużelecki, G. Heitz, D. Floreano, and B. Rimoldi, "Dynamic routing for flying ad hoc networks," *IEEE Transactions on Vehicular Technology*, vol. 65, no. 3, pp. 1690–1700, 2016.

[64] A. Briod, P. Kornatowski, J.-C. Zufferey, and D. Floreano, "A collision-resilient flying robot," *Journal of Field Robotics*, vol. 31, no. 4, pp. 496–509, 2014.

[65] J. M. Peschel and R. R. Murphy, "On the human–machine interaction of unmanned aerial system mission specialists," *IEEE Transactions on Human-Machine Systems*, vol. 43, no. 1, pp. 53–62, 2013.

[66] C. Carignan, J. Tang, and S. Roderick, "Development of an exoskeleton haptic interface for virtual task training," in *2009 IEEE/RSJ International Conference on Intelligent Robots and Systems*. IEEE, 2009, pp. 3697–3702.

[67] A. Cherpillod, S. Mintchev, and D. Floreano, "Embodied flight with a drone," *arXiv preprint arXiv:1707.01788*, 2017.

[68] A. Sanna, F. Lamberti, G. Paravati, and F. Manuri, "A kinect-based natural interface for quadrotor control," *Entertainment Computing*, vol. 4, no. 3, pp. 179–186, 2013.

[69] K. Pfeil, S. L. Koh, and J. LaViola, "Exploring 3d gesture metaphors for interaction with unmanned aerial vehicles," in *Proceedings of the 2013 international conference on Intelligent user interfaces*. ACM, 2013, pp. 257–266.

[70] W. S. Ng and E. Sharlin, "Collocated interaction with flying robots," in *2011 Ro-Man*. IEEE, 2011, pp. 143–149.

[71] A. Stoica, F. Salvioli, and C. Flowers, "Remote control of quadrotor teams, using hand gestures," in *2014 9th ACM/IEEE International Conference on Human-Robot Interaction (HRI)*. IEEE, 2014, pp. 296–297.

[72] J. Miehlbradt, A. Cherpillod, S. Mintchev, M. Coscia, F. Artoni, D. Floreano, and S. Micera, "Data-driven body–machine interface for the accurate control of drones," *Proceedings of the National Academy of Sciences*, vol. 115, no. 31, pp. 7913–7918, 2018.

[73] T. M. Lam, M. Mulder, and M. R. van Paassen, "Haptic interface in uav tele-operation using force-stiffness feedback," in *2009 IEEE International Conference on Systems, Man and Cybernetics.* IEEE, 2009, pp. 835–840.

[74] X. Hou, R. Mahony, and F. Schill, "Comparative study of haptic interfaces for bilateral teleoperation of vtol aerial robots," *IEEE Transactions on Systems, Man, and Cybernetics: Systems*, vol. 46, no. 10, pp. 1352–1363, 2016.

[75] A. Kanso, I. H. Elhajj, E. Shammas, and D. Asmar, "Enhanced teleoperation of uavs with haptic feedback," in *2015 IEEE International Conference on Advanced Intelligent Mechatronics (AIM).* IEEE, 2015, pp. 305–310.

[76] J. D. Brown, M. K. Shelley, D. Gardner, E. A. Gansallo, and R. B. Gillespie, "Non-colocated kinesthetic display limits compliance discrimination in the absence of terminal force cues," *IEEE transactions on haptics*, vol. 9, no. 3, pp. 387–396, 2016.

[77] A. Schiele and F. C. van der Helm, "Influence of attachment pressure and kinematic configuration on phri with wearable robots," *Applied Bionics and Biomechanics*, vol. 6, no. 2, pp. 157–173, 2009.

[78] H. S. Lo and S. Q. Xie, "Exoskeleton robots for upper-limb rehabilitation: State of the art and future prospects," *Medical engineering & physics*, vol. 34, no. 3, pp. 261–268, 2012.

[79] NASA, "Nasa-std-3000, antropometry and biomechanics, vol.1, sect. 3," NASA, Washington D.C., Tech. Rep., 1994.

[80] T. G. Sugar, J. He, E. J. Koeneman, J. B. Koeneman, R. Herman, H. Huang, R. S. Schultz, D. Herring, J. Wanberg, S. Balasubramanian *et al.*, "Design and control of rupert: a device for robotic upper extremity repetitive therapy," *IEEE transactions on neural systems and rehabilitation engineering*, vol. 15, no. 3, pp. 336–346, 2007.

[81] Y. Mao and S. K. Agrawal, "A cable driven upper arm exoskeleton for upper extremity rehabilitation," in *2011 IEEE International Conference on Robotics and Automation.* IEEE, 2011, pp. 4163–4168.

[82] D. Park and K.-J. Cho, "Development and evaluation of a soft wearable weight support device for reducing muscle fatigue on shoulder," *PloS one*, vol. 12, no. 3, p. e0173730, 2017.

[83] R. Natividad and C.-H. Yeow, "Development of a soft robotic shoulder assistive device for shoulder abduction," in *2016 6th IEEE International Conference on Biomedical Robotics and Biomechatronics (BioRob).* IEEE, 2016, pp. 989–993.

Bibliography

[84] C. T. O'Neill, N. S. Phipps, L. Cappello, S. Paganoni, and C. J. Walsh, "A soft wearable robot for the shoulder: Design, characterization, and preliminary testing," in *2017 International Conference on Rehabilitation Robotics (ICORR)*. IEEE, 2017, pp. 1672–1678.

[85] S. O. Madgwick, A. J. Harrison, and R. Vaidyanathan, "Estimation of imu and marg orientation using a gradient descent algorithm," in *2011 IEEE international conference on rehabilitation robotics*. IEEE, 2011, pp. 1–7.

[86] B. L. Day and R. F. Reynolds, "Vestibular reafference shapes voluntary movement," *Current biology*, vol. 15, no. 15, pp. 1390–1394, 2005.

[87] J. J. LaViola Jr, "A discussion of cybersickness in virtual environments," *ACM SIGCHI Bulletin*, vol. 32, no. 1, pp. 47–56, 2000.

[88] C. T. Fuentes and A. J. Bastian, "Where is your arm? variations in proprioception across space and tasks," *Journal of neurophysiology*, 2009.

[89] H. Kobayashi and H. Nozaki, "Development of muscle suit for supporting manual worker," in *2007 IEEE/RSJ International Conference on Intelligent Robots and Systems*. IEEE, 2007, pp. 1769–1774.

[90] K. Stadler, W. J. Elspass, and H. W. van de Venn, "Robo–mate: Exoskeleton to enhance industrial production: Special session: Exoskeletons for emerging applications," in *Mobile Service Robotics*. World Scientific, 2014, pp. 53–60.

[91] K. S. Stadler, R. Altenburger, E. Schmidhauser, D. Scherly, J. Ortiz, S. Toxiri, L. Mateos, and J. Masood, "Robo-mate an exoskeleton for industrial use—concept and mechanical design," in *Advances in Cooperative Robotics*. World Scientific, 2017, pp. 806–813.

[92] C. Constantinescu, D. Popescu, P. Muresan, and T. Oliver, "Optimisation of advanced manufacturing environments with integrated intelligent exoskeletons," in *2016 International Conference on Production Research–Africa, Europe and the Middle East, Cluj-Napoca, Romania*, 2016, pp. 24–27.

[93] S. Roderick, M. Liszka, and C. Carignan, "Design of an arm exoskeleton with scapula motion for shoulder rehabilitation," in *ICAR'05. Proceedings., 12th International Conference on Advanced Robotics, 2005*. IEEE, 2005, pp. 524–531.

[94] L. Cappello, D. K. Binh, S.-C. Yen, and L. Masia, "Design and preliminary characterization of a soft wearable exoskeleton for upper limb," in *2016 6th IEEE International Conference on Biomedical Robotics and Biomechatronics (BioRob)*. IEEE, 2016, pp. 623–630.

[95] S. Lessard, P. Pansodtee, A. Robbins, J. M. Trombadore, S. Kurniawan, and M. Teodorescu, "A soft exosuit for flexible upper-extremity rehabilitation," *IEEE Transactions on Neural Systems and Rehabilitation Engineering*, vol. 26, no. 8, pp. 1604–1617, 2018.

116

[96] A. R. Tilley, *The measure of man and woman: human factors in design.* John Wiley & Sons, 2002.

[97] C. E. Clauser, J. T. McConville, and J. W. Young, "Weight, volume, and center of mass of segments of the human body," Antioch Coll Yellow Springs OH, Tech. Rep., 1969.

[98] Q. Lu, C. Ortega, and O. Ma, "Passive gravity compensation mechanisms: technologies and applications," *Recent Patents on Engineering*, vol. 5, no. 1, pp. 32–44, 2011.

[99] G. Rauter, J. von Zitzewitz, A. Duschau-Wicke, H. Vallery, and R. Riener, "A tendon-based parallel robot applied to motor learning in sports," in *2010 3rd IEEE RAS & EMBS International Conference on Biomedical Robotics and Biomechatronics.* IEEE, 2010, pp. 82–87.

[100] S. Omari, M.-D. Hua, G. Ducard, and T. Hamel, "Bilateral haptic teleoperation of vtol uavs," in *2013 IEEE International Conference on Robotics and Automation.* IEEE, 2013, pp. 2393–2399.

[101] M. Mulder, D. A. Abbink, and E. R. Boer, "The effect of haptic guidance on curve negotiation behavior of young, experienced drivers," in *2008 IEEE International Conference on Systems, Man and Cybernetics.* IEEE, 2008, pp. 804–809.

[102] B. A. Forsyth and K. E. MacLean, "Predictive haptic guidance: Intelligent user assistance for the control of dynamic tasks," *IEEE transactions on visualization and computer graphics*, vol. 12, no. 1, pp. 103–113, 2006.

[103] R. A. Schmidt and C. A. Wrisberg, *Motor learning and performance: A situation-based learning approach.* Human kinetics, 2008.

[104] S. McGill, J. Seguin, and G. Bennett, "Passive stiffness of the lumbar torso in flexion, extension, lateral bending, and axial rotation. effect of belt wearing and breath holding." *Spine*, vol. 19, no. 6, pp. 696–704, 1994.

[105] T. Mcneill, D. Warwick, G. Andersson, and A. Schultz, "Trunk strengths in attempted flexion, extension, and lateral bending in healthy subjects and patients with low-back disorders." *Spine*, vol. 5, no. 6, pp. 529–538, 1980.

[106] J. E. Graves, M. L. Pollock, D. M. Carpenter, S. H. Leggett, A. Jones, M. MacMILLAN, and M. Fulton, "Quantitative assessment of full range-of-motion isometric lumbar extension strength," *Spine*, vol. 15, no. 4, pp. 289–294, 1990.

[107] S. G. Hart and L. E. Staveland, "Development of nasa-tlx (task load index): Results of empirical and theoretical research," in *Advances in psychology.* Elsevier, 1988, vol. 52, pp. 139–183.

[108] M. H. Zadeh, D. Wang, and E. Kubica, "The effect of sub-threshold forces on human performance in multi-modal computer-aided design," *Computer-Aided Design*, vol. 42, no. 5, pp. 471–477, 2010.

Bibliography

[109] J. M. Wolfe, K. R. Kluender, D. M. Levi, L. M. Bartoshuk, R. S. Herz, R. L. Klatzky, S. J. Lederman, and D. M. Merfeld, *Sensation & perception*. Sinauer Sunderland, MA, 2006.

[110] J. C. Baird and E. J. Noma, *Fundamentals of scaling and psychophysics*. John Wiley & Sons, 1978.

[111] S. S. Stevens, "On the psychophysical law," *Psychological review*, vol. 64, no. 3, p. 153, 1957.

[112] ——, *Psychophysics: Introduction to its perceptual, neural and social prospects*. Routledge, 2017.

[113] ——, "To honor fechner and repeal his law," *Science*, vol. 133, no. 3446, pp. 80–86, 1961.

[114] T. N. Cornsweet, "The staircase-method in psychophysics," *The American journal of psychology*, vol. 75, no. 3, pp. 485–491, 1962.

[115] J. K. Holden, E. M. Francisco, Z. Zhang, C. Baric, and M. Tommerdahl, "An undergraduate laboratory exercise to study weber's law," *Journal of Undergraduate Neuroscience Education*, vol. 9, no. 2, p. A71, 2011.

[116] E. Francisco, V. Tannan, Z. Zhang, J. Holden, and M. Tommerdahl, "Vibrotactile amplitude discrimination capacity parallels magnitude changes in somatosensory cortex and follows weber's law," *Experimental brain research*, vol. 191, no. 1, p. 49, 2008.

[117] S. Weinstein, "Intensive and extensive aspects of tactile sensitivity as a function of body part, sex and laterality," *The skin senses*, 1968.

[118] L. Marchal-Crespo and D. J. Reinkensmeyer, "Review of control strategies for robotic movement training after neurologic injury," *Journal of NeuroEngineering and Rehabilitation*, vol. 6, no. 1, p. 20, Jun. 2009. [Online]. Available: https://doi.org/10.1186/1743-0003-6-20

[119] J. L. Patton, M. E. Stoykov, M. Kovic, and F. A. Mussa-Ivaldi, "Evaluation of robotic training forces that either enhance or reduce error in chronic hemiparetic stroke survivors," *Experimental brain research*, vol. 168, no. 3, pp. 368–383, 2006.

[120] D. M. Wolpert, J. Diedrichsen, and J. R. Flanagan, "Principles of sensorimotor learning," *Nature Reviews Neuroscience*, vol. 12, no. 12, p. 739, 2011.

[121] M.-H. Milot, L. Marchal-Crespo, C. S. Green, S. C. Cramer, and D. J. Reinkensmeyer, "Comparison of error-amplification and haptic-guidance training techniques for learning of a timing-based motor task by healthy individuals," *Experimental brain research*, vol. 201, no. 2, pp. 119–131, 2010.

[122] L. Marchal-Crespo, P. Wolf, N. Gerig, G. Rauter, L. Jaeger, H. Vallery, and R. Riener, "The role of skill level and motor task characteristics on the effectiveness of robotic training: first results," in *2015 IEEE international conference on rehabilitation robotics (ICORR)*. IEEE, 2015, pp. 151–156.

[123] F. C. Huang, J. L. Patton, and F. A. Mussa-Ivaldi, "Negative viscosity can enhance learning of inertial dynamics," in *2009 IEEE International Conference on Rehabilitation Robotics*. IEEE, 2009, pp. 474–479.

[124] J. L. Patton, Y. J. Wei, P. Bajaj, and R. A. Scheidt, "Visuomotor learning enhanced by augmenting instantaneous trajectory error feedback during reaching," *PloS one*, vol. 8, no. 1, p. e46466, 2013.

[125] A. Tonazzini, J. Shintake, C. Rognon, V. Ramachandran, S. Mintchev, and D. Floreano, "Variable stiffness strip with strain sensing for wearable robotics," in *2018 IEEE International Conference on Soft Robotics (RoboSoft)*. IEEE, 2018, pp. 485–490.

[126] U. Yang, Y. Jang, and G. J. Kim, "Designing a vibro-tactile wear for close range interaction for vr-based motion training," in *International Conference on Artificial Reality and Telexistence*, 2002, pp. 4–9.

[127] R. W. Lindeman, R. Page, Y. Yanagida, and J. L. Sibert, "Towards full-body haptic feedback: the design and deployment of a spatialized vibrotactile feedback system," in *Proceedings of the ACM symposium on Virtual Reality Software and Technology*, 2004, pp. 146–149.

[128] W. Karlen, S. Cardin, D. Thalmann, and D. Floreano, "Enhancing pilot performance with a SymBodic system," in *Annual International Conference of the IEEE Engineering in Medicine and Biology Society (EMBC)*, 2010, pp. 6599–6602.

[129] J. K. S. Teh, A. D. Cheok, R. L. Peiris, Y. Choi, V. Thuong, and S. Lai, "Huggy pajama: a mobile parent and child hugging communication system," in *Proceedings of the 7th international conference on Interaction Design and Children*, 2008, pp. 250–257.

[130] J. Cha, M. Eid, L. Rahal, and A. El Saddik, "Hugme: An interpersonal haptic communication system," in *IEEE International Workshop on Haptic Audio Visual Environments and Games*, 2008, pp. 99–102.

[131] D. Tsetserukou, "Haptihug: A novel haptic display for communication of hug over a distance," in *International Conference on Human Haptic Sensing and Touch Enabled Computer Applications*. Springer, 2010, pp. 340–347.

[132] A. Israr, S. Zhao, K. Schwalje, R. Klatzky, and J. Lehman, "Feel effects: enriching storytelling with haptic feedback," *ACM Transactions on Applied Perception (TAP)*, vol. 11, no. 3, p. 11, 2014.

[133] F. Arafsha, K. M. Alam, and A. El Saddik, "Emojacket: Consumer centric wearable affective jacket to enhance emotional immersion," in *IEEE International Conference on Innovations in Information Technology (IIT)*, 2012, pp. 350–355.

[134] L. A. Jones, M. Nakamura, and B. Lockyer, "Development of a tactile vest," in *Haptic Interfaces for Virtual Environment and Teleoperator Systems, 2004. HAPTICS'04. Proceedings. 12th International Symposium on*, 2004, pp. 82–89.

Bibliography

[135] J. Van Erp, C. Jansen, T. Dobbins, and H. Van Veen, "Vibrotactile waypoint navigation at sea and in the air: two case studies," in *Proceedings of EuroHaptics*, 2004, pp. 166–173.

[136] S. W. Wu, R. E. Fan, C. R. Wottawa, E. G. Fowler, J. W. Bisley, W. S. Grundfest, and M. O. Culjat, "Torso-based tactile feedback system for patients with balance disorders," in *IEEE Haptics Symposium*, 2010, pp. 359–362.

[137] R. E. Fan, C. Wottawa, A. Mulgaonkar, R. J. Boryk, T. C. Sander, M. P. Wyatt, E. Dutson, W. S. Grundfest, and M. O. Culjat, "Pilot testing of a haptic feedback rehabilitation system on a lower-limb amputee," in *IEEE International Conference on Complex Medical Engineering*, 2009, pp. 1–4.

[138] P. Kapur, S. Premakumar, S. A. Jax, L. J. Buxbaum, A. M. Dawson, and K. J. Kuchenbecker, "Vibrotactile feedback system for intuitive upper-limb rehabilitation," in *IEEE World Haptics*, 2009, pp. 621–622.

[139] M. F. Rotella, K. Guerin, X. He, and A. M. Okamura, "HAPI bands: a haptic augmented posture interface," in *IEEE Haptics Symposium*, 2012, pp. 163–170.

[140] S. Kulkarni, C. J. Fisher, P. Lefler, A. Desai, S. Chakravarthy, E. Pardyjak, M. A. Minor, and J. M. Hollerbach, "A full-body steerable wind display for a locomotion interface," *IEEE Transactions on Visualization and Computer Graphics*, vol. 21, pp. 1146–1159, 2015.

[141] K. O. Johnson, "The roles and functions of cutaneous mechanoreceptors," *Current Opinion in Neurobiology*, vol. 11, no. 4, pp. 455–461, 2001.

[142] G. Ambrosi, A. Bicchi, D. D. Rossi, and E. Scilingo, "The role of contact area spread rate in haptic discrimination of softness," in *IEEE International Conference on Robotics and Automation*, 1999, pp. 305–310.

[143] E. Coevoet, T. Morales-Bieze, F. Largilliere, Z. Zhang, M. Thieffry, M. Sanz-Lopez, B. Carrez, D. Marchal, O. Goury, J. Dequidt *et al.*, "Software toolkit for modeling, simulation, and control of soft robots," *Advanced Robotics*, vol. 31, no. 22, pp. 1208–1224, 2017.

[144] R. A. Schmidt and T. D. Lee, *Motor learning and performance: From principles to application.* Human Kinetics, 2013.

[145] A. R. Jensen and E. Munro, "Reaction time, movement time, and intelligence," *Intelligence*, vol. 3, no. 2, pp. 121–126, 1979.

[146] M. Raitor, J. M. Walker, A. M. Okamura, and H. Culbertson, "Wrap: Wearable, restricted-aperture pneumatics for haptic guidance," in *Robotics and Automation, IEEE International Conference on*, 2017, pp. 427–432.

[147] L. He, C. Xu, D. Xu, and R. Brill, "Pneuhaptic: delivering haptic cues with a pneumatic armband," in *Proc. ACM International Symposium on Wearable Computers*, 2015, pp. 47–48.

[148] H. Tan, R. Gray, J. J. Young, and R. Taylor, "A haptic back display for attentional and directional cueing," *Haptics-e*, vol. 3, no. 1, 2003.

[149] R. W. Beard and T. W. McLain, *Small unmanned aircraft: Theory and practice*. Princeton university press, 2012.

[150] N. Smolyanskiy and M. Gonzalez-Franco, "stereoscopic first person view system for drone navigation," *Frontiers in Robotics and AI*, vol. 4, p. 11, 2017.

[151] S. Ionta, R. Gassert, and O. Blanke, "Multi-sensory and sensorimotor foundation of bodily self-consciousness–an interdisciplinary approach," *Frontiers in psychology*, vol. 2, p. 383, 2011.

[152] R. Colombo, F. Pisano, A. Mazzone, C. Delconte, S. Micera, M. C. Carrozza, P. Dario, and G. Minuco, "Design strategies to improve patient motivation during robot-aided rehabilitation," *Journal of neuroengineering and rehabilitation*, vol. 4, no. 1, p. 3, 2007.

[153] B. Robins, K. Dautenhahn, R. Te Boekhorst, and A. Billard, "Robotic assistants in therapy and education of children with autism: can a small humanoid robot help encourage social interaction skills?" *Universal Access in the Information Society*, vol. 4, no. 2, pp. 105–120, 2005.

CARINE ROGNON

PhD STUDENT IN ROBOTICS

✉ rognon.carine@gmail.com 📞 +4179-450-3115 📍 Lausanne, Switzerland
in linkedin.com/in/carinerognon 🔗 flyjacket.epfl.ch

EDUCATION

PhD
Ecole Polytechnique Fédérale de Lausanne (EPFL)

📅 September 2015 – ongoing 📍 Lausanne, Switzerland

Thesis title: Wearable Technologies for Embodied Human-Robot Interaction

Video: youtu.be/KEhSUZdRtm8

- Study of Human-Robot interactions, human proprioception of wearable devices, and influence of haptic feedback on guidance and immersion
- Design and fabrication of a soft exoskeleton (FlyJacket) to control a drone with body movements and receive haptic feedback
- March to September 2018: exchange at the Collaborative Haptics and Robotics in Medicine Laboratory (Stanford, USA) to develop of a new soft haptic actuator to render the sensation of flying
- Supervision of thirteen student projects and four semester of teaching assistant for the Master program in Robotics
- Twelve national and international public demonstrations of the FlyJacket project (CES Las Vegas, World Economic Forum in Davos, Lates at Science Museum in London, FoST in NYC, Hubweek in Boston, etc.). Appearance on Swiss National TV and radio
- Member of the Equal Opportunity committee of NCCR Robotics

Master Thesis
The University of Tokyo

📅 January 2015 – July 2015 📍 Tokyo, Japan

- Development and characterization of a new pneumatic actuator that mimic muscle behavior
- Design and construction of a robotic arm and shoulder that mimic the bone and muscular structure of the human body

M. Sc. in Biomedical Engineering, track core in Mechanics
Eidgenössische Technische Hochschule Zürich (ETHZ)

📅 September 2013 – July 2015 📍 Zurich, Switzerland

- Design of a reliability test procedure and characterization of four new polymer implants for intervertebral discs repair.
- Tests on biological samples. Dissection of cow tails, insertion of implants, and fatigue testing with INSTRON machine

B. Sc. in Microengineering
Ecole Polytechnique Fédérale de Lausanne (EPFL)

📅 September 2008 – July 2013 📍 Lausanne, Switzerland

- Bachelor's degree in five years to follow a swimming practice and compete at an international level

MOTIVATION

"I am passionate about human-robot interactions, particularly haptic communication. To me, the world is an amazing playground that I draw inspiration from to develop new technologies that can influence it"

SKILLS

Human-Robot interaction:
Design of haptic feedback actuators, human tactile perception, human proprioception, soft wearable devices design, exoskeletons, user study

Biomechanical Engineering:
Physiology, anatomy, orthopedics, biomechanics, design of mechanical implants, biocompatibility and material science, intervertebral disc implants, rehabilitation, prosthesis

Mechanics:
3D printing, design and modelization, CAD, conventional machining

Electronics:
Analysis and conception of electrical circuits, embedded electronics, electrical motors, sensors

Soft skills:
Creative thinking, innovation, project management, written, verbal and non-verbal communication, open-mindedness

Software:
SolidWorks, MATLAB and Simulink, Arduino, Qt Creator, Unity, C language, LaTeX, Adobe

EXPERIENCE

Engineering Intern
Mount Sinai Hospital, Orthopaedics Department

📅 October 2014 – January 2015 📍 New York City, USA

- Mechanical characterization of a new gel for nucleus pulposus replacement and polymer implants for anulus fibrosus repair in the intervertebral discs

Engineering Intern
INSTANT-LAB, EPFL

📅 July 2013 – August 2013 📍 Neuchâtel, Switzerland

- Design, characterization and prototyping of a smart insert for a knee prosthesis which enables post-operation long term tuning of the prosthesis orientation

PUBLICATIONS AND PATENT

- Rognon, C., Mintchev, S., Dell'Agnola, F., Cherpillod, A., Atienza, D., and Floreano, D., FlyJacket: An Upper Body Soft Exoskeleton for Immersive Drone Control. IEEE Robotics and Automation Letters, 3(3), 2362-2369. 2018. *Video: youtu.be/L0FTPYkLKHI*

- Rognon, C., Koehler, M., Duriez, C., Floreano, D., and Okamura, A. M., Soft haptic device to render the sensation of flying like a drone. IEEE Robotics and Automation Letters, 4(3), 2524-2531. 2019. *Video: youtu.be/SXCGDjWTc0I*

- Rognon, C., Ramachandran, V., Wu, A. R., Ijspeert, A. J., and Floreano, D. Haptic feedback perception and learning with cable-driven guidance in exosuit teleoperation of a simulated drone. IEEE Transactions on Haptics, 2019

- Rognon, C., Wu, A. R., Mintchev, S., Ijspeert, A., and Floreano, D., Haptic Guidance with a Soft Exoskeleton Reduces Error in Drone Teleoperation. In International Conference on Human Haptic Sensing and Touch Enabled Computer Applications (pp. 404-415). Springer, Cham. June 2018. *Video: youtu.be/zjb_dsSgn8s*

- Rognon, C., Koehler, M., Floreano, D., and Okamura, A. M., Perception of a Wearable Haptic Feedback Device to Render the Sensation of Flight, accepted at IEEE World Haptics conference, July 2019

- Tonazzini, A., Shintake, J., Rognon, C., Ramachandran, V., Mintchev, S., and Floreano, D.,. Variable stiffness strip with strain sensing for wearable robotics. In IEEE International Conference on Soft Robotics (RoboSoft) (pp. 485-490). April 2018

- Niiyama, R., Rognon, C., and Kuniyoshi, Y., Printable pneumatic artificial muscles for anatomy-based humanoid robots. In IEEE-RAS 15th International Conference on Humanoid Robots (Humanoids), (pp. 401-406). November 2015

- Rognon, C., Floreano, D., Mintchev, S., Concordel, A., Dell'Agnola, F., Atienza, D., Jacket for embodied interaction with virtual or distal robotic device, International Patent Application n ° PCT/IB2017/055410

LANGUAGES

French: Native Proficiency

English: Full Professional Proficiency

German: Professional Working Proficiency

Japanese: Elementary Proficiency

STRENGTHS

Hard-working Responsible
Time management Curiosity
Perseverance Communication skills
Motivator & Leader Tolerance

VOLUNTEERING

- La Soupe Populaire, Fondation Mère Sofia, Lausanne
- Ingénieurs du Monde, EPFL student association

INTERESTS

- Sports : swimming at international level from 2005 to 2013, currently triathlon team member, cross-country and alpine skiing, hiking and camping
- Humanitarian aid
- Sustainable development
- Equal opportunities causes
- Discovering new places